Investigating In-Situ Alloying During Blended Elemental (BE) and Master Alloy (MA) Sintering of Ti6Al4V

by

Gavin Steedman

Submitted in partial fulfilment of the requirements
for the degree of Master of Applied Science

at

Dalhousie University
Halifax, Nova Scotia
March 2014

DEDICATION PAGE

I wish to dedicate this work to both my parents and Nora Spencer, who have been immensley supportive during my studies, and provided continuous support at all times. Their guidance has been instrumental to me, and I am deeply grateful for it. I also wish to thank my supervisor, Dr. Stephen Corbin, who has been very supportive of me. His guidance and wisdom have been a huge benefit to this work.

TABLE OF CONTENTS

LIST OF TABLES

LIST OF FIGURES

ABSTRACT

Despite an increasing body of research, there exists a lack of understanding about the alloying behaviour of PM titanium alloys. Specifically, Ti6Al4V, which is the most common alloy, has not been investigated sufficiently to understand the behavior of alloying additions in the various forms that exist. The objective of this research was to investigate the role of alloying additions via in-situ analysis with differential scanning calorimetry (DSC). Mixtures of Ti6Al4V were prepared using master alloy (MA) and blended elemental (BE) additions, and analyzed during sintering profiles where the specimens were heated to 1200°C and held for various amounts of time. Of particular interest was the allotropic phase transformation that occurs during sintering, transforming from α-Ti to β-Ti on heating and then reversing on cooling. The reverse transformation was analyzed in detail using DSC in hopes of understanding how the nature of the alloying additions and the sintering profile affected various characterisitics of this transformation. Measurements of the onset, end, and peak temperature of the transformation were taken, along with the specific enthalpy and temperature span. A full compositional and microstructural analysis was performed on these DSC specimens as well in order to corroborate the findings of the DSC. Analysis of the binary BE mixtures of Ti6Al and Ti4V gave significant insight to the role of each alloying addition in the Ti matrix. Aluminum was found to reach a homogeneous state within a 1hr, but significant porosity formed as a result of highly dissimilar diffusion rates between Ti and Al, creating titanium aluminides. The binary Ti4V mixture required significantly more thermal exposure in order to reach homogeneity, but produced a denser product. The ternary BE Ti6Al4V mixture exhibited many of the characterisitics of the two binary systems. The measured enthalpy of transformation of the BE Ti6Al4V mixture was considerably lower than both MA mixtures, due to the porosity formed by the melting and spreading of the elemental Al additions. Results from the DSC suggested that the use of coarse and fine MA additions led to relatively homogeneous specimens after more that 2hrs at 1200°C. The smaller particle size of the fine MA led to faster homogenization than the coarse, however, in both cases the homogeneity of V in the matrix was the limiting factor. Unlike the BE mixutres, the addition of Al in MA particle did not result in the formation of porosity because it was introduced as an intermetallic. All DSC results were supported by both XRD and SEM/EDS analysis. Overall, a more complete understanding of the alloying behavior of PM Ti6Al4V has been developed along with a methodology for the use of DSC to analyze the sintering behavior in-situ.

LIST OF ABBREVIATIONS USED

BE	Blended elemental
CP	Commercially pure
DSC	Differential scanning calorimetry
DTA	Differential thermal analysis
EDS	Energy dispersion spectroscopy
FWHM	Full width half maximum
HDH	Hydride dehydride
HSPT	Hydrogen sintering phase and phase transformation
IM	Ingot metallurgy
MA	Master alloy
PM	Powder metallurgy
SEM	Scanning electron microscope
XRD	X-Ray diffraction

ACKNOWLEDGEMENTS

The authors would like to acknowledge the funding support provided by NSERC through the Automotive Partnership of Canada grant program, with additional funding provided by Wescast Industries Inc and Kingston Process Metallurgy Inc. The authors would also like to acknowledge the support of the following people: Daniel Cluff, Julian O'Flynn, Clark Murray, Cathy Whitman, Nick Koch, Logan Smith, Joannie Lapointe, Patricia Scallion, Dr Paul Bishop, and Dr Darrel Doman.

1.0. INTRODUCTION

1.1. Background

For decades engineers have seen the potential that titanium has for applications where a high strength-to-weight metal is required. Since the 1950s, the use of titanium has seen few applications outside of aerospace and defence applications. Titanium's inherent strength-to-weight advantage, corrosion resistance, and biocompatibility have not been fully exploited, due to the high cost of producing wrought titanium.

Powder metallurgy (PM) offers a processing route that could potentially open up the use of titanium to many new markets, such as massive-production industries. PM has been applied to other metals, particularly ferrous alloys, to reduce the cost of producing parts. PM offers near-net shaping production which will reduce waste and post-processing machining. Due to the processing of the mineral forms of titanium, PM offers additional savings because titanium powder is an intermediary when producing wrought titanium and therefore could represent a low cost feedstock for PM manufacturing. Further cost savings are possible with the higher material utilization that is possible with PM.

Before titanium PM alloys can achieve widespread use they must have mechanical properties which are comparable to those of wrought alloys. To date, certain properties such as yield strength and ultimate tensile strength of PM alloys are comparable to their wrought counter parts. However, other properties such as ductility and creep strength are inferior. The properties can be improved by reducing porosity, developing a homogeneous composition and minimizing contamination. Investigating the sintering behaviour of titanium can lead to significant gains in the previously mentioned properties by maximizing the effect of the diffusion mechanisms that occur during sintering. This can be accomplished by using thermal analysis techniques to investigate sintering of titanium.

1.2. Sintering

The consolidation of powders is a critical step in PM. Typically this occurs in a two-step process that first involves mechanical compaction. This compresses the powder particles both plastically and elastically into a form that should be very similar to the final shape. Compaction can achieve a very high level of consolidation and density. However, the bonds between the powder particles are very weak and are not sufficiently strong enough for most applications. Therefore, further densification is required to achieve the desired properties.

Sintering is a thermally activated bonding process that allows powders to bond at points of contact and lower their surface area. This results in a more coherent and mechanically suitable material. There are several mechanisms for bonding that occur during sintering, but primarily it is a result of solid and/or liquid state diffusion [1].

Following mechanical compaction powder particles form a semi-coherent structure that is held together by mechanical bonds resulting from compaction. Sintering can then be initiated at this stage. As temperature is increased, the system acts to reduce its overall surface energy. Typically this is achieved through a reduction in surface area. Smaller particles have a larger surface and thus, a higher surface energy. A reduction in surface energy results in mass transportation at points of contact between the particles to surrounding areas. This is known as “neck” growth, and is shown in Figure 1.2.1 in the classical example of two spherical powder particles. Ultimately neck growth reduces surface area and therefore lowers energy.

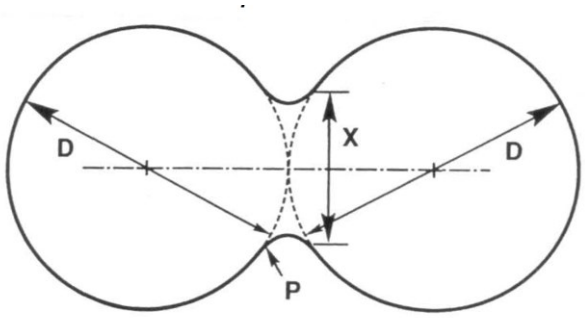

Where:

D = Particle Diameter
X = Neck Diameter
P = Radius o Curvature of the Neck

Figure 1.2.1: Neck growth between two spherical powder particles [2]

Neck growth reduces porosity and causes a change in pore shape, i.e. pores take on a more rounded structure. As a result, the discrete shapes of the original powder particles become less evident. While the rounding of the pore structure proceeds, the length of contact between particles grows and a more coherent structure is produced. As the pores continue to spheroidize, they become closed-off and are no longer connected to the surface. This causes pressure within these pores to increase. Eventually the external pressure that has caused these shaped pores equals the internal gas pressure. At this point the kinetics of sintering slow considerably and further increases in density are negligible.

These changes that occur during sintering are commonly categorized in to three stages: initial, intermediate and final and are shown schematically and described in Figure 1.2.2.

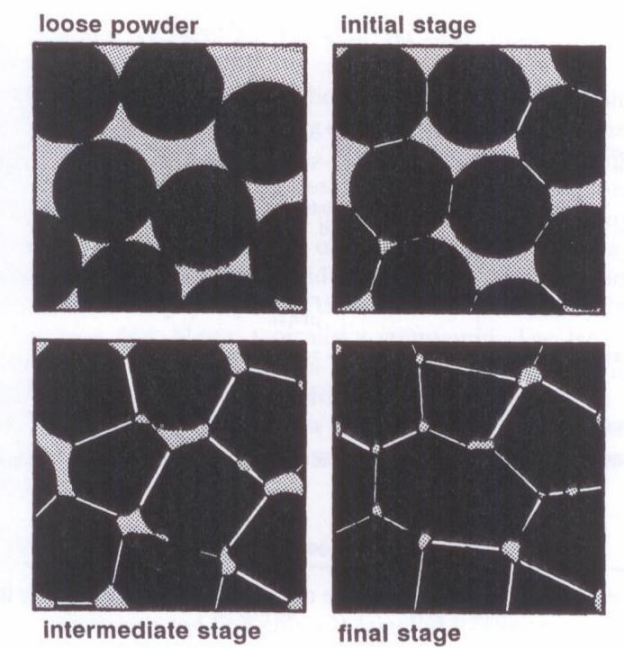

Stage	Process	Surface Area Loss	Densification	Coarsening
Adhesion	Contact formation	Minimal unless compacted at high pressures	None	None
Initial	Neck growth	Significant, up to 50% loss	Small at first	Minimal
Intermediate	Pore rounding and elongation	Near total loss of open porosity	Significant	Increase in grain size and pore size
Final	Pore closure, final densification	Negligible further loss	Slow and relatively minimal	Extensive grain and pore growth

Figure 1.2.2: Discrete stages of sintering with relative changes in microstructure [1].

Mass transport is necessary for neck growth to occur. Mass transport occurs through surface transport and bulk transport; where surface transport involves the movement of atoms from one surface to another, and bulk transport involves the movement of atoms from within a particle to the surface. Both forms of transport involve several atomistic mechanisms [1]. These mechanisms are summarized in Table 1.2.1. The transport of

mass can be visualised as the movement of vacancies, where the movement of mass creates a counter flow of vacancies. Vacancy concentration is lowered by thermally activated mass transport mechanisms causing either their accumulation or annihilation. This causes particles to coalesce creating neck growth and/or particle densification depending on the mechanism that is occurring.

Table 1.2.1: Summary of atomistic mass transport mechanisms

Atomistic Mechanism	**Type of Transport**
Evaporation-Condensation	Surface Transport
Surface Diffusion	Surface Transport
Volume Diffusion	Bulk and Surface Transport
Grain Boundary Diffusion	Bulk Transport

1.2.1. Evaporation-Condensation

During evaporation-condensation, vapour from the surface of a particle condenses on a nearby surface. The site where condensation occurs is determined by slight variations in pressure. As this is a surface transport mechanism there is no net increase in density. Instead, evaporation-condensation leads to a significant decrease in surface area as particles become rounded and particle necks grow. At the neck regions there is a continual deposition of atoms at these sites creating layers of growth. This reduces the amount of surface atoms neighboring the particle neck where the evaporation occurred. Evaporation-condensation is a temperature controlled mechanism following an Arrhenius

dependence. Increasing temperature leads to a higher vapour pressure at the surface of a particle, which increases the rate of evaporation. Evaporation occurs preferentially at flat or convex surfaces, while condensation occurs at concave surfaces where the vapour pressure is slightly lower than equilibrium, such as particle necks. Neck growth due to evaporation-condensation will continue until an equilibrium dictated by the solid-vapour dihedral angle is reached [1]. This equilibrium is expressed by Equation 1.2.1.

Equation 1.2.1

$$\gamma_{SS} = 2\gamma_{SV} cos \frac{\phi}{2}$$

where:

γ_{SS} = the grain boundary energy

γ_{SV} = the solid-vapour surface energy

ϕ = the dihedral angle

1.2.2. Surface Diffusion

Surface diffusion involves the motion of atoms across the surface of a particle to sites where a type of imperfection exists. Surface imperfections can include: ledges, kinks, atoms or vacancies. In order for surface diffusion to occur the current bond holding an atom must be broken. Once freed, the atom then must diffuse to the site of the imperfection across the surface. Finally, the atom must reattach to the crystal lattice at the site of the imperfection. The rate of these three steps is primarily controlled by temperature. In addition, the quantity of sites where imperfections exist and the ease of motion greatly affects surface diffusion [1]. The activation energy for surface diffusion, which is the activation energy for the slowest of the three steps, is lower than other forms

of mass transport. As a result, surface diffusion is the first of the different mass transport mechanisms to initiate. The effect of surface diffusion slows at higher temperature as the quantity of surface imperfections decreases. Similar to evaporation-condensation, surface diffusion increases particle rounding without any shrinkage.

1.2.3. Volume Diffusion

Volume diffusion is a mass transport mechanism that is controlled by temperature, composition, and pressure. Volume diffusion involves the movement of atoms through the bulk of the material, and can also be termed lattice diffusion. Vacancy concentration is an important variable for volume diffusion, and its dependence on temperature, composition, and pressure determine the driving force for volume diffusion. Volume diffusion is active at higher temperatures due to the temperature effect on vacancy concentration. Temperature determines the equilibrium concentration of vacancies, with increasing vacancy concentration at higher temperatures. Pressure also affects vacancy concentration; however this is due to local variations in pressure caused by differences in curvature of particles. More highly curved surfaces experience a change in vacancy concentration away from equilibrium, such as the neck region [1]. Concave regions have a vacancy concentration lower than equilibrium, and convex regions have a vacancy concentration above equilibrium. This creates diffusion paths between concave and convex regions of the material. The combined effect of temperature and pressure on vacancy concentration leads to volume diffusion sintering, with a sintering rate that can be quantified by Fick's first law as shown in Equation 1.2.2.

Equation 1.2.2

$$J = -D_V \frac{dC}{dx}$$

where:

J = atomic flux

D_V = diffusivity

dC/dx = vacancy concentration change over distance

Compositional effects on volume diffusion are due to a loss of stoichiometry. Off-stoichiometric compounds contain excess vacancies to neutralize charge [1]. This creates an increased atomic flux from phases that are off-stoichiometric.

1.2.4. Grain Boundary Diffusion

Grain boundary diffusion involves mass transport along grain boundaries, and is prominent in most alloys. Grain boundaries form in the neck region at the sinter bond between two particles. There is a misalignment between the crystal lattice of the two particles. This region then acts as a pathway for atomic movement. Additional grain boundaries exist within the powder particles, and also act as diffusion pathways. Movement occurs simultaneously with vacancy annihilation along the grain boundary. Mass is deposited at the neck region for diffusion along the sinter bond grain boundary. Transport along interparticle grain boundaries is usually between pores, causing them to coarsen.

Several different sintering processes have been developed to address the requirements for different applications. All of these processes are intended to progress sintering to the desired stage while satisfying any other requirements. Pressureless solid-state sintering is a very common sintering process and will be the focus of this report. With this form of sintering, the material is under no external load to enhance densification and no persistent liquid phases evolve during the process. Both external pressure and liquid phase evolution are commonly used to enhance densification and sintering kinetics, but are not a requirement to achieve high density.

1.3. Titanium/Titanium Alloys

Titanium is relatively exotic and expensive engineering metal that has found applications since the 1950s. The Soviet Union pioneered the use of titanium alloys for military applications such as aircraft and submarines [2]. These applications benefitted from titanium's relatively high strength-to-weight ratio, high temperature properties and corrosion resistance. The use of titanium remained limited to military applications throughout the cold war and was classified as a Strategic Material by the US government [3].

The expansion of titanium to other areas outside of military and aerospace applications has been limited by the cost of producing wrought titanium. Several sophisticated and energy intensive steps are required to produce titanium. This is primarily due to the metal's high reactivity and affinity for interstitial elements such as oxygen, nitrogen, hydrogen, and carbon [4]. Compared to the production of steel, a great deal more care and control is required to produce titanium that is low in impurities. In spite of the cost of producing titanium, there is a large body of work that is focusing on using titanium for novel applications due to its superior properties. These areas include: the automotive industry, food and chemical facilities, and biomedical applications. As a result, new methods for producing titanium are also being developed that hope to reduce both the cost and time [5].

Titanium is abundant in nature, and is the seventh most abundant metal. It is commonly found bonded with oxygen in the mineral forms rutile and ilmenite. Titanium is extracted from these two minerals almost exclusively by the Kroll process. This multi-step batch process begins with the conversion of titanium oxide to titanium tetrachloride ($TiCl_4$). The $TiCl_4$ is then purified using fractional distillation in order to remove any other chlorides. Following this step, the $TiCl_4$ is then reacted with liquid magnesium between 773 to 873°C [4], as shown below.

$$TiCl_{4_g} + 2Mg_l \rightarrow Ti_s + 2MgCl_{2_l}$$

The reduced titanium is a "sponge" form which is then physically removed from the reactor. The titanium sponge is then formed into long electrodes in preparation for vacuum arc melting. Melting under vacuum is necessary because the reactivity of titanium to oxygen and nitrogen. At this step alloying elements are mixed with the sponge to produce the electrodes. The sponge electrode acts as the anode and is lowered towards a water cooled copper crucible which acts as the cathode. The melt then collects in the copper crucible after the arc is struck. Double melting of the titanium ingots is common to ensure homogeneity of the alloying elements throughout.

1.3.1. Physical Properties

Titanium is uniquely situated between aluminum and iron alloys for many of its physical properties. Table 1.3.1 summarizes some of these properties.

Table 1.3.1: Summary of physical properties of titanium, aluminum and iron

	Titanium	**Aluminum**	**Iron**
Density (g/cm^3)	4.54	2.70	7.87
Modulus of elasticity (GPa)	115	72	215
Melting Point (°C)	1668	660	1536
Crystal Structure at RT	HCP	FCC	BCC
Hardness (Brinell)	120	23	86

Pure titanium exists in two crystal forms depending on temperature; below 883°C the α form of titanium is a hexagonal close-packed (HCP) structure. Above this temperature, termed the beta transus temperature, the structure changes to a body-centered cubic (BCC) known as the β phase. These alpha and beta phases of titanium form the basis for classifying different titanium alloys. Despite being an HCP structure, alpha titanium possesses a relatively high ductility due to numerous slip systems and twinning planes. This ductility is greatly affected by the concentration of interstitial impurities such as oxygen and nitrogen.

Titanium alloys are classified by the predominant stabilized phase of titanium that exists in the microstructure, these include: commercially pure (CP), alpha-alloys, beta-alloys, and alpha-beta alloys. In alpha-stabilized alloys, the alloying elements are added to help stabilize the α phase and increase the beta transus temperature. For beta-stabilized alloys, the alloying additions are intended to both lower the beta transus temperature and prevent the decomposition of the beta phase upon cooling. Alpha-beta alloys are a mixed-microstructure where all alpha is transformed to beta during heating. During cooling, transformation back to alpha occurs for most of the beta titanium, but some remains retained in the alpha microstructure. Figure 1.3.1 summarizes many of the common titanium alloys including composition and beta transus temperature.

Common Name	Alloy Composition (wt%)	T_β (°C)
α Alloys and CP Titanium		
Grade 1	CP-Ti (0.2Fe, 0.18O)	890
Grade 2	CP-Ti (0.3Fe, 0.25O)	915
Grade 3	CP-Ti (0.3Fe, 0.35O)	920
Grade 4	CP-Ti (0.5Fe, 0.40O)	950
Grade 7	Ti-0.2Pd	915
Grade 12	Ti-0.3Mo-0.8Ni	880
Ti-5-2.5	Ti-5Al-2.5Sn	1040
Ti-3-2.5	Ti-3Al-2.5V	935
α+β Alloys		
Ti-811	Ti-8Al-1V-1Mo	1040
IMI 685	Ti-6Al-5Zr-0.5Mo-0.25Si	1020
IMI 834	Ti-5.8Al-4Sn-3.5Zr-0.5Mo-0.7Nb-0.35Si-0.06C	1045
Ti-6242	Ti-6Al-2Sn-4Zr-2Mo-0.1Si	995
Ti-6-4	Ti-6Al-4V (0.20O)	995
Ti-6-4 ELI	Ti-6Al-4V (0.13O)	975
Ti-662	Ti-6Al-6V-2Sn	945
IMI 550	Ti-4Al-2Sn-4Mo-0.5Si	975
β Alloys		
Ti-6246	Ti-6Al-2Sn-4Zr-6Mo	940
Ti-17	Ti-5Al-2Sn-2Zr-4Mo-4Cr	890
SP-700	Ti-4.5Al-3V-2Mo-2Fe	900
Beta-CEZ	Ti-5Al-2Sn-2Cr-4Mo-4Zr-1Fe	890
Ti-10-2-3	Ti-10V-2Fe-3Al	800
Beta 21S	Ti-15Mo-2.7Nb-3Al-0.2Si	810
Ti-LCB	Ti-4.5Fe-6.8Mo-1.5Al	810
Ti-15-3	Ti-15V-3Cr-3Al-3Sn	760
Beta C	Ti-3Al-8V-6Cr-4Mo-4Zr	730
B120VCA	Ti-13V-11Cr-3Al	700

Figure 1.3.1: Summary of titanium alloys classified by stabilized phase of Ti [7]

Besides the general properties for all titanium alloys, there are desired properties in either alpha, beta or alpha-beta alloys that make them suitable for any particular application. In most cases it is necessary to differentiate between commercially pure (CP) titanium and alpha titanium alloys due to the desired properties that each possess.

1.3.2. CP Titanium

The lack of alloying elements in CP titanium means it is the lowest strength alloy. Consequently, CP titanium is not usually used in applications where excellent mechanical properties are required. Instead, the corrosion resistance of oxidized CP titanium is its most beneficial quality. Most grades of CP titanium require impurities (usually iron) to not exceed 0.3 at% [6]. In addition to iron, interstitial impurities such as nitrogen, oxygen, and carbon are usually present in CP titanium. As mentioned earlier, titanium has a very high affinity for these interstitial impurities, and as a result, it is very difficult to eliminate them. While the concentrations of these interstitial elements must be kept very low, they can still have a significant effect of the strength of CP titanium due to interstitial strengthening. Yield strength of CP titanium can range from 175MPa to 480MPa depending on the concentration of interstitial elements. This increase in strength, however, comes at the expense of ductility.

1.3.3. Alpha Titanium

As a general definition alpha titanium alloys contain significant quantities of alpha-stabilizing elements, and minute quantities of beta-stabilizing elements. Aluminum and tin are the primary alpha-stabilizing elements, with aluminum being the most common. Due to the higher temperature limits of the alpha-beta transition, alpha alloys are the most suited to higher temperature applications, and are generally insensitive to heat treatment [7]. Weldability of alpha alloys is the best of all titanium alloys due to the higher alpha-beta transus temperature. Microstructure refinement of alpha alloys can be accomplished by inducing recrystallization through cold work and annealing [6]. The most important characteristic of alpha alloys is their excellent creep resistance, even at high temperatures. This can be further improved if very small amounts of retained beta is allowed to form.

1.3.4. Beta Titanium

Beta alloys are metastable alloys that contain significant quantities of beta-stabilizing elements. Beta-stabilizing elements include: vanadium, chromium, and molybdenum. Retainment of the beta phase is accomplished by quenching from temperatures above the alpha-beta transus temperature. The BCC structure of beta alloys makes them excellent for forging. Additionally, beta alloys possess high ductility, hardenability, and toughness. The metastable nature of beta alloys means that any elevated temperature expose can cause partial transformation to the equilibrium alpha phase. This is undesirable during any sort of forming process, but can be advantageous afterwards to form a finely dispersed alpha phase within the retained beta.

1.3.5. Alpha-Beta Titanium

Alpha-beta alloys are more complex systems, and are intended to be a compromise between the somewhat opposing properties of alpha and beta alloys. These alloys require a combination of alpha and beta-stabilizing alloying elements, with exact chemistries depending on what quantity of each phase is desired. The transformation to beta, above the beta-transus temperature, is intended to be a complete transformation, or nearly complete. As a result, the transformation back to alpha upon cooling can be carefully controlled in order to produce a refined microstructure. The nucleation and growth of alpha is controlled by cooling rates, and by subsequent heat treatment if desired. With rapid cooling rates, retained beta can experience a martensitic transformation [7]. This shear transformation, designated α', usually forms an acicular structure that is very similar in appearance to the plate-like structure of the alpha phase. This martensite phase is non-equilibrium, and is supersaturated in beta-stabilizing elements. During heat treatment the α' phase will decompose to form α+β by precipitation of the incoherent β [7]. Figure 1.3.2 summarizes the effect of beta-stabilizing element concentration, showing the relative range for each of the different classes of titanium alloys.

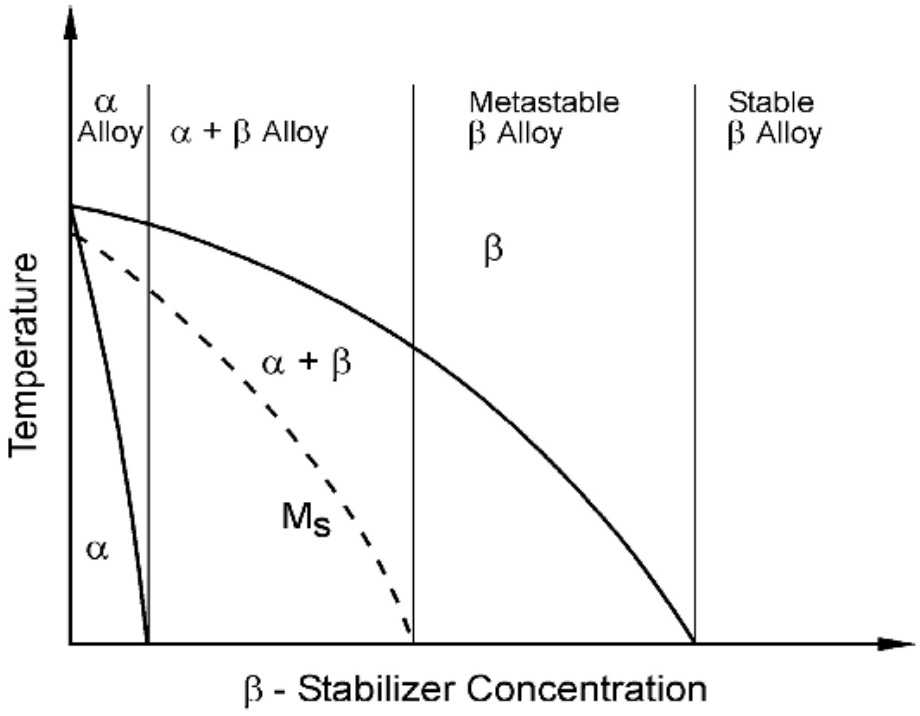

Figure 1.3.2: Pseudo-binary section of a β isomorphous phase diagram [7]

1.4. Differential Scanning Calorimetry

Differential scanning calorimetry (DSC) is a thermal analysis technique that is used to analyze and quantify thermal events. These thermal events can include: phase transitions, melting events, thermal decomposition, and glass transition [8]. Thermal events are measured relative to an inert reference sample during a temperature profile. The two samples are contained in crucibles that sit in a carrier inside a furnace. Due to the high sensitivity, small sample specimens are preferred for this analysis (~50mg). DSC also allows for the use of powders samples, either as loose powders or compacted.

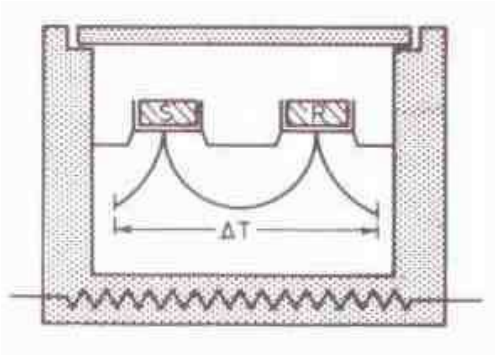

Figure 1.4.1: Schematic of DSC with sample (S) and reference (R) crucibles [9]

The crucibles used for both the sample and reference side of the DSC must be made of the same material so that the thermal conductivity is identical. It is important that the crucible material chosen does not experience any thermal events during the temperature program, and that there is not a significant chemical interaction with the sample or the sample carrier, which holds the two crucibles in the heating zone of the furnace. The crucibles and carrier should be of minimal mass so that they have little effect on the recorded measurements [8].

Measurements for DSC are taken from thermocouples bonded to the sample carrier. This induces some thermal resistance from the carrier, but eliminates any problem caused by thermocouple interaction with the sample. Temperature and sensitivity calibration runs are necessary with both crucibles empty prior to adding a sample.

Typically, DSC measures heat flow in and out of the sample throughout the temperature program. The measurement of heat flow is calculated from the instantaneous difference in temperature between the sample and the reference. This differs from traditional differential thermal analysis (DTA), where only the difference in temperature is measured. This differential in temperature is measured using Equation 1.4.1.

Equation 1.4.1

$$\Delta T = T_R - T_S$$

Thermal events that are measured by the DSC are either endothermic, where the measured temperature of the sample lags behind the measured temperature of the reference (ΔT is positive), or exothermic, where the measured temperature of the sample is higher than the reference (ΔT is negative).

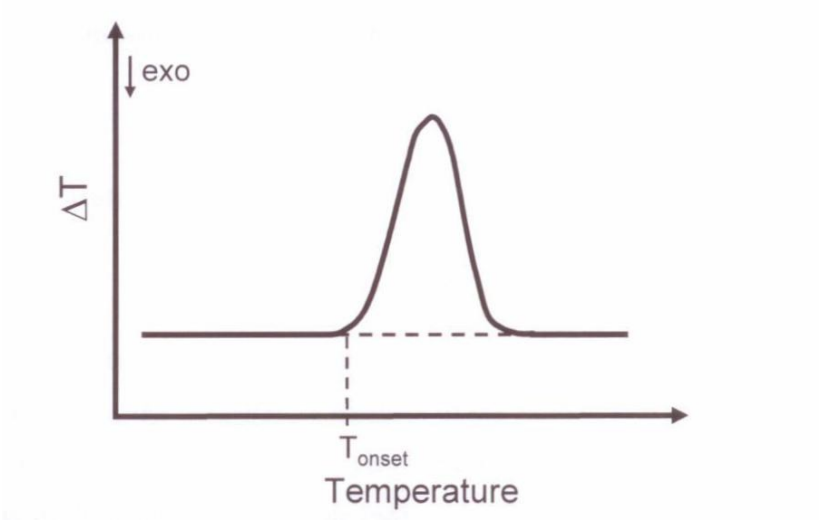

Figure 1.4.2: DTA curve showing endothermic peak [10]

Figure 1.4.2 shows a characteristic endothermic peak, typical of a melting event. Determination of heat flow (*dq/ds*) for DSC can be determined by understanding the relative heat flow on both the sample and reference side of the carrier. Equation 1.4.2 gives the heat flow for the sample crucible:

Equation 1.4.2

$$\frac{dq_s}{dt} = \frac{1}{R}(T_H - T_{SM})$$

where:

dq_s/dt= heat flow into the sample crucible

R= thermal resistance

T_H= temperature of the heat source

T_{SM}= temperature of sample

This equation can also be used for the reference side:

Equation 1.4.3

$$\frac{dq_s}{dt} = \frac{1}{R}(T_H - T_{RM})$$

where:

T_{RM}= temperature of reference

Heat flow to the sample side will heat the sample and crucible in relation to the specific heat capacity of both the sample and the sample crucible, C_s and C_{sm} respectively. This is expressed in Equation 1.4.4.

Equation 1.4.4

$$\frac{dq_s}{dt} = C_{SM}\frac{dT_{SM}}{dt} + C_S\frac{dT_S}{dt}$$

where:

T_S = sample temperature

This equation can also be used for the reference side:

Equation 1.4.5

$$\frac{dq_s}{dt} = C_{SM}\frac{dT_{RM}}{dt} + C_S\frac{dT_R}{dt}$$

where:

T_R = reference temperature

Subtracting Equation 1.4.4 from Equation 1.4.3 will give the differential temperature, ΔT, similar to Equation 1.4.1, except that it is now in terms of differential heat flow and thermal resistance. This is shown in Equation 1.4.6.

Equation 1.4.6

$$\Delta T = T_{RM} - T_{SM} = R\left(\frac{dq_S}{dt} - \frac{dq_R}{dt}\right)$$

If the carrier holding the crucibles is the same structure, and both sample and reference crucibles are made of the same material and have the same conductivity, then the assumption that $C_{SM} = C_{RM}$ is valid. In addition, the heating rate for both sides will also

be the same, such that $dT_R/dt = dT_S/dt$. By substituting Equation 1.4.4 and Equation 1.4.5 into Equation 1.4.6, we can express ΔT as a function of heat capacity of the sample and reference. This is shown in Equation 1.4.7.

Equation 1.4.7

$$\Delta T = T_{RM} - T_{SM} = R\frac{dT}{dt}(C_S - C_R)$$

The temperature differential is now expressed as a function of thermal resistance, heating rate and the specific heat of both the sample and reference crucibles. By running a correction, where both crucibles are empty, the effect of C_R is removed and changes C_S are due to the actual sample [10]. The thermal resistance, R, is value based on several thermal resistances within the machine, and in DTA, includes the thermal resistance of the sample because the thermocouples are in contact with the sample. Due to the placement of the thermocouples on the carrier thermal resistance in DSC is independent of the sample. In order to determine R, and its dependence on temperature, calibration runs are performed using pure metallic standards. These standards are chosen based on their melting points, falling within the desired temperature range. Once thermal resistance is determined the DSC can measure heat flow (dq_S/dt) using Equation 1.4.6.

In addition to heat flow measurements, DSC can also provide information about the enthalpy of different thermal events. As the DSC trace deviates from the baseline, forming peaks (Figure 1.4.2), the enthalpy of this transformation can be calculated, whether it is endothermic or exothermic. This is accomplished by measuring the area underneath the curve, with an approximation for the continuation of the baseline (the dotted line in Figure 1.4.2). This integrated area is proportional to the enthalpy of that particular thermal event [10]:

Equation 1.4.8

$$\Delta H = A\left(\frac{K}{m}\right)$$

where:

ΔH = enthalpy change

A = area under curve

K = enthalpy calibration constant

m = mass of sample

The proportionality of enthalpy to the area under the curve from Equation 1.4.8 is calculated with the known mass of the sample and the enthalpy calibration constant. This constant is also determined from the prior calibration runs; during melting and freezing, the enthalpy of these changes is compared to reference data. The approximation for the continuation of the baseline is taken from the correction file, which is constantly compared to the sample run to determine any deviations.

1.4.1. DSC for Blended Elemental (BE) and Master Alloy (MA) Sintering

The application of DSC to study sintering mechanisms is a relatively new area of study for most metallic systems [11]. In the particular case of BE or MA sintering, the BE and MA powder additions, alloy with the parent or base metal powder during heating. This "in-situ" alloying has the potential to introduce new thermal events or phase transformations (e.g. liquid phase formation) in the powder mixture. It can also alter the phase transformation behaviour inherent in the base metal powder. These evolving phase transformations can be identified and quantitatively measured by DSC. Both the

temperatures of the and enthalpy of a the specific transformation can then be determined and used to analyze the nature of in-situ alloying during BE and MA sintering.

1.5. BE and MA Sintering of Titanium alloys

Titanium PM has been identified as an effective method for reducing the cost of producing titanium alloys [12]. Titanium produced by PM is classified into two groups based on the type of processing: blended elemental (BE), or master alloy (MA), and prealloyed (PA). BE alloys are comprised of a mixture of elemental powders with the alloying of these elements occurring during sintering. MA mixtures are similar to BE mixtures except that they alloy addition is added as a pre-alloyed powder. For example, the composition of Ti6Al4V could achieved through the blending of elemental Ti, Al and V powderes (i.e. BE) or through the blending of elemental Ti powder with a pre-alloyed MA powder of 60% Al and 40 % V. PA powders have the desired quantity of alloying elements contained in the individual particles. In the case of BE and MA mixtures the alloying process occurs during sintering. In the cae of PA the powder is alloyed during the powder production stage. PA powders are reported to be advantageous due to a increased homogeneity of the alloying elements. However, PA alloyed powders are significantly more expensive to produce than the elemental powders which make up the majority of the powder content in a BE or MA mixture [13]. As such, a considerable effort has been put into developing titanium alloys following the BE or MA approach. This avenue is seen as the most promising for producing lost-cost titanium alloys for high volume markets such as the automotive industry.

For industrial applications it is necessary for PM titanium to match the properties of IM titanium, outlined in standards such as ASTM B348. In several areas BE or MA titanium alloys can match IM alloys, such as Ti-6Al-4V, by far the most common IM alloy [14]. Historically, the fatigue strength of PM Ti6Al4V has been inferior to that of IM Ti6Al4V. This inferior fatigue strength was likely due to residual contaminants, and open porosity.

Both of these have been found to be detrimental to fatigue strength [15]. But with improvements to powder production, which have resulted in lower contaminant levels, this effect has been reversed [16].

Of the different steps in the titanium PM process, sintering is both the most complex and the least understood. As such, a comprehensive study to understand the sintering mechanisms of BE titanium is required. Significant gains in contaminant levels and porosity reduction can be achieved by properly investigating the sintering process along with other gains in yield strength and ductility. There are several variables that can influence the sintering process including: alloying elements, powder processing route, and sintering thermal program.

1.5.1. Alloying Elements

In addition to alloying elements controlling phase structure in PM alloys, they can also be added to alter the sinterability. By improving the sinterability of titanium it is possible to achieve higher sintered density. This is accomplished by adding alloying elements which increase diffusion rates, either in solid state or liquid state. Alloying elements that are added to improve the sinterability of titanium include: nickel, iron, and niobium. Nickel and iron in particular are commonly used to increase the rate of densification during sintering [17,18]. These elements have significantly higher diffusion rates in titanium than that of titanium self-diffusion, some as high as 100x faster [19]. It is expected that these elements will homogenize within the matrix of titanium very rapidly. This increases the rate at which sinter bonds are created, and increases the rate of neck growth.

Table 1.5.1: Iron content of specimens quenched from various temperatures in Ti-5Fe [19]

Quenched Temperature °C	Iron content of different positions, wt%				
	1	2	3	4	5
950	83.3	11.8	X	X	X
1020	56.4	28.6	14.4	X	X
1080	4.5	5.3	X	X	X
1120	4.9	4.9	5.1	5.0	4.9
1250	5.0	5.1	5.2	4.9	4.9

Table 1.5.1 indicates the effective diffusion rates and the extent of homogenization of iron in titanium. A deleterious effect can occur when the relative inter-diffusion rates between two elements differs by a significant amount. This disproportionate rate of diffusion between two constituents can impede densification [18,20–24]. This is due to the Kirkendall effect which can cause swelling as a result of highly disproportionate diffusion rates between a couple. One element will rapidly diffuse into the other, but due to the slower diffusion in the opposite direction, a void space will be created.

Additional increases in densification can be achieved through liquid-phase and transient liquid-phase sintering. The existence of a liquid phase greatly increases diffusion rates

between powder particles [1]. However, in some instances the existence of a liquid phase, especially a persistent liquid phase, can limit the sinterability of an alloy. Aluminum, nickel and silicon have been identified as elements that can form a eutectic liquid phase within the normal sintering temperature profile of titanium alloys that contain these elements [17,18,25]. In these cases, the liquid phase formed during sintering leads to "swelling", caused by a low solubility of solid in the liquid phase, and high solubility of liquid in the solid phase. This scenario causes little densification when the liquid phase forms, as the liquid rapidly diffuses into the surrounding matrix. The area occupied by the liquid phase creates large pores that are very difficult to remove. Because aluminum is used in nearly all structural titanium alloys, its tendency to form a liquid phase and swelling during sintering is of great concern [26]. Analysis completed by dilatometry has shown that in alloys contain 5wt% aluminum there is a significant expansion at the melting temperature of aluminum [25]. The magnitude of this expansion was found to increase with increasing weight content of aluminum. The porosity created by aluminum is also partly due to the highly exothermic reaction that occurs when the liquid aluminum reacts with titanium to produce various intermetallics.

Tin has been identified as an alloying element that can improve sinterability, both directly and indirectly . The addition of tin helps to improve compaction, increasing the green density of titanium compacts. Increased green density improves the sinterability of alloys by bringing particles in closer contact with each other, allowing diffusion to occur sooner. Tin may also cause transient liquid phase sintering in titanium, with a liquid phase forming above 231°C [27]. This liquid phase is then absorbed into solid solution at higher temperatures.

1.5.2. Powder Processing Route

The processing route for titanium powders has many effects on the final product such as: sintering kinetics, porosity, and mechanical properties. Typically, titanium PM is

produced using hydride-dehydride powders. The powders start with the sponge produced by the reduction with magnesium discussed earlier. In this form the titanium particles are far too large to be useful for PM. In order to facilitate size reduction, the powders are heated in the presence of hydrogen to form TiH_2. In this state the sponge is much more brittle and can easily be milled down to the desired size. Following this, the powder is then dehydrided under vacuum.

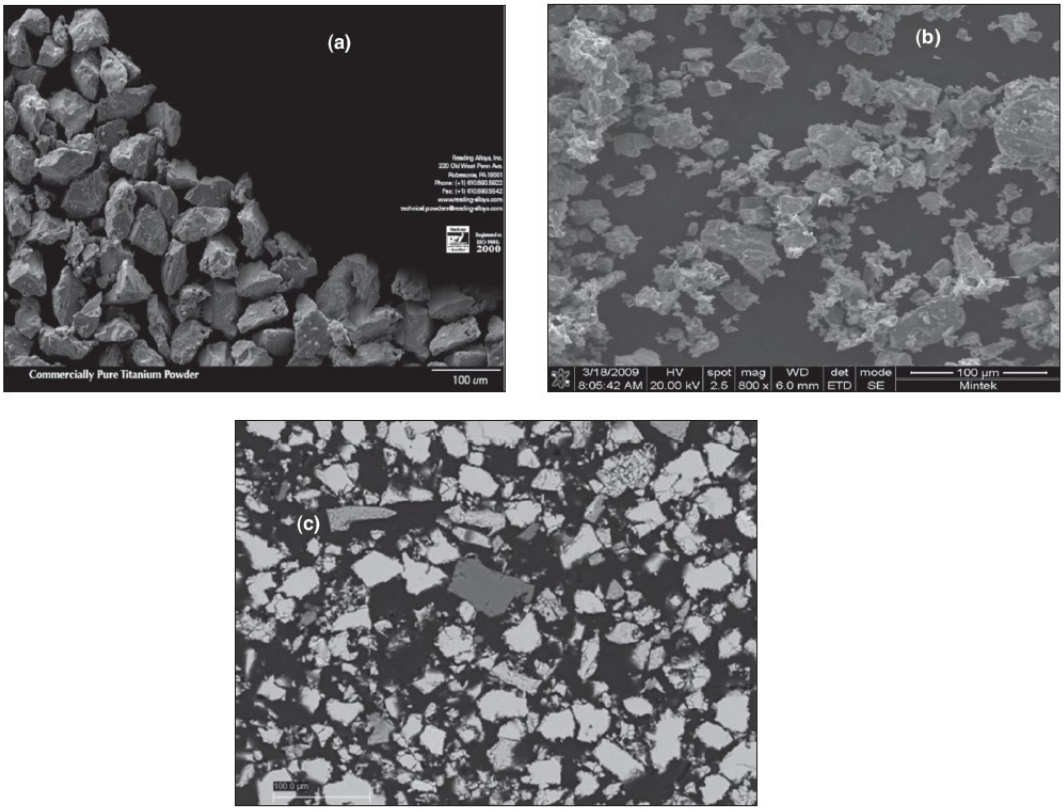

Figure 1.5.1: Titanium HDH powder a) commercial b) planetary milled c) roller milled [28]

Figure 1.5.1 shows three examples of titanium HDH powder. From these micrographs it is apparent that HDH powder has an angular morphology. This is a result of cleavage fracture due to milling. HDH powders are relatively inexpensive to produce, with

smaller particle size increasing the cost (<100 μm). Contaminants, such as chlorine, hydrogen and oxygen, are the most significant limitation of HDH powders. The content of these contaminants increases as the powder is milled to a finer size, which must then be reduced. As a result, it becomes cost prohibitive to produce HDH powder below 45μm.

There are several novel powder processes that have been proposed in the last 10 years [13]. Of these, the Armstrong process has matured the furthest towards large-scale commercial production [13]. The Armstrong process is essentially a continuous process based on the Hunter/Kroll process discussed earlier. Gaseous $TiCl_4$ is injected into a liquid stream of sodium. The sodium reduces the $TiCl_4$ to titanium and sodium chloride. Filtration and distillation are used to remove the sodium, leaving the titanium powder. Prealloyed powders can be produced with the Armstrong process by adding the alloying elements in chloride form to the sodium stream with the $TiCl_4$.

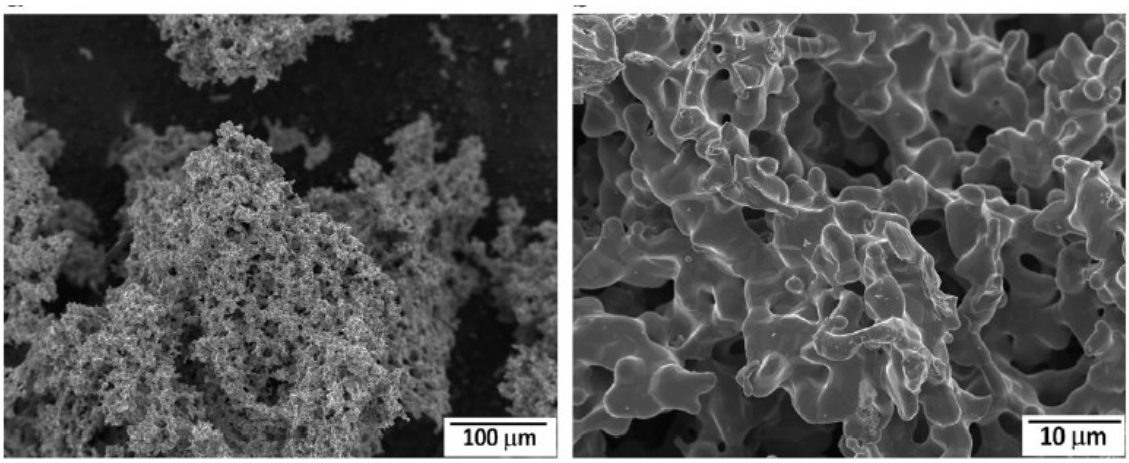

Figure 1.5.2: As-received CP titanium Armstrong powder [14]

Armstrong powder displays a coral-like dendritic morphology. These particles are quite large, up to 1mm, but are composed of smaller dendrites, less than 25μm in size. This

coral-like structure is very advantageous for compaction. Higher green density and green strength are achieved with Armstrong powders over HDH powder. Green strength in particular can see marked increases with Armstrong powders due to interlocking of the powder dendrites during compaction [16].

Atomization processes are a group of powder processes that can be divided into three main groups: plasma rotating electrode process (PREP), plasma atomization (PA), and gas atomization (GA). All three of these processes have been adapted to produce titanium powders. While there are distinct differences between them, all three of these processes produce highly spherical powders with very low amounts of contaminants [29]. The spherical morphology is a result of the rapid cooling rates that the powder experiences during the process, up to 1000°C/s for plasma atomization. The PREP process involves the melting of a high purity stock bar under inert atmosphere as it rotates at very high speed. The melting is accomplished by a plasma arc from a tungsten cathode to the bar which is the anode. As the bar melts, the droplets experience centrifugal acceleration, and form spheres to minimize their surface area. The main advantage to this process is that the powders are produced in a completely inert atmosphere and make no contact with any other material as they melt and solidify. This creates powders of extremely high purity. Due to the fact that it is a batch process and the need for a high-purity wrought bar as the feed material, PREP production is significantly more expensive than other processes. Gas and plasma atomization incorporate melting with rapid cooling steps. During PA, a wire is feed into an argon plasma which melts the wire. As the droplets fall, they experience aerodynamic drag which rapidly cools them, and causes them to form spheres to minimize their surface area. Similarly for the GA process, a liquid stream is blasted with an argon jet stream that disrupts the stream liquid. The droplets formed by the gas rapidly solidify as they fall. PA can achieve purity levels that are very similar to PREP, and as a result, PA is also cost prohibitive for the majority of titanium PM applications. GA powder is more

widely available and is also less cost prohibitive. It is possible to produce powders by GA that have a particle size distribution suitable for metal injection molding (<45μm).

1.5.3. Thermal Program

The thermal program, which is the temperature, heating rate and time that a specimen is exposed to thermal energy, has a significant role during sintering. Temperature is the most significant variable, as it directly affects sintering kinetics. Typically, sintering temperatures are chosen to maximize kinetics, without any undesirable reactions occurring. Studying the equilibrium phase diagram for the desired system will provide useful information about what temperature is appropriate for sintering. This typically ranges from 0.5 to 0.8 of the melting temperature for pure metals.

Isothermal holds are commonly used during sintering when it is necessary increase homogeneity within a specimen before changing the temperature. Isothermal holds are used frequently at the maximum temperature of a thermal program to provide additional time for diffusion to occur before cooling. Isothermal holds can also be used at various points during heating to ensure that certain reactions do not occur. Dissolution of a phase into solid solution may prevent it from reacting unfavorably. By holding at a certain temperature below the reaction temperature can ensure that the phase has been dissolved and can not react.

1.6. Current PM Ti6Al4V Literature

Current research of PM Ti64AlV has diversified significantly, encompassing a wide range of research efforts to improve the basic properties of this alloy. This research usually focuses on improving the sinterability of the Ti6Al4V system, and focuses on three primary areas: powder chemistry/production method, compaction methods, and thermal conditions.

Powder morphology and chemistry are key aspects of Ti6Al4V research. Powder morphology is a result of the production process which itself is a result of the main driving factors for PM Ti6Al4V. These are primarily enhancement of mechanical properties and cost reduction. Many researchers are looking the use of either elemental powders [15,18,30–32] or pre-alloyed powders [34–36] made by a variety of production processes. Many of these investigations used a variety of BE and PA powders in different combinations to achieve the desired chemistry. Additionally, many use master alloy additions, which are powders containing two or more of the desired elements. The use of MA additions is growing area of research for Ti6Al4V. MA additions strike a balance between BE and PA powders. They offer the improved homogeneity in the green state compared with BE compacts, with lower material cost and improved compaction characteristics compare to PA powders. MA alloy powders are added for greater flexibility when dividing the bulk chemistry amongst the powder constituents. The is particularly useful for the addition of Al, which as an elemental addition has been found to causing significant swelling above its melting point in a Ti matrix [22]. The addition of Al in the form of a Ti-Al MA powder can eliminate this problem by preventing the formation of any liquid phase.

Another important area of research is concerned with use of TiH_2 as the base powder instead of the elemental powder [23]. Despite the brittle nature of this type of powder, high green densities are achieved. A network of very fine pores exists after compaction which then heals during sintering. It is this finely dispersed porosity and high crystal lattice defect concentration that accelerates mass transfer through interparticle boundaries. The TiH_2 is reduced under high vacuum during heating, while also reducing other surface oxides. The remaining active Ti surfaces then rapidly sinter, and results in lower concentrations of O. The sintering of TiH_2 powders can result in near fully density (99%), however, this does result in significant shrinkage due to the hydride reduction.

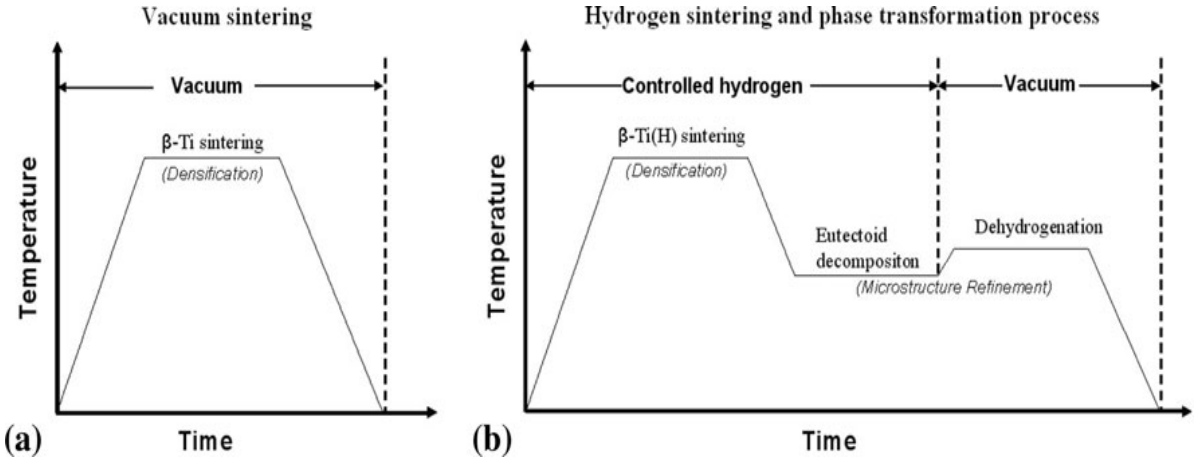

Figure 1.6.1: Sintering profile for vacuum sintering (a) and HSPT (b) [36]

A second process utilizing TiH_2 is shown schematically in Figure 1.6.1. The process is called hydrogen sintering phase and phase transformation (HSPT). This process differs from the sintering of TiH_2 by maintaining a concentration of hydrogen in solution throughout the sintering phase. Hydrogen concentration sustained because it has the following beneficial effects on Ti6Al4V: it acts as a β stabilizer, lowering the transition temperature, allows the formation of δTi(H) phase, and induces a eutectoid phase transformation when cooling from the βTi(H) phase. A hydrogen/argon atmosphere is used to maintain sintering in the βTi(H) phase [37]. By maintaining a certain concentration of hydrogen in solution, the process is able to control the allotropic phase transformation. Sintering in the beta-stabilized phase reduces the required sintering temperature while also increasing the self-diffusion of Ti, Al and V. Upon cooling from the βTi(H) region, a eutectoid decomposition occurs creating αTi(H) and δTi(H), which nucleate in the interior of the βTi(H) grains. The final step is to vacuum anneal the material, removing hydrogen from solution. The resulting microstructure is highly refined, and oxygen and hydrogen levels are lower than ASTM B348 standards [38].

Powder compaction is great area of research for all PM materials. As the first step in the densification of powdered materials, compaction plays a significant role in determining

the final product. Most current research utilizes uniaxial die compaction as the method for consolidation. Many researchers have looked outside the scope of traditional uniaxial compaction in order to improve compaction performance. This includes the use of isostatic compaction [39,40], powder forging [41], and equal channel angular pressing (ECAP) [42–44]. ECAP subjects the powder to severe plastic deformation resulting in green compacts that are approach full density (99%).

Optimization of the sintering atmosphere and thermal profile is an area that shows the most variability between researchers, particularly time and temperature. Because of the difficulties of producing a fully homogenized material, especially with elemental powders, many researchers choose temperatures that will maximize the kinetics and improve diffusion rates. Typically, sintering temperatures range from 1100°C to 1400°C [18,34,35,45,46]. This considerable range in sintering temperature is partially due to variability in the processing route that different groups choose, but also shows the relatively nascent state of PM Ti6Al4V research compared to more established alloys. Lower sintering temperatures are usually favored in order to limit effects of grain growth while ensuring sufficient bonding and homogenization has occurred. Another benefit is the reduced process cost of sintering at lower temperatures. Sintering atmosphere is almost exclusively high-vacuum [36]. The considerations for this choice are primarily concerned with the reactivity of titanium with C,N,O, and H. Sintering under high vacuum ensures that contamination from these elements is minimal, and that any of these contaminants contained in the powders are reduced.

The difficulties with optimizing the homogenization of aluminum and vanadium in Ti6Al4V have noted by several researchers [30,47,48]. The challenges with homogenization both beta and alpha-phase stabilizing elements within titanium is not unique to Ti6Al4V, but a larger body of work exists because it is very common system. Typically this problem has been approached by looking for suitable substitutes for either vanadium, aluminum, or both.

Improving the mechanical properties of Ti6Al4V has focused several key process parameters. There is a general agreement that the goal is to develop a process that results in a near full density material with a homogenized fine-grained microstructure. Because titanium's allotropic phase transformation is a critical factor for all the desired properties, ensuring that a uniform transformation occurs, particularly on cooling, has been an area of focused research [22,45,49–51]. Characterization of this transformation is not unique to PM, but is given greater importance because the additional difficulties of homogenizing alloying elements that are introduced as powder particles. There is an opportunity to provide great insight into the sintering behaviour of Ti6Al4V with the use of an insitu measurement technique. There has been some work utilizing thermal analysis techniques such as DSC [35], DTA [41,44,45,50], and dilatometry [21,25,30,46,49,52]. However, an opportunity exists to further investigate the alloying characteristics of PM Ti6Al4V with thermal analysis techniques.

2.0. RESEARCH OBJECTIVES

The objective of this research is to develop to a methodology for analyzing the sintering behaviour of PM Ti6Al4V with thermal analysis techniques, specifically DSC. With this methodology it is expected that the alloying behaviour of different powder additions can be characterized and compared in order to determine the optimum parameters. The differences between MA and BE blends will be analyzed by DSC with a focus on the β to α phase transformation on cooling. Additional characterization will be performed with microstructural analysis and phase/chemical analysis.

3.0. IN-SITU ALLOYING AND HOMOGENIZATION OF BLENDED ELEMENTAL Ti6Al4V POWDER MIXTURES

3.1. Introduction

A significant challenge to the adoption of Ti in high volume automobiles is its cost, as outlined by Froes et al and others [5,34,53,54]. Powder metallurgy (PM) has been identified as a cost effective route for producing Ti components [5,34,36,53–55]. The α/β alloy Ti6Al4V has the potential for wide application in the automotive industry [53]. There have been numerous studies on the PM processing of Ti6Al4V using both blended element (BE) or master alloy (MA) sintering [22,23,31,34,51,55,56]. The BE (or MA) approach compared to the sintering of pre-alloyed (PA) powders can offer further cost reductions within the PM process. In this method, the alloying elements (e.g. Al and V) are introduced through the mixing of elemental powders or master alloy powders (e.g. 60Al:40V) with pure Ti powder. In-situ alloying then occurs during high temperature sintering with the intent of achieving a uniform distribution of the added Al and V and a homogeneous final microstructure similar to that present in an ingot or wrought material.

The main focus of previous work on BE and MA sintering of Ti PM alloys has been on the final sintered density, microstructure and mechanical properties achieved in the final material. This work has demonstrated that the BE or MA powder metallurgy route can produce components with mechanical properties similar to those achieved in wrought Ti6Al4V, particularly if a hot isostatic pressing (HIP) operation is performed to increase the final density.

It is widely recognized that diffusion of the BE and MA alloy elements throughout the pure Ti powder compact matrix is critical to creating a homogeneous alloy composition [36]. This required homogeneity insures the formation of a uniform microstructure during

cooling through the β to α transformation which is important in developing mechanical properties similar to those achieved through traditional ingot metallurgy (IM). As recently pointed out in [48] chemical homogenization in most Ti alloys which contain both alpha and beta stabilizers, can be a complex process which is sensitive to the relative diffusion rates of the elements involved and the method in which they are introduced (i.e. BE versus MA). Therefore a detailed understanding of chemical homogenization is needed to further advance the BE or MA sintering routes.

Despite the importance of homogenization during BE and MA in-situ alloying, studies which have investigated the phenomena in detail have been limited [57]. A summary of some of these studies has been outline by Robertson and Schaffer [46]. More recent studies of microstructural development and homogeneity have also been completed [34,51,56,57]. These works evaluated homogeneity through observation of the localized microstructural development and x-ray diffraction pattern as a function of sintering temperature. While these results offer valuable insight, a more quantitative method of measuring the extent and rate of homogeneity is needed.

The objective of the current work is to develop a method using differential scanning calorimetry (DSC) capable of providing a more quantitative measurement of the extent of diffusion and homogenization during BE and MA sintering, as well as the rate at which it occurs. The principle behind the approach can be explained through an examination of the pseudo-binary phase diagram for the Ti6Al4V alloy system (see Figure 3.1.1). The β to α phase transformation behaviour of a Ti-Al-V ternary alloy is a strong function of the alloy content. In one extreme, a Ti-6Al binary alloy would exhibit a relatively high β Transus temperature (i.e. >1000° C) and a narrow temperature range over which the complete transformation would take place (i.e. cooling path B). On the other hand an alloy with a high V content (eg. Ti-6Al-12V) would have a low β-transus temperature and a wider temperature range of transformation (i.e. cooling path C). The alloy Ti-6Al-

4V would exhibit a moderate β-transus temperature and phase transformation temperature range.

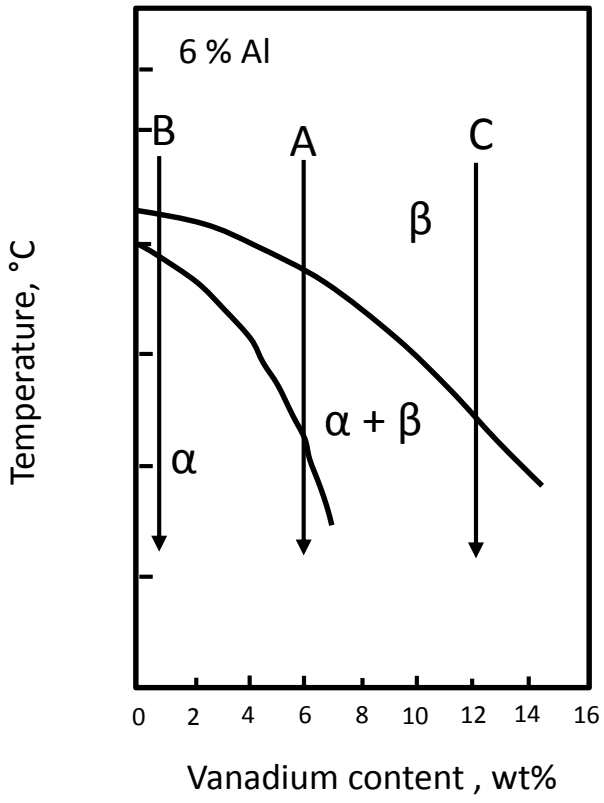

Figure 3.1.1: Schematic of the transformation paths during cooling in a Ti 6 wt% Al mixture with different Vanadium contents

In the case of a BE mixture containing elemental Al and V powder additions, it can be assumed that, if little homogeneity has been achieved, the microstructure would consist of Al and V rich regions. Upon cooling from the Beta region (e.g. 1200 °C), the Al rich regions would follow cooling path B and begin to transform at high temperatures, while V rich regions would follow cooling path C and transform at low temperatures. The net result would be an overall phase transformation that would occur over a very wide temperature range. As homogenization proceeded, the transformation temperature range

would narrow and become closer to that of the Ti-6Al-4V composition (i.e. cooling path A).

As will be demonstrated below, the DSC instrument is capable of measuring the temperature range over which the β to α phase transformation occurs in an alloy as a function of sintering time and temperature. This has the potential of providing direct evidence of the extent of homogenization.

3.2. Experimental Methods

The blended elemental mixtures used for this investigation were prepared using a hydride-dehydride (HDH) CP Ti (ASTM Grade 3) powder obtained from Reading Alloys, a pure Al powder obtained from Ecka and a pure V powder purchased from Alfa Aeasar. For comparison purposes a prealloyed T6Al4V powder obtained from Reading Alloys and an ingot metallurgy (IM) pre-alloyed Ti6Al4V rod was obtained from McMaster Carr. The chemical composition of all received powders and the IM rod was verified by an independent third party laboratory to ensure purity, including the concentration of C, O, N, and H. Additionally, the received size fraction of all powders was verified by laser particle size analysis. The d_{50} from these laser measurements are given in Table 3.2.1.

Table 3.2.1: As-received powder composition (wt%) and characteristics

Powder	Size Fraction (mesh)	d_{50} (μm)	Ti	Al	V	C	O	N	H
CP-Ti	-100/ +325	106	balance	<50 ppm	<50 ppm	0.008	0.161	0.018	0.013
Al	-100/ +325	110	0.008	balance	n/a	0.011	0.310	0.004	0.008
V	-325	25m	<100 ppm	n/a	balance	0.029	0.530	0.120	0.012
PA Ti6Al4V	-100/ +325	98	balance	6.11	4.06	0.024	0.163	0.018	0.008
IM Ti6Al4V	N/A	N/A	Balance	6.01	3.98	0.023	0.153	0.013	0.007

Three BE mixtures with compositions of Ti-6wt% Al, Ti-4 wt% V and Ti-6 wt% Al -4 wt% V using the appropriate powders of Table 3.2.1 were blended with the CP Ti in a Turbula mixer for approximately 1 hour. Consolidation of all the powders was performed using manual uniaxial die compaction with a Carver press to 850MPa. Licowax lubrication was applied to the die walls to reduce wear. Sample weight and dimensions were recorded in both the green and sintered state. The samples were 4.8mm

in diameter and approximately 1mm in thickness. Discs were cut from the purchased Ti6Al4V rod to a nominal thickness of 1 mm.

Thermal analysis of the sintering behaviour of the different PM alloys was performed using a Netzsch 404 F1 DSC. Samples were sintered in a yttria crucible to limit reaction between the crucible and Ti samples. Heating was performed under a high purity flowing argon atmosphere (99.999%) with a titanium "getter" ring placed below the hot zone to ensure minimal contamination of the samples by impurities in the gas stream. The DSC was temperature and sensitivity calibrated using 6 standards (i.e. In, Bi, Sn, Al, Ag and Au). Each thermal profile involved heating to 1200°C at 20°C/min with either an immediate cooling or increasing isothermal hold times from 30 minutes to 2 hours. The samples were then cooled to room temperature at a controlled rate.

Microstructural examination on post DSC treated samples was performed using both a Hitachi S-4700 FEG SEM with an Oxford INCA EDS analysis system for phase composition, and a Zeiss optical microscope. Samples were mounted in a conductive resin and polished to a mirror-like finish using SiC papers, diamond suspension and colloidal silica (Struers). A Bruker D8 Advance XRD with a Cu Kα source was used for phase identification of as pressed and DSC heated powder compact samples.

3.3. Preliminary Results and Experimental Development

Differential Scanning Calorimetry (DSC) has been used by Malinov et al. [50] to study the β to α transformation for IM Ti6Al4V. The work by Malinov et. al. focused on the effects of different cooling rates for the β to α transformation. Their work validated the use of DSC as a technique for measuring the β to α transformation for Ti6Al4V. In particular, it determined the influence of cooling rate on the start (Beta Transus) and finish (alpha Transus) temperatures and therefore transformation peak width.

In order to validate the current DSC procedure, the β to α phase transformation of the IM Ti6Al4V sample described in Table 3.2.1 was determined for 4 separate samples. The transformation peaks for these samples are shown in Figure 3.3.1. Table 3.3.1 illustrates the various measurements performed on these peaks. A cooling rate of 40 °C/minute was used for these experiments. This cooling rate was chosen because it allowed the DSC instrument to establish a constant cooling rate from approximately 1075 to 675 °C which encompassed the temperature of interest with respect to the β to α transformation. This constant cooling rate was important in establishing a stable baseline in the DSC signal before and after the transformation peak. Cooling rates lower than 40 °C/minute produced transformation peaks that were not as visible with respect to the baseline level. A cooling rate of 40 °C/minute was also included in the study of Malinov et al. so direct comparison could be made.

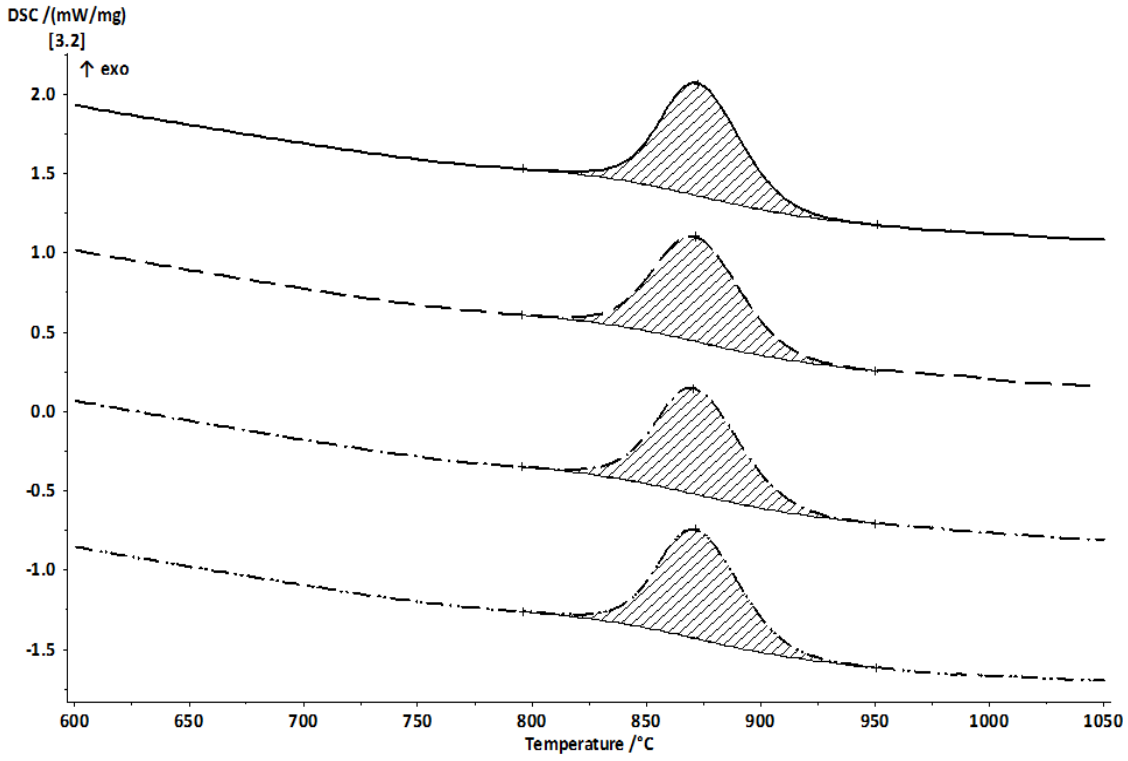

Figure 3.3.1: Illustration of the β to α transformation for four IM Ti6Al4Vsamples cooled at 40°C/min from 1200 °C.

Included in Figure 3.3.1 is an example of the baseline construction used to determine the area under the peak (i.e. the enthalpy of transformation), the temperature at the maximum peak height (i.e. peak temperature) and the peak width. Peak width was determined by the Netzsch software through a construction of a second baseline parallel to the first, but offset a magnitude of 1% of the maximum peak height in the heat flow direction. The lower and upper temperatures at which this 1% offset construction intersects the DSC trace was used to determine the peak width. The beta transus temperature was determined by the point at which the DSC trace and baseline construction coincide as indicated in Figure 3.3.1. The alpha transus was determined by subtracting the peak width calculation from the beta transus temperature.

The DSC traces of Figure 3.3.1 indicate that the β to α phase transformation behaviour in the Ti6Al4V ingot is very reproducible. The first row of Table 3.3.1 presents the averaged values for the enthalpy and temperature measurements determined from the transformation peaks of Figure 3.3.1. The standard deviation of all measurements were less than 1.5%. The enthalpy of transformation, beta transus, peak temperature and peak width measurements made on Ti6Al4V by Malinov et al are also given in Table 3.3.1 for a 40 °C/minute cooling rate. Agreement with the current study is very good considering the different measurement conditions. The Ti6Al4V alloy of Malinov's study contained a higher Al and O content than the alloy studied in Figure 3.3.1 (i.e. 6.59 and 0.19 wt% respectively) which increases the beta transus temperature. Reports on the β transus of low oxygen containing Ti6Al4V are 945 °C [6], which is in better agreement with the current value. Peak width is partially determined by the thermal lag of the DSC system. Helium was used as the process gas in the DSC experiments of Malinov, while Argon was used in the current study. Helium is known to decrease transformation peak widths, thus explaining the small difference in peak width between Malinov and this study. The most significant discrepancy between reference Malinov et al and the current study is the enthalpy of transformation measurements.

Table 3.3.1: Average values for DSC Measurements made for the β to α Phase Transformation in a Ti6Al4V ingot and 100% CP-Ti pressed powder.

Sample	Enthalpy (J/g)	Peak Temperature (°C)	β Transus Temperature (°C)	α Transus Temperature (°C)	Peak Width (°C)
Ti6Al4V IM	51.0	870.5	926.5	768.9	157.6
Ti6Al4V [50]	27	873	970	830	140
100% CP-Ti	75.15	870.1	928.5	828.6	99.9

The Ti6Al4V BE powder mixtures initially contain 90 wt% of CP-Ti powder. For this reason it was considered important to characterise the transformation behaviour of 100% CP-Ti powder compacts as a baseline comparison. Figure 3.3.2 illustrates the cooling curves for four 100% CP-Ti samples while row 3 of Table 3.3.1 presents the average values measurement from the transformation peaks of Figure 3.3.2. The phase transformation behaviour of the CP-Ti is also very reproducible, with standard deviations on temperature measurements of less than 0.5% and variations of 4% on the enthalpy and peak width measurements. The beta and alpha transus temperatures agree well with that reported by Kim and Park for a CP-Ti ingot material for a similar cooling rate (i.e. 925 °C and 850°C respectively) made using resistivity measurements [58].

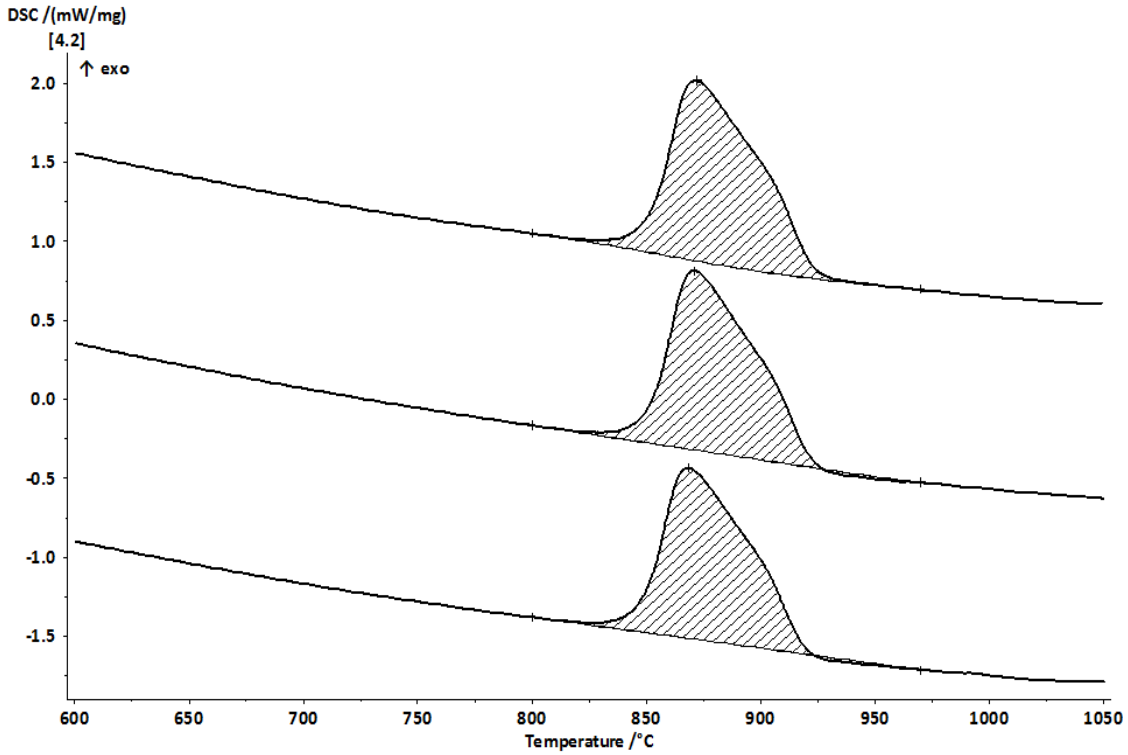

Figure 3.3.2: Repeatability of Cp-Ti cooled from 1200°C at 40°C/min

3.4. Blended Elemental Experimental Results

3.4.1. Initial Heating to 1200 °C

Figure 3.4.1 illustrates the heating traces for the Ti4V, Ti6Al and Ti6Al4V blended elemental mixtures in comparison to the 100% CP-Ti powder compact. The 100% CP-Ti and Ti4V have similar DSC traces with no thermal events evident until the alpha to beta phase transformation, which onsets at approximately 879 °C. This is close to the published theoretical onset temperature of 882 °C for high purity Titanium. The slightly lower temperature measured in this study is due to the small amount of impurities in the powders as reported in Table 3.2.1.

The Ti6Al and Ti6Al4V BE samples exhibit an exothermic reaction which onsets at 565 °C. This exothermic peak is associated with the reaction of Ti and Al to form Ti aluminide intermetallics. A doublet exothermic peak in the Ti6Al4V BE mixture indicates that there may also be reactions between Al and V to form Al-V intermetallic phases. At higher temperatures, the Al containing mixtures also exhibit the alpha to beta phase transformation over a similar temperature range to that observed in the 100% CP-Ti and Ti4V mixtures. One notable measurement made from the DSC traces of Figure 3.4.1 is the enthalpy of transformation of the alpha to beta phase transformation for the different mixtures (i.e. 68.8 J/g, 46.7 J/g and 42.9 J/g for the Ti4Al, Ti6Al and Ti6Al4V respectively). Based on the measured enthalpy of transformation for the 100% CP-Ti, if all of the pure Ti powder transformed in such a way that it was unaffected by the presence of the BE powder additions, the theoretical enthalpies for the mixtures, accounting for the weight fraction of pure Ti powder, would be 64, 62.7 and 60.0 J/g for the Ti4Al, Ti6Al and Ti6Al4V respectively. The measured enthalpy for the Ti4Al sample is within the standard deviation of it's theoretical enthalpy. However, the enthalpy values for the Ti6Al and Ti6Al4V samples are significantly below the theoretical value, indicating that metallurgical interaction between the Ti and Al powder addition begins during heating. More specifically, the lower enthalpy for the Ti6Al and Ti6Al4V mixtures, is an indication that the exothermic reaction at lower temperatures consumes a measureable amount of Ti in the formation of intermetallic compounds prior to the alpha to beta phase transformation.

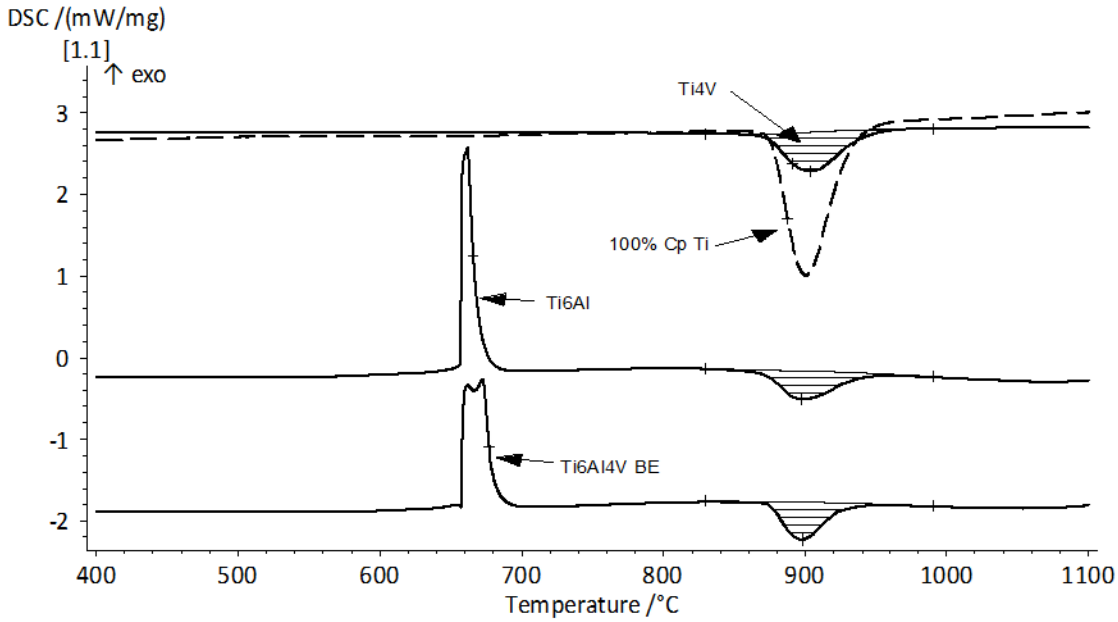

Figure 3.4.1: Comparison of heating traces including α to β transformation for blended elemental mixtures

3.4.2. Cooling Transformations and Microstructural Development

Ti6Al

The DSC traces shown in Figure 3.4.2 includes the cooling traces for Ti6Al following increased sintering time. The cooling trace for a 100% CP-Ti sample is also included. In comparison to the 100% CP-Ti it is evident that the presence of Al shifts the β to α phase transformation to higher temperatures even after zero hold time at 1200 °C. This is consistent with the fact that Al is an alpha stabilizing element. The sample with no hold time at 1200 °C, exhibits a relatively broad phase transformation with a high onset temperature and low end temperature. With increasing hold time, peak width reduces due to a lower onset temperature and higher end temperature. The majority of change in the phase transformation behaviour occurs within the first 30 minutes of sintering.

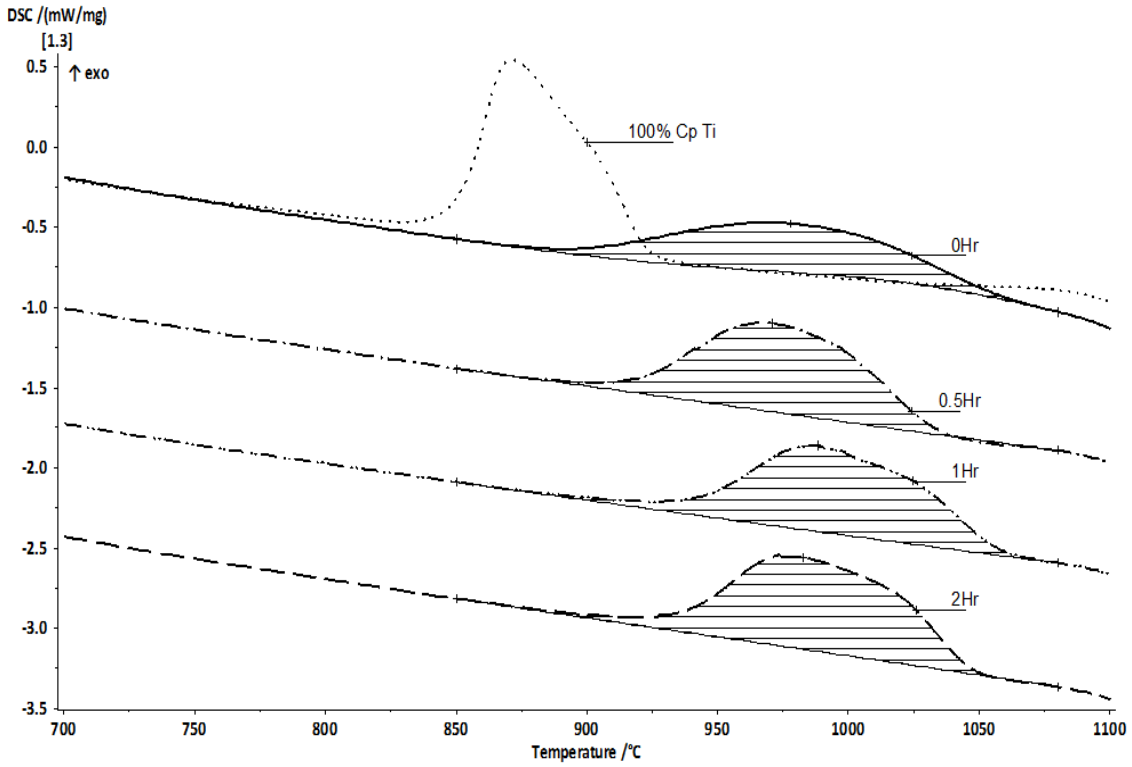

Figure 3.4.2: Comparison of the β to α transformation for Ti6Al resulting from increasing isothermal holds: No Hold, 30min, 1 hour, 2 hours, compared to pure Ti

Optical micrographs of Kroll's reagent etched samples for zero and 2 hour holds at 1200 °C are illustrated in Figure 3.4.3. Both samples exhibit large scale irregularly shaped porosity which was introduced at lower temperatures due to the melting of the Al powder and its exothermic reaction with the Ti powder. Both samples also indicate a similar grain structure with a relatively coarse platelike microstructure which arises from the beta to alpha phase transformation in these alloys during cooling. The scale of the platelike features are more variable in the zero hold sample, which is indicative of a variable Al content. Figure 3.4.4 presents an SEM image and EDS spot analysis in a region of a large pore in the no hold sample. These results confirm a higher Al content near the pore and a lower Al content further away from the pore location for the zero hold sample. Mixtures sintered for 0.5 and 1 hour exhibited microstructures similar to the 2 hour sample.

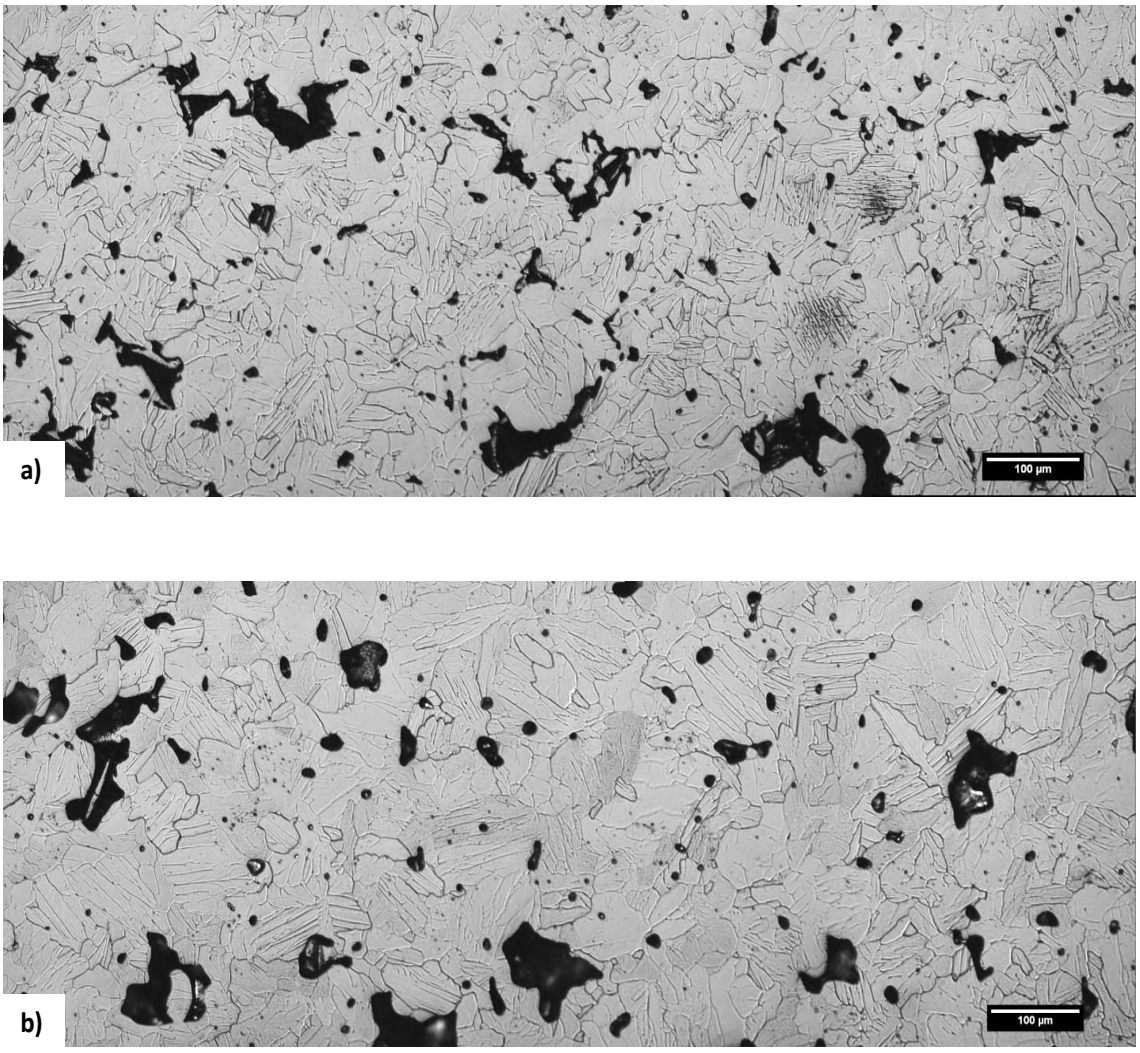

Figure 3.4.3: Optical micrograph of Ti6Al sintered with a) no hold and b) 2 hours

Spectrum	Al	Ti
1	6.94	93.06
2	7.14	92.86
3	7.31	92.69
4	5.88	94.12
5	4.01	95.99
6	3.06	96.94
Mean	5.72	94.28

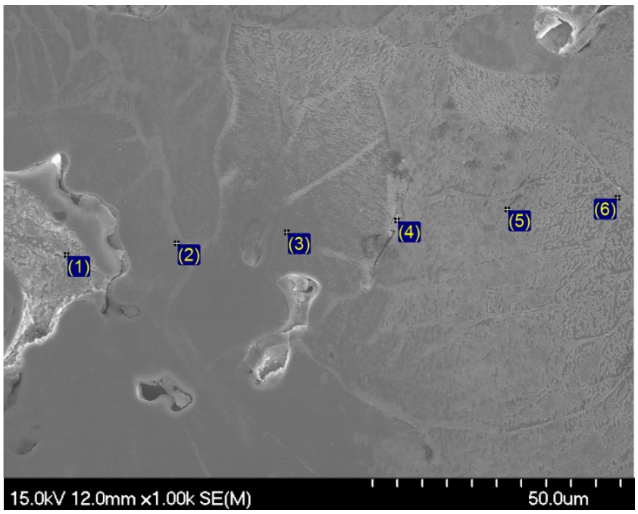

Figure 3.4.4: SEM/EDS chemical analysis at designated points for a Ti6Al sample heated to 1200 °C with no hold.

Figure 3.4.5 presents XRD results for an unheated, green sample and samples after sintering at 1200 °C for various hold times. The presence of the elemental Al powder addition is clearly visible in the green sample as is the α-Ti phase of the 100% CP-Ti powder. The primary change in phase evolution as a result of sintering is the disappearance of the Al phase and, in some cases (i.e. 30 minute hold at 1200 °C) some minor peaks which may be associated with oxide phases. These minor peaks were not characterisitic of any singular oxide phase, and would need further investigation. Alpha-Ti is the predominant phase present in all samples, indicating a complete transformation of the β-Ti phase during cooling. The relative peak intensities fluctuate from sample to sample. This is expected to be due to the preferred orientation developed in the platelike structure during the β to α transformation upon cooling. Note that the α-Ti peak positions shift slightly to higher angles in the sintered samples compare to the green sample. This is due to the solid solution alloying of Al in the Ti crystal lattice.

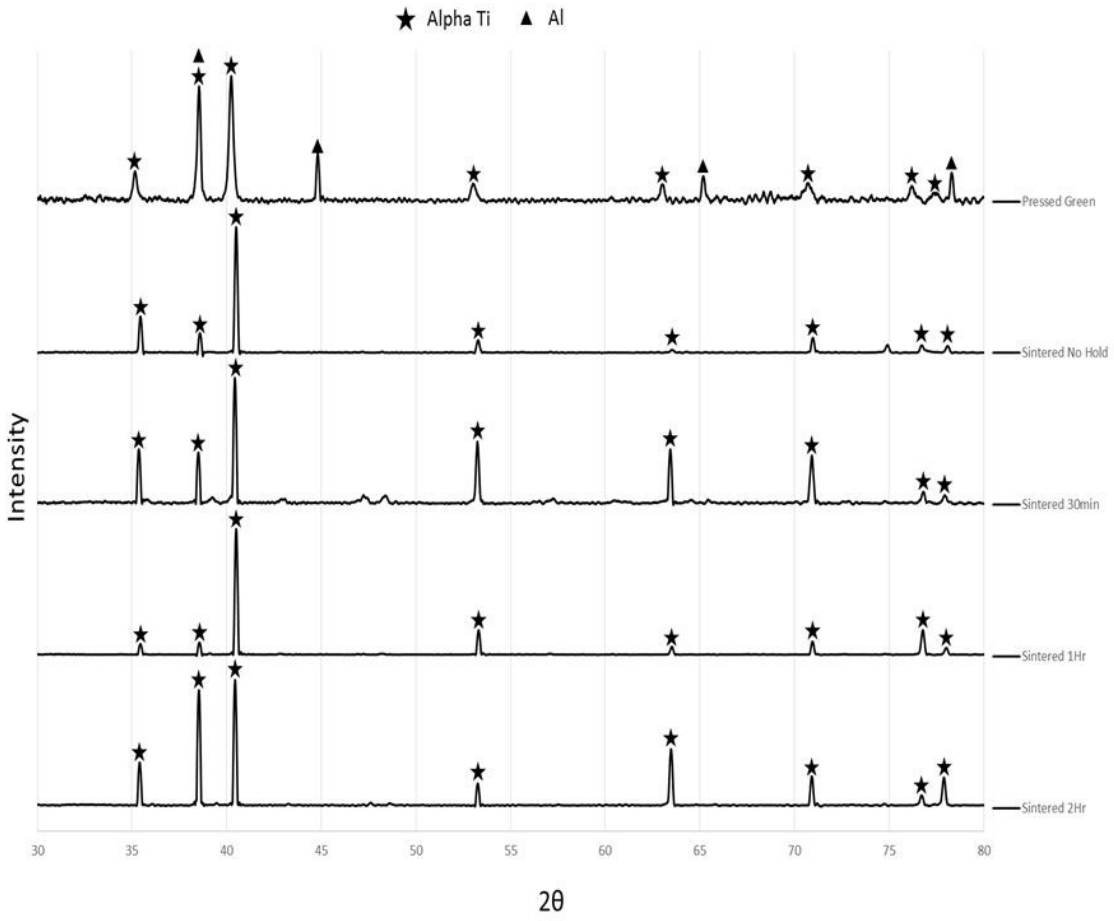

Figure 3.4.5: Measured spectra by XRD for Ti6Al mixture with corresponding phase composition

Ti4V

Figure 3.4.6 includes the cooling DSC traces for Ti4V with increasing hold time and a 100 % CP-Ti sample. Compared with 100% CP-Ti, the presence of V in the binary mixture shifts the β to α phase transformation to lower temperatures even after zero hold time at 1200 °C. This is consistent with the fact that V is a beta stabilizing element. The 0 hold trace for Ti4V shows the broadest peak on cooling with a low peak height. With increased sintering time, this transformation peak shifts to lower temperatures up to 1 hour. After 1 hour and up to 2 hours, the most significant changes occur. Firstly, the

peak shifts back to higher temperatures. And secondly, the start and end temperatures of this peak narrow.

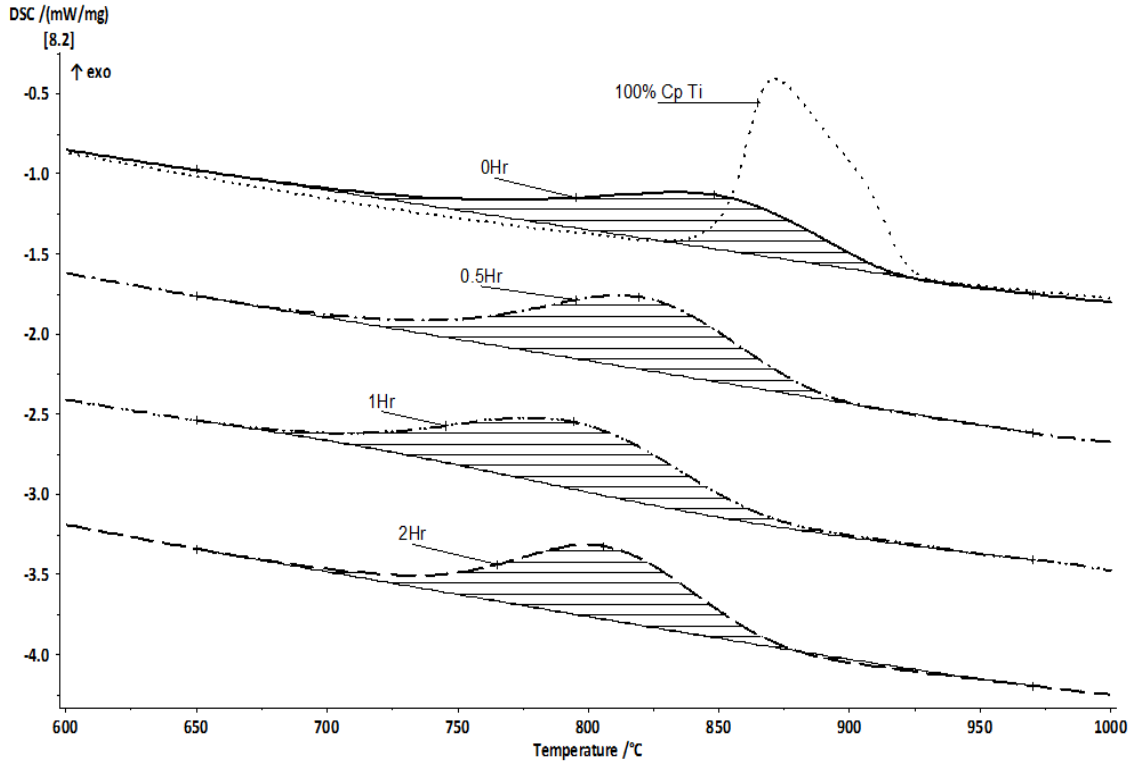

Figure 3.4.6: Comparison of the β to α transformation for Ti4V resulting from increasing isothermal holds: No Hold, 30min, 1 hour, 2 hours, compared to pure Ti

Optical micrographs of the Ti4V BE mixture with a zero and 2 hour hold time at 1200 °C are shown in Figure 3.4.7. Undissolved V particles (light grey) are clearly visible throughout the microstructure for the zero hold sample. The matrix surrounding these particles is fairly uniform and the equiaxed grain structure is similar to that observed in the 100 % CP-Ti samples. Figure 3.4.8 a) presents an SEM image and EDS elemental map for the Ti4Al no hold, 1200 °C sample in the region of an undissolved V particle. The image indicates and extensive interdiffusion and solid solution zone which is penetrating to the core of the original V BE particle.Figure 3.4.8 b) illustrates that the

diffusion of V into the surrounding CP-Ti matrix extends less than 100 µm at this stage. Samples sintered for 0.5, 1 and 2 hours exhibited similar microstructures exemplified by Figure 3.4.7 b). At these sintering times no V particles remained in the structure and a uniform equiaxed microstructure was produced. Figure 3.4.7 illustrates the absence of the large scale irregular pores in the Ti4Al samples compared to the Ti6Al samples.

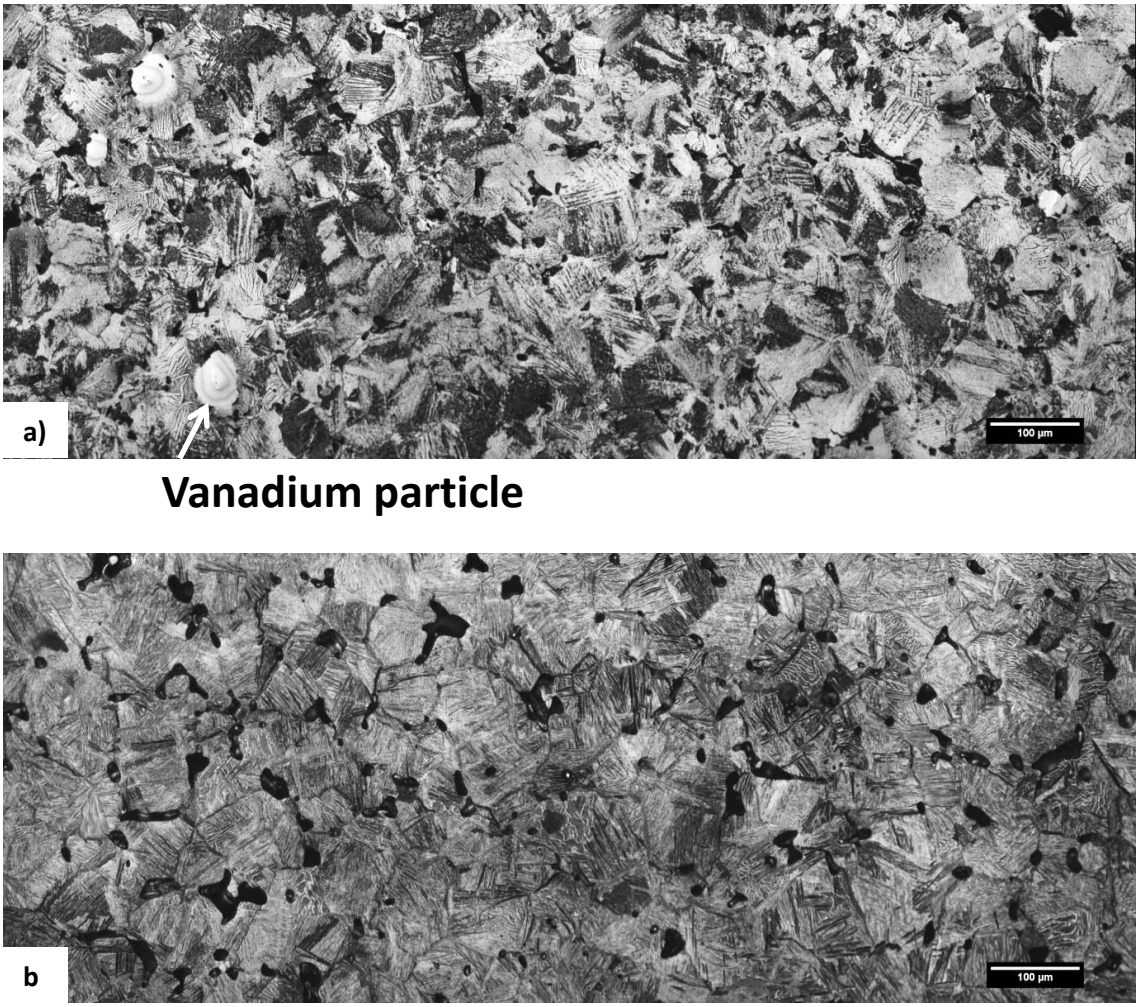

Figure 3.4.7: Optical micrograph of Ti4V sintered at 1200 °C with a) no hold and b) 2 hour hold

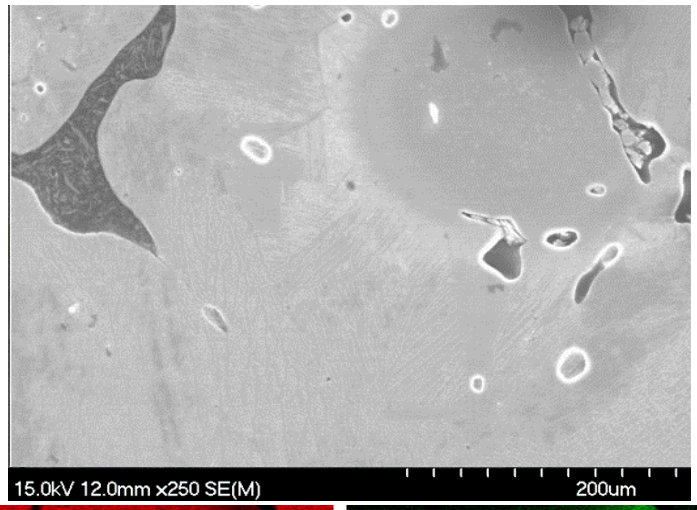

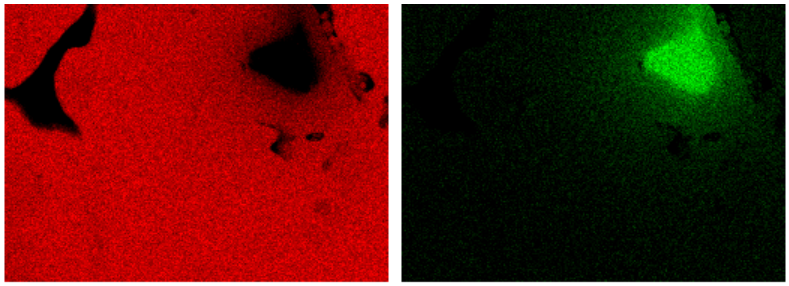

a)

Spectrum	Ti	V	Total
1	1.43	98.57	100.00
2	97.32	2.68	100.00
3	99.04	0.96	100.00
4	99.74	0.26	100.00
5	100.00	0.00	100.00

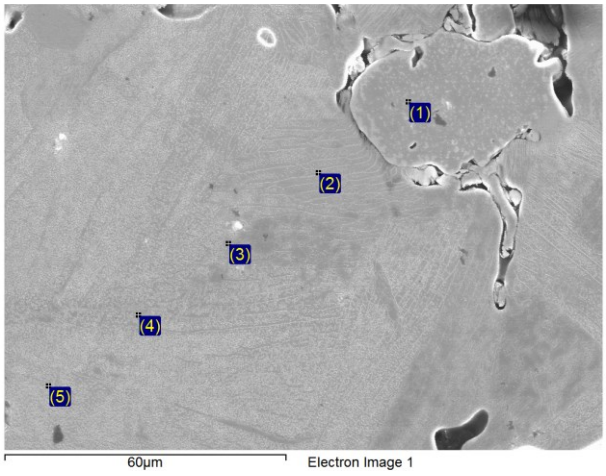

b)

Figure 3.4.8: SEM/EDS analysis of Ti4V sintered at 1200 °C with no hold; a) EDS map and b) compositional profile in the vicinity of a V particle.

Phase composition and evolution of sintered Ti4V measured using XRD was very similar to that determined for Ti6Al (see Figure 3.4.9). The pressed green sample consists of α-Ti and V. In the sintered samples the predominant phase is α-Ti, however there is a small peak approximately at 38° which has been reported by many researchers to correspond to retained beta phase [18,32,59]. This peak is most obvious at intermediate sintering times and nearly disappears at 2 hours. Some degree of retained beta is consistent with the presence of the beta stabilizing V alloy addition. No intermetallic phase formation occurred but a similar peak shift to higher angles occurred due to the solid solution alloying of V in Ti.

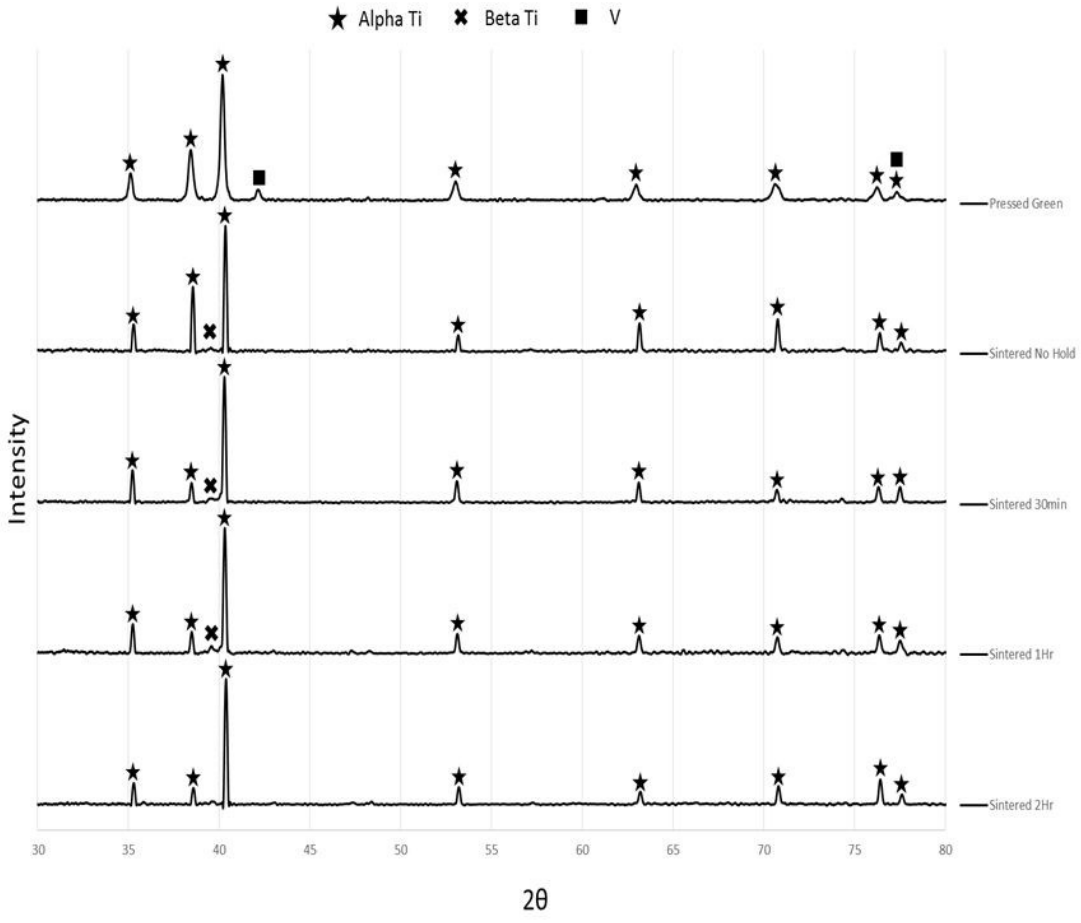

Figure 3.4.9: Measured spectra by XRD for Ti4V mixture with corresponding phase composition

Ti6Al4V

The DSC traces for the BE mixture of Ti6Al4V with increasing hold times compared to the 100 % CP-Ti sample are shown in Figure 3.4.10. The observed peaks for the β to α transformation for all the BE samples have a significantly reduced intensity and a wider peak width compared to the CP-Ti sample. The onset temperature of the cooling transformation is lower than the Ti6Al mixture while the end temperature is higher than the Ti4Al mixture. This makes sense since the Ti6Al4V mixture experiences the influence of both V and Al. In general the change in the cooling transformation peak in the Ti6Al4V mixture is less influenced by the sintering time and the temperature range over which it occurs remains relatively broad in comparison to the binary mixtures.

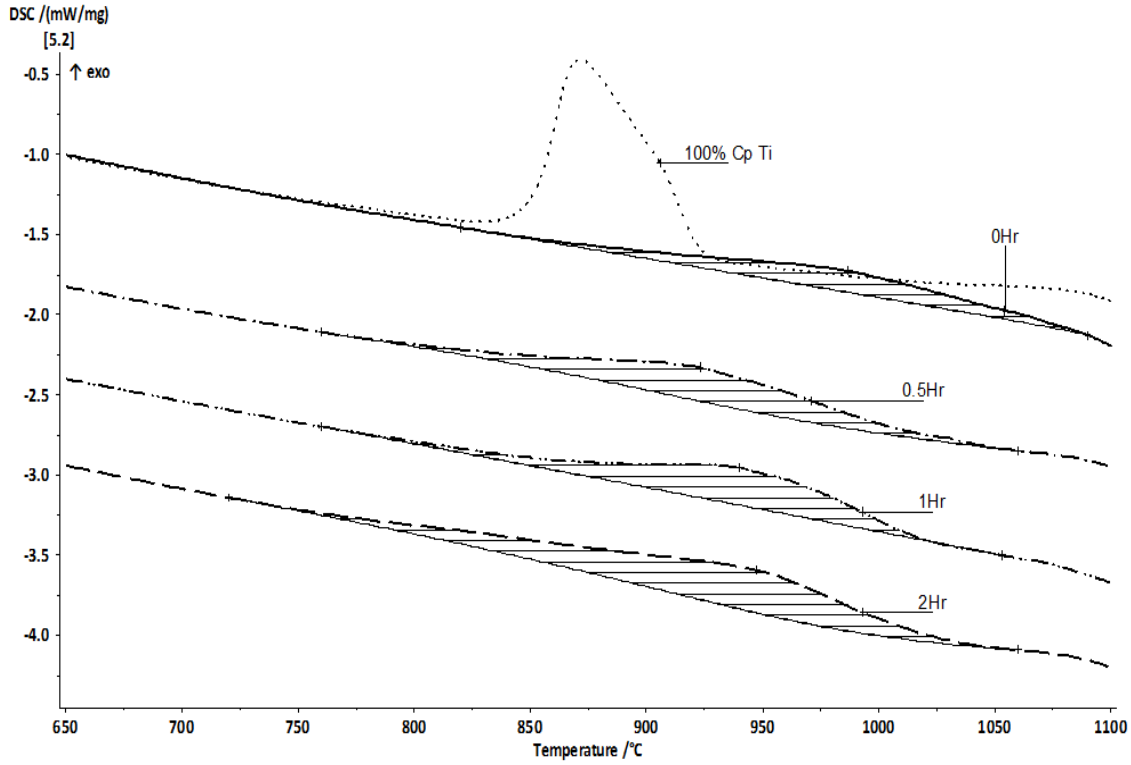

Figure 3.4.10: Comparison of the β to α for Ti6Al4V BE transformation resulting from increasing isothermal holds: No Hold, 30min, 1 hour, 2 hours, compared to pure Ti

Optical micrographs of the Ti6Al4V BE mixture with zero, 0.5, 1 and 2 hour hold times at 1200 °C are shown in Figure 3.4.11. Undissolved V particles (light grey) are clearly visible throughout the microstructure of the zero hold sample, similar to that seen in the Ti4Al binary mixture. However, unlike the Ti4Al, the surrounding matrix exhibits a more noticeable acicular microstructure. In addition, the scale of the acicular microstructure varies from very fine near the V particles (i.e. darkly etched regions) to coarsely spaced platelets.

Figure 3.4.12 presents an SEM image and EDS elemental map for the Ti6Al4V no hold sample in the region of a partially dissolved V particle. The very core of the particle has retained a pure V content. However, extensive diffusion of both Ti and Al through the outer surface of the original V particle has occurred. Surrounding the original V particle surface is a fine, acicular microstructure noted in the optical micrograph.

Like the Ti4V mixture, the dissolution of V particles was completed after sintering for 30 minutes. However regions of darkly etched, fine acicular structure and lightly etched platelike structures remain. These regions are expected to have different alloy content, indicating that inhomogeneity still exists at 30 minutes. Some non-uniformity in the acicular spacing exists after 1 hour, but this is not as extensive as that observed at 0.5 hours. After 2 hours the microstructure is very uniform indicating a homogeneous distribution of the alloy elements has been achieved.

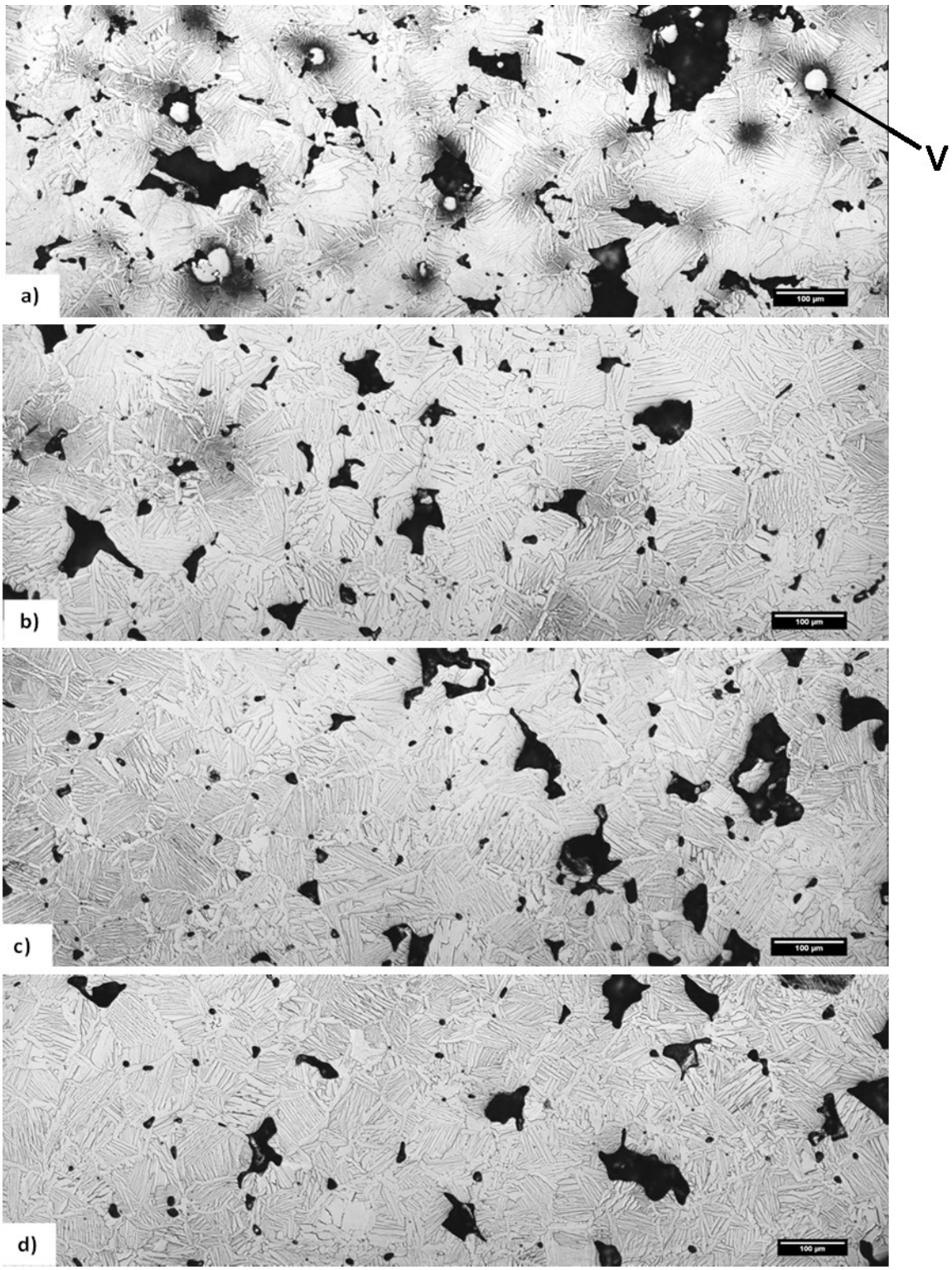

Figure 3.4.11: Optical micrograph of Ti6Al4V BE sintered at 1200 °C; a) with no hold, b) 0.5, c) 1, d) 2 hours

Element	Weight%	Atomic%
Al K	4.54	7.83
Ti K	83.06	80.81
V K	12.41	11.35

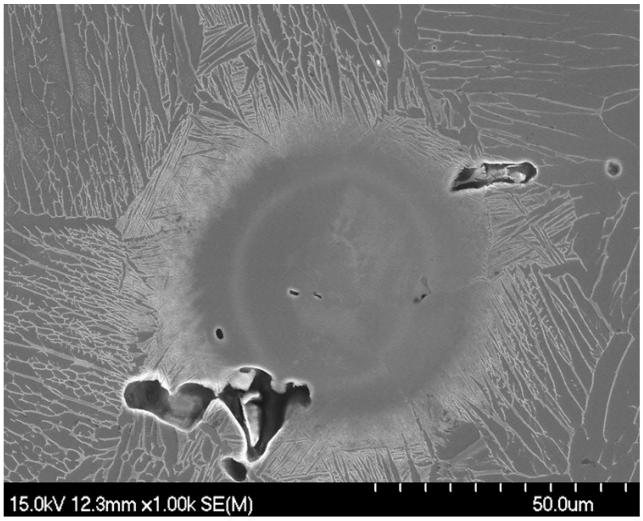

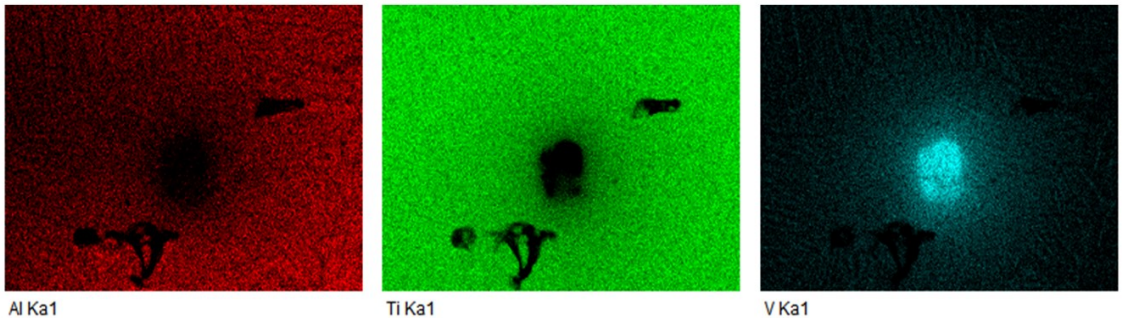

Figure 3.4.12: SEM/EDS analysis of Ti6Al4V BE sintered at 1200 °C with no hold

It should be noted that the irregularly shaped, large scale porosity created by the presence of the elemental Al particles is present in the Ti6Al4V BE mixture and is similar to that observed in the binary Ti6Al sample.

The measured phase composition for BE Ti6Al4V in both the green and sintered states is shown in Figure 3.4.13. In the green state, the majority of the measured peaks corresponded to α-Ti with evidence of the added elemental V and Al particles. A significant feature of the XRD pattern for the sintered materials is the development of a pronounced retained beta peak. This peak appears in the no hold sample, grows in intensity at 30 minutes and 1 hours and then greatly reduces after 2 hours. Extensive

retained beta would be expected if regions of the microstructure contained elevated V content. Such a region is clearly noted in the SEM-EDS results of Figure 3.4.12. Therefore the XRD results indicate significant levels of inhomogeneity in the Ti6Al4V up to at least 1 hour of sintering time. It is worth noting that the retained beta XRD peak in the Ti4V sample was present over a shorter sintering time and at a lower magnitude compared the Ti6Al4V BE samples. This suggests that the combination of Al and V added through elemental particle additions has a detrimental effect on V dissolution and homogenization.

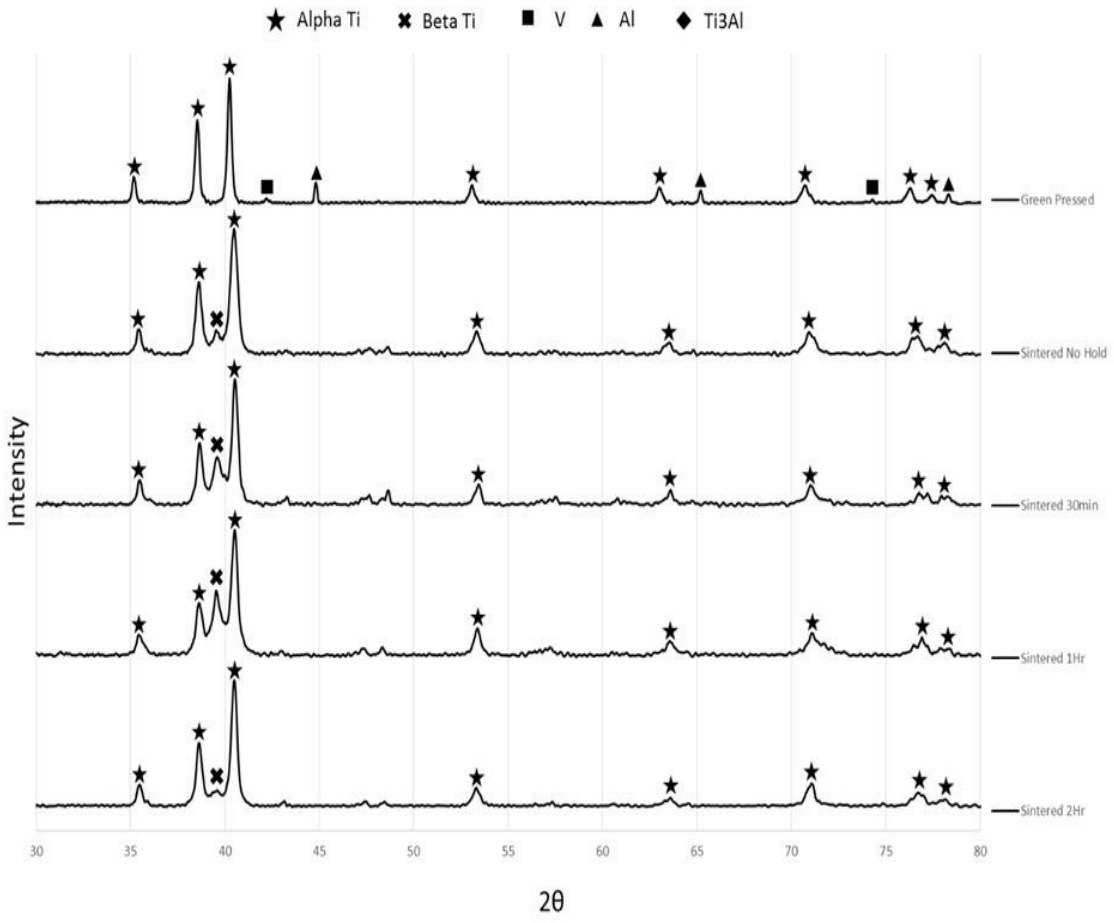

Figure 3.4.13: Measured spectra by XRD for Ti6Al4V mixture with corresponding phase composition

Prealloyed (PA) Ti6Al4V powder

The results shown in Figure 3.4.14 are a comparison of the DSC cooling traces for increasing hold time at 1200°C for the PA Ti6Al4V powder. Unlike the blended elemental binary and ternary mixtures described above, the β to α phase transformation peak is relatively unaffected by the sintering time at 1200 °C. There does appear to be an increase in the enthalpy of the transformation with increasing hold time, but unlike the BE mixtures, there is no appreciable change in the shape of the measured peaks.

The microstructure of the PA Ti6Al4V after heating to 1200 °C but with no hold and after 2 hours is shown in Figure 3.4.15. There are two main distinctions between the PA powder and the BE mixtures. Firstly, the formation of the Widmanstätten microstructure typical in Ti6Al4V is uniform throughout the sample. The subsequent samples sintered for 0.5, 1 and 2 hours exhibited identical microstructures. The second distinction is the substantially higher porosity in these samples. The porosity is well distributed and appears to be open and continuously connected throughout the structure.

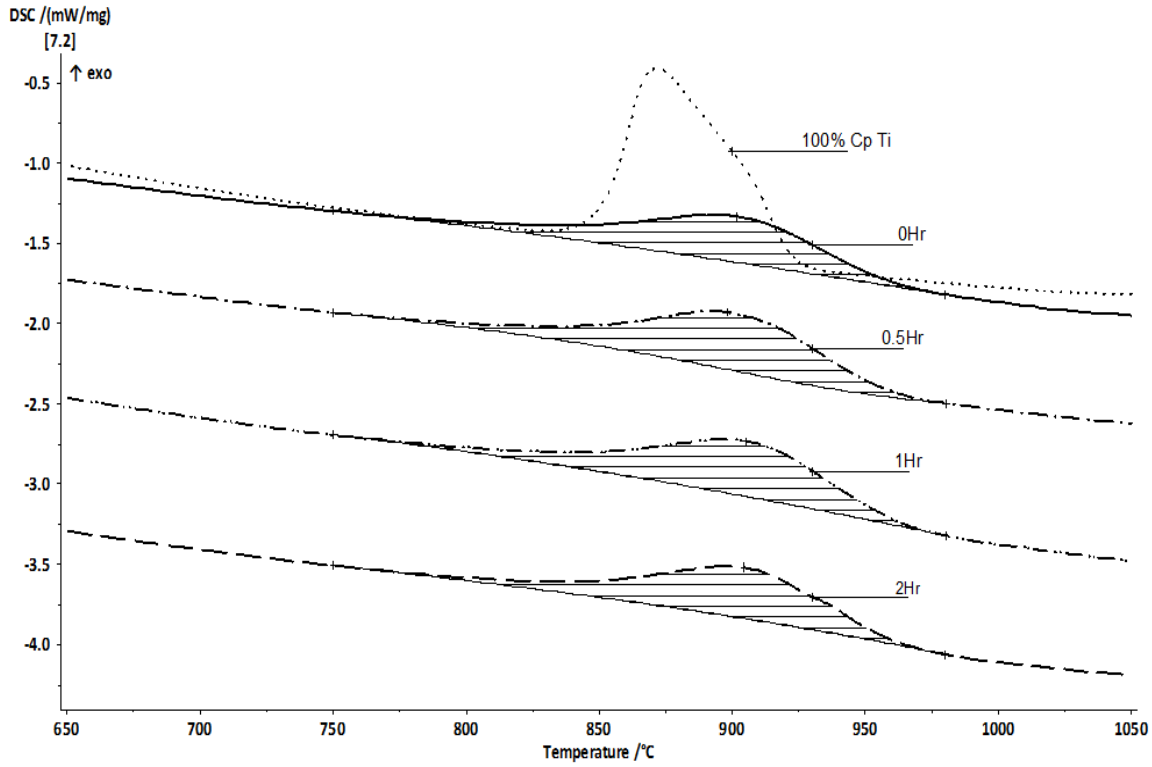

Figure 3.4.14: Comparison of the β to α with PA transformation resulting from increasing isothermal holds: No Hold, 30min, 1 hour, 2 hours, compared to pure Ti

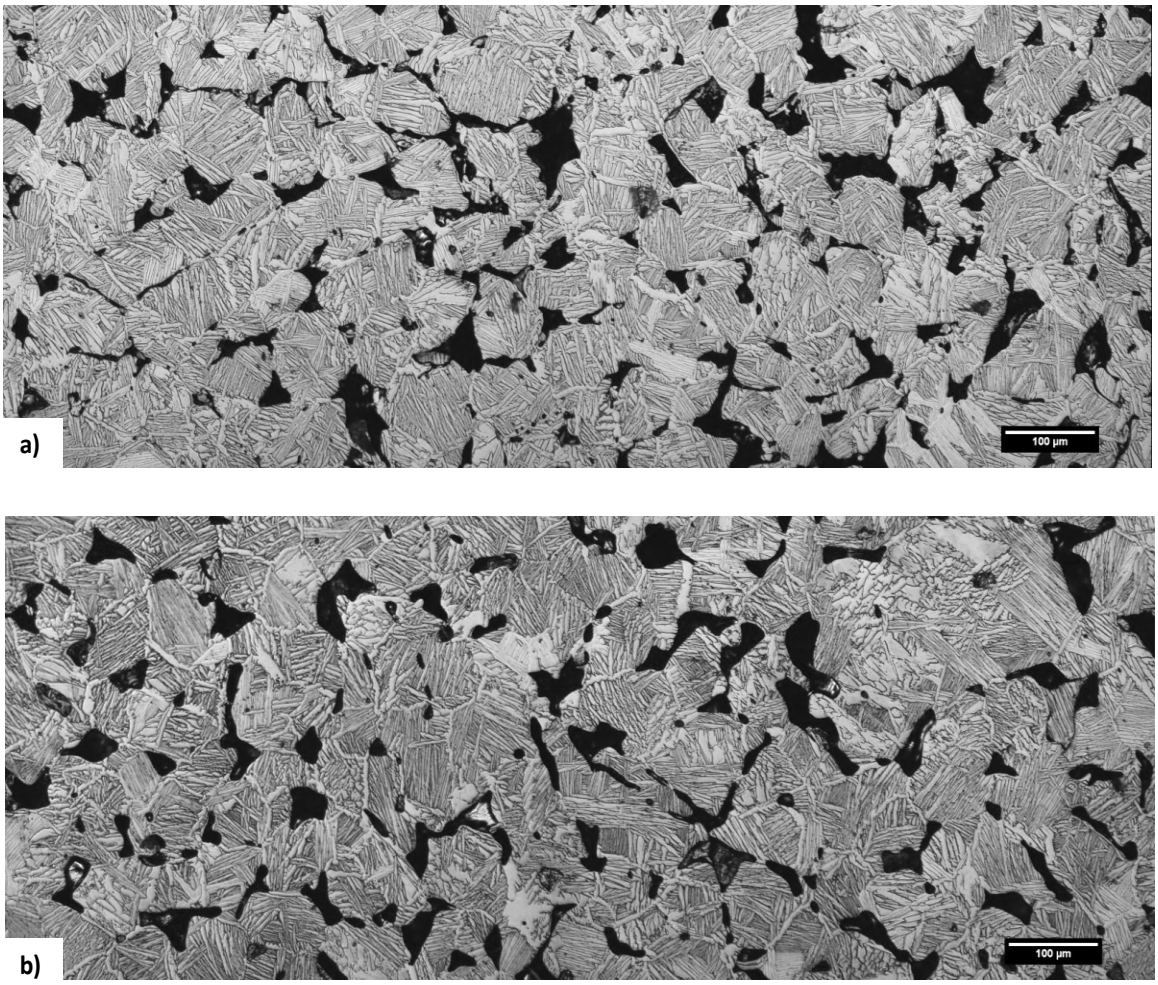

Figure 3.4.15: Optical micrograph of sintered Ti6Al4V Prealloyed powder sintered at 1200 °C; a) with no hold and b) for 2 hours.

SEM/EDS analysis to the sintered PA Ti6Al4V samples confirmed a uniform distribution of the alloy elements. XRD results for the PA samples as a function of sintering time are presented in Figure 3.4.16. As with the BE mixtures above, the predominant phase present at room temperature is (α-Ti). There is some evidence that a small about of retained beta and perhaps some intermetallic compounds or oxides exist in the microstructure. Similar results were reported by Malinov for an ingot metallurgy Ti6Al4V. Therefore, the formation of small amounts of these phases, is a result of the complex phase transformation that occurs during cooling in Ti6Al4V. For example, the

presence of a certain level of retained beta results from microsegregation on the scale of the Widmanstätten structure, and does not reflect larger scale bulk inhomogeneity that would be expected from the incomplete diffusion of alloying elements in a BE sintering process.

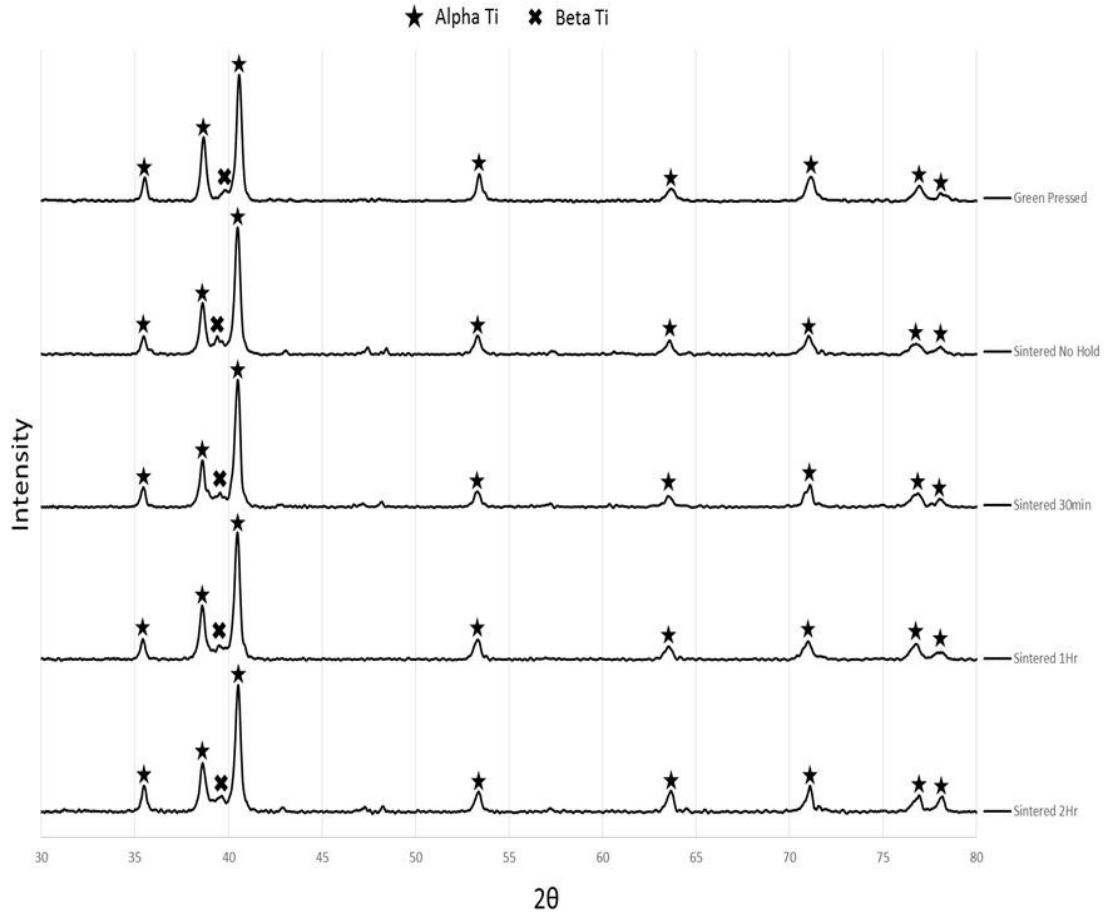

Figure 3.4.16: Measured spectra by XRD for the PA powder with corresponding phase composition

3.5. Analysis and Discussion

Overall the above DSC, microstructural and XRD results indicate homogenization of BE powder additions occurs to a significant extent over a 2 hour sintering period at 1200 °C. However, there are some trends within the individual alloys studied, which can be further

understood from the summarized DSC measurements presented in Figure 3.5.1-Figure 3.5.4. As would be expected, the Ti6Al mixture consistently exhibits a high beta transus temperature, both in terms of onset and end temperature. Conversely, the Ti4V mixture exhibits the lowest onset and end temperature for the beta to alpha transformation. The measured behaviour of the ternary systems fell in the region between the two binary in terms of start and end temperature for the transformation. The IM Ti6Al4V maintained the most stable results in all the metrics, while all the PM systems had larger degree of variability after different periods of sintering. Peak width was greater for all PM than the IM, but this did not correlate into a higher enthalpy of transformation.

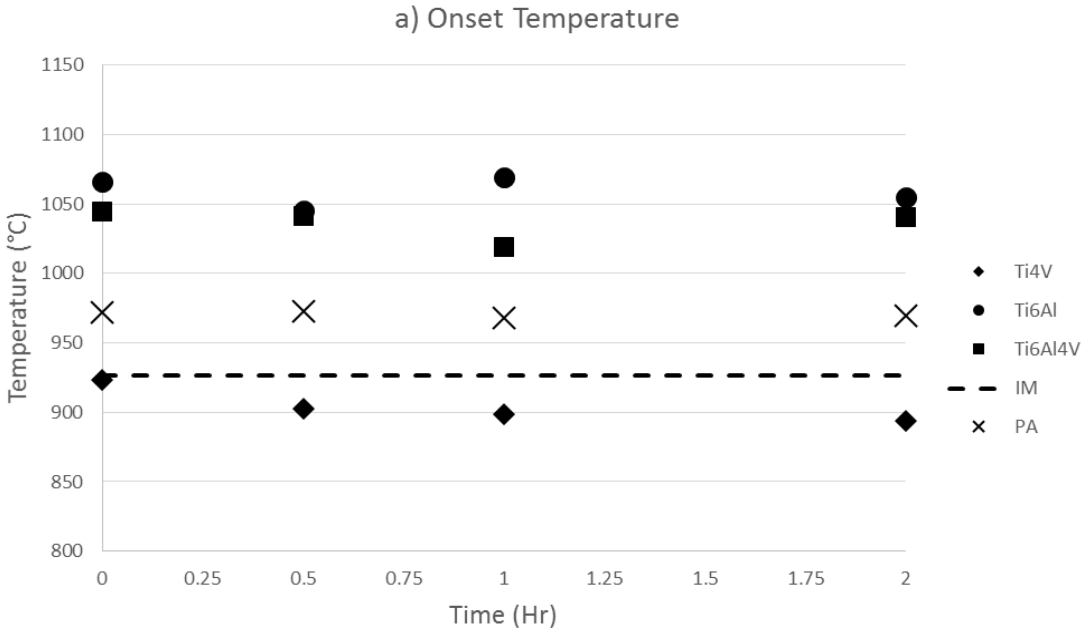

Figure 3.5.1: Onset temperature measurements made from the DSC cooling traces of the materials of this study

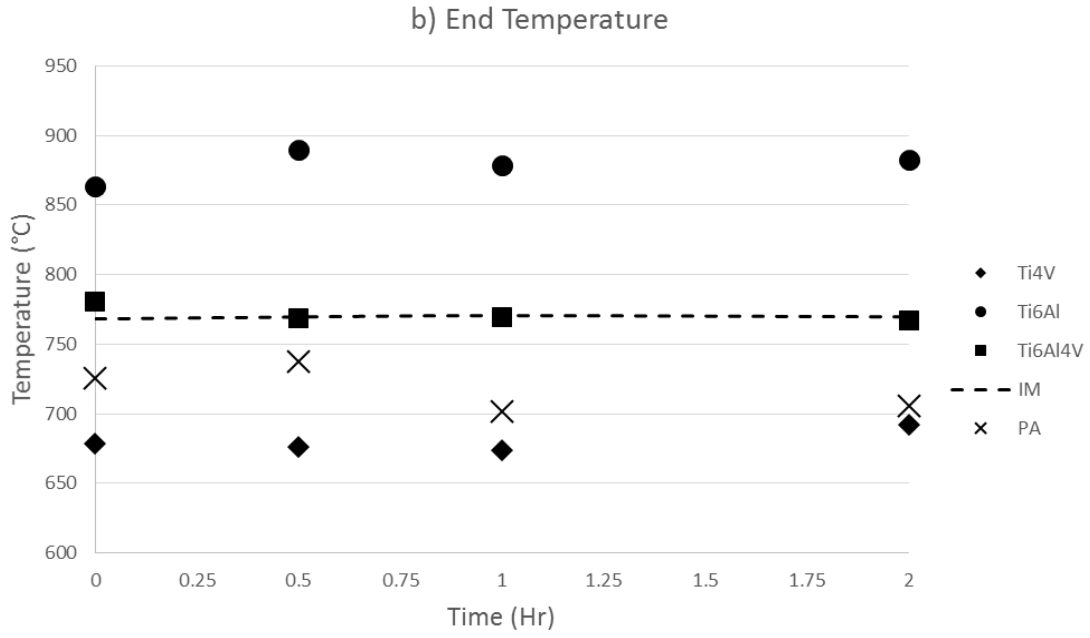

Figure 3.5.2: End temperature measurements made from the DSC cooling traces of the materials of this study

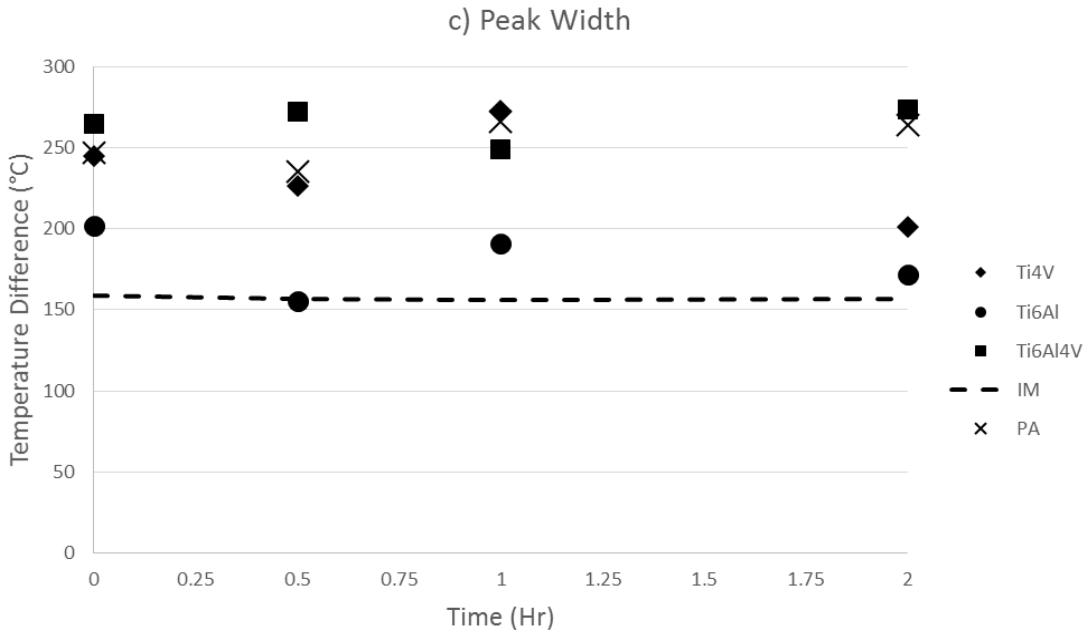

Figure 3.5.3: Peak width measurements made from the DSC cooling traces of the materials of this study

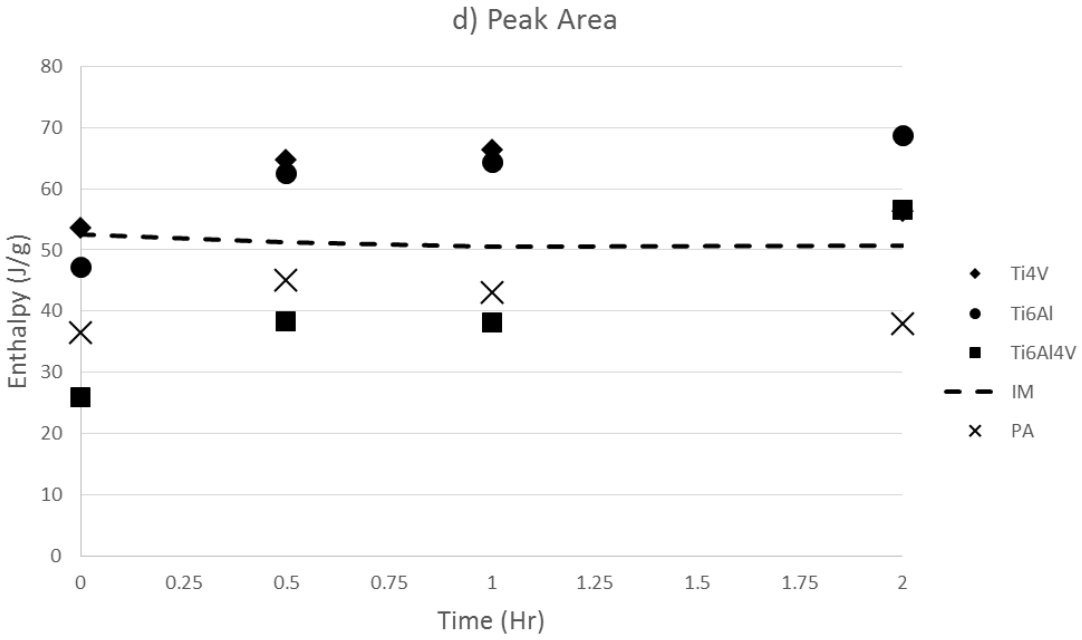

Figure 3.5.4: Enthalpy of transformation measurements made from the DSC cooling traces of the materials of this study.

3.5.1. Ti6Al

In order to elucidate the results gathered from DSC and other sources, a conceptual diffusion model was developed for the progression of alloying for the Ti6Al system, and is shown in Figure 3.5.5.

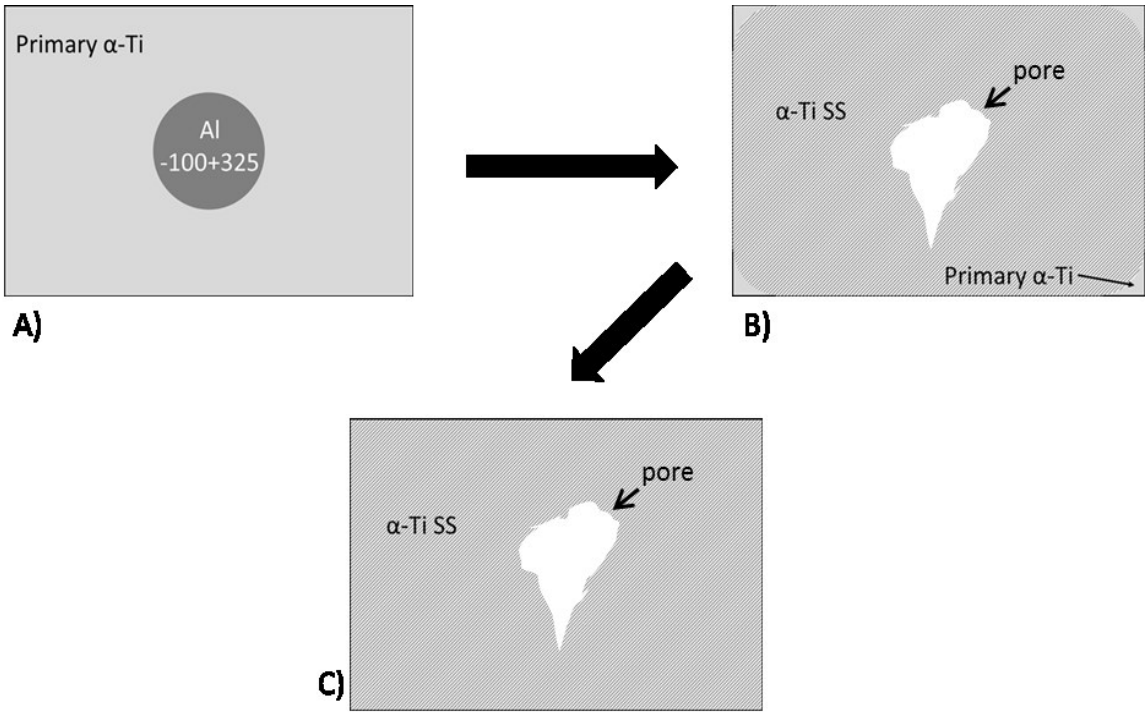

Figure 3.5.5: Diffusion model for Ti6Al at A) Green state, B) No hold state, and C) 2hr state

The behaviour of the DSC traces for the different sintered states shown in Figure 3.4.2 provide insight into the alloying behaviour of the Ti6Al system. In the no hold state, the DSC trace for the β to α transformation has changed significantly in comparison to the CpTi trace. The two most notable features of this measured transformation are its extremely broad shape and the considerable shift to higher temperatures for both the start and end of the transformation. The broad shape of the transformation suggests a non-uniform phase transformation. This is due to incomplete diffusion of Al at this early period. As mentioned previously, Al increases the stability of α-Ti phase at higher temperatures. The measured onset for the transformation in this state is 1065.7°C, indicating that regions in the microstructure exist with high Al concentration. This variation in Al concentration was confirmed by SEM/EDS in Figure 3.4.4 where a marked change in concentration of Al corresponds with the transition from the plate-like

region (Points 2-4) and the equiaxed region (Points 5,6). The broad shape of the DSC peak suggests that these variations in Al concentration result in a large temperature span for the β to α transformation. Both SEM/EDS and XRD were unable to locate the existence of pure Al in this state. Therefore, despite the variation in microstructure, at this relatively premature state of sintering there is significant homogenization of Al. This is due to the melting of Al which helps distribute the element throughout the microstructure. The phase composition changes that occurred from the green state to the no hold state are primarily due to the elimination of pure Al, resulting in an α-Ti solid solution.

There was less observed variation in the measured DSC peaks with increased sintering after the no hold state. From the no hold state there is a significant increase in measured enthalpy for the β to α transformation peak, increasing by 32% at the 0.5Hr state. Peak heatflow also increased significantly, with both characteristics pointing to a more homogeneous transformation SEM/EDS analysis confirmed that small variations in Al concentration lead to visibly distinct variations in microstructure. Additionally, EDS analysis showed that increased Al concentration was found segregated in the regions between the plate formations. XRD analysis of the 0.5Hr state produced a similar spectra to the no hold state, however, variations in peak intensity were observed. This intensity variation is caused by high α-Ti stabilized plate growth along preferred crystal planes.

The DSC traces for the latter two states showed little variation, with no observable changes due to the increased sintering time. This suggests that in both the 1Hr and 2Hr states changes to the β to α transformation due to Al concentration had homogenized. Measured enthalpy for the transformation had little variation between 1 and 2Hrs, as well as peak heatflow and peak width. The microstructure seen in Figure 3.4.3 has a coarse plate-like formation, similar to that found in the 0.5Hr state. This suggests that some degree of grain growth has occurred up to this period, causing the individual plates to widen with increasing sintering. SEM/EDS chemical analysis of the microstructure of

both states showed that bulk homogenization of Al was complete, with the less variation in Al composition at the 2Hr state. Variation in peak intensity of the α-Ti phase was also noted in the 1Hr and 2Hr states, which was due to preferred orientations of the alpha Ti transformation.

3.5.2 Ti4V

A conceptual model for alloying and diffusion for the binary Ti4V mixture is shown in Figure 3.5.6.

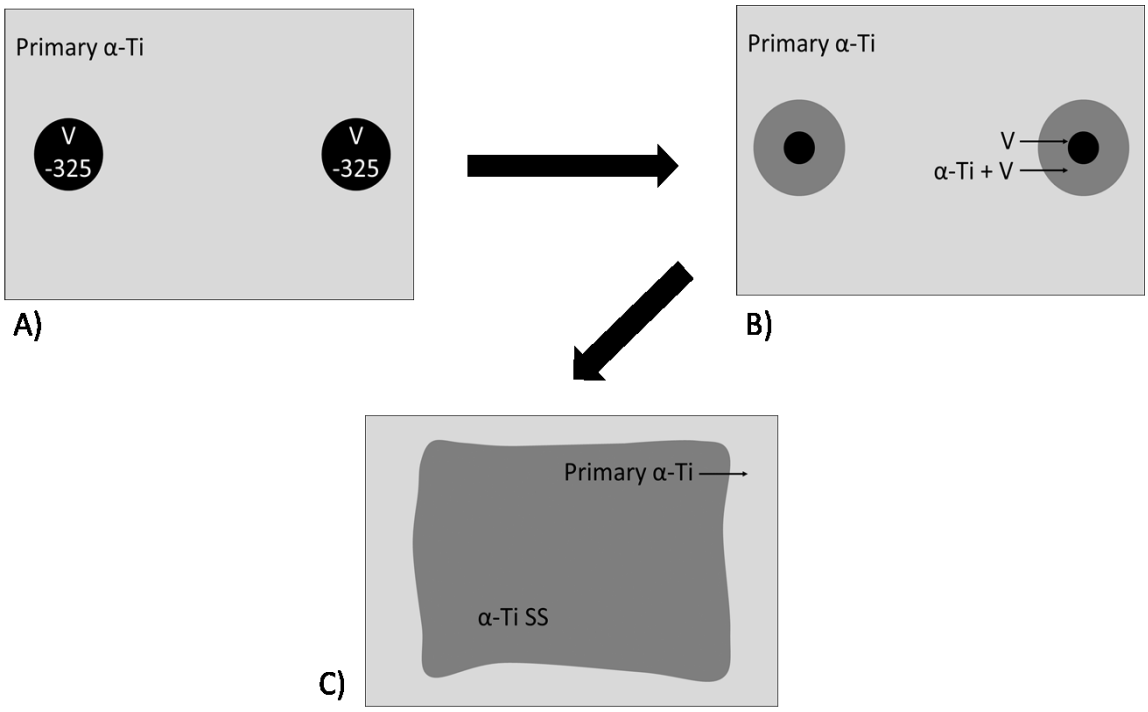

Figure 3.5.6: Diffusion model for Ti4V at A) Green state, B) No hold state, and C) 2hr state

Similar to the Ti6Al system, significant insight into the alloying behaviour of the Ti4V system can be inferred from the DSC traces shown in Figure 3.4.6. In the 0Hr state the

DSC trace for the β to α transformation was significantly altered compared to the CpTi trace. The measured peak had broadened significantly, with a temperature span of 244.7°C compared to 101°C for the transformation of the pure Ti powder. This broadening occurred with a corresponding marked reduction in peak heatflow. Another observation made for the Ti4V system was the apparent shift of the phase transformation to lower temperatures. This is due to the isomorphous β-phase stabilizing effects of V, and that diffusion of V in to the Ti matrix would shift the transformation temperature below the beta transus for pure Ti. The measured onset for the 0Hr state is close to the onset for the CpTi trace, suggesting that the effect of V to lower the transformation temperature has not affected some regions of the sample. Additionally, retained V particles were visible in this state. This contrasts the Ti6Al system where there was no visible remaining Al particles in the microstructure. Another visual difference from the Ti6Al system was the lack of large voids in this state. SEM/EDS analysis in

Figure 3.4.8 confirmed the existence of retained V particles at the 0Hr state, however, there was significant concentration of Ti in the peripheral areas of these V sites. XRD analysis of this state did not detect elemental V that was found in the green state, suggesting that the concentration was too low to resolve the peak using the scanning parameters for this investigation. Therefore, at this state, the site of the elemental V particles exists with Ti diffusion into the center of these particles without any appreciable counter diffusion of V.

In the 0.5Hr state, further changes to the DSC trace occur. The onset temperature of the β to α transformation occurs at a lower temperature (902.8°C vs 923.4°C) than the 0Hr state. This suggests that the β-stabilizing effects of V have been enhanced with increased thermal exposure by allowing further diffusion. Peak temperature has also shifted to a lower temperature (819.3°C vs 848.1°C) than the 0Hr state, with a higher heatflow at the peak temperature. The higher heatflow at the peak temperature is due a greater portion of the material transforming at this temperature, whereas in the 0Hr, the shorter

transformation peak is the result of a more inhomogeneous transformation. An increased enthalpy of transformation was also measured for the 0.5Hr state (53.65J/g vs 64.69J/g). In the 0.5Hr state the V sites seen in the 0Hr state were no longer present. The equiaxed grain structure of the 0Hr state appeared to have changed little with additional thermal exposure, however, upon closer examination a plate-like structure had formed. This likely occurred in the regions that had previously been occupied by the V particles. Additionally, there was evidence of pore shrinkage and rounding, a result of densification due to increased sintering. The dissolution of the V sites suggested increased diffusion of V throughout the Ti matrix. Analysis with SEM/EDS confirmed that longer range diffusion of V had occurred. Due to the smaller particle size of the V powder, there is an inherent increase in the homogeneity of the V once in is in solution. However, the long range diffusion of V at this state had not progressed to the same extent as Al in the Ti6Al system despite the smaller particle size. This is likely due to the slow self-diffusion rate of V which would have increased the amount of thermal exposure necessary to create a Ti-V solid solution [48]. Identification of phase composition by XRD revealed a similar composition to the 0Hr state. As the characteristic peaks for V were no longer present in the previous state, there was only changes to the two remaining phases, α-Ti, and β-Ti. There was only minute changes to β-Ti, with a broader peak occurring at 39.7°.

In the final two states of sintering the observed variations in the DSC traces suggest improved alloying due to the increased thermal exposure. The observed transformation peak in the 1Hr state had the largest temperature span, increasing from the 0.5Hr state by nearly 50°C. It should be noted that both at the onset and end of the transformation of the 1Hr state, the measured deviations from baseline were very subtle. This small increase in heat flow at both ends of the transformation means that there is little thermodynamic activity and that this represents a very small portion of the total transformation. This is evidence of the slow diffusion of V in the Ti matrix. The observed microstructure of the 1Hr state by optical microscopy reveals a large volume fraction of plate-like structure relative to the 0.5Hr state, and the equiaxed grain structure is no longer present. Regions

of a lighter coloured phase that have persisted in all states now have a plate-like structure within these regions. SEM/EDS analysis of these regions found a higher V concentration, close to the desired bulk concentration, and the surrounding regions to be lower in V concentration. The transition from 0.5Hr to 1Hr appears to represent a significant transition for the sintering of the Ti4V system. SEM/EDS and DSC support the transition in the 0.5Hr of a relatively inhomogeneous microstructure with some regions of high-V concentration to a much more homogeneous microstructure at the 1Hr state. Variations in V concentration in the 1Hr state have less variation and appear to be the result of two distinct regions, with the previously mentioned lighter-coloured phase having a V concentration of approximately 4wt% and the surrounding darker region having an average V concentration on 2.2wt%. Further changes occur for the measured transformation peak in the 2Hr state. The DSC trace for the β to α transformation had the highest end temperature of all the sintered states. The measured end temperature of 692°C was nearly 70°C higher than the 1Hr state (625.6°C). The onset temperature for the transformation was similar to the 1Hr state (898.5°C for the 1Hr state vs 893.5°C for the 2Hr state), resulting in the shortest temperature span for the measured transformation of the Ti4V sintered states (272.9°C for the 1Hr state vs 201.1°C for the 2Hr state). This decrease in the temperature span of the phase transformation suggests the degree of alloying of V is more homogeneous. In Figure 3.4.7, the optical micrograph of this sintered state, shows a nearly complete plate-like structure throughout. This structure is apparent in both of the two light and dark coloured regions described earlier. Additionally, on inspection there does not appear to be any reduction in volume fraction of the lighter V-rich regions when compared to the 1Hr state. This is surprising because with increased sintering it was expected that volume fraction of these regions would be reduced as diffusion of V continued. SEM/EDS analysis of the microstructure reveals many regions that are still below the desired bulk composition. Area scans of specific regions of the microstructure found the composition of V to vary between 1.8wt% to 2.3wt%. Interestingly, this includes some of the lighter V-rich regions, meaning that the V concentration in these specific regions has decreased but there is still more diffusion

required before a homogeneous composition is obtained. XRD analysis of both the 1Hr and 2Hr sintered states is shown in Figure 3.4.9. In both cases, α-Ti constitutes the bulk of the phase composition. In the 1Hr state a small peak corresponding with β-Ti is observed. This is expected due to the incomplete diffusion of V resulting in V-rich regions in the microstructure that are able to stabilize β-Ti. This peak is not observed in the 2Hr state, further supporting the improved homogenization of V that was found with SEM/EDS.

3.5.3 Ti6Al4V BE

With an analysis of the alloying behaviour of both Al and V completed to determine the behaviour of each in the Ti matrix, the ternary mixture was then analyzed. A conceptual model for alloying and diffusion for the ternary Ti6Al4V BE mixture is shown in Figure 3.5.7.

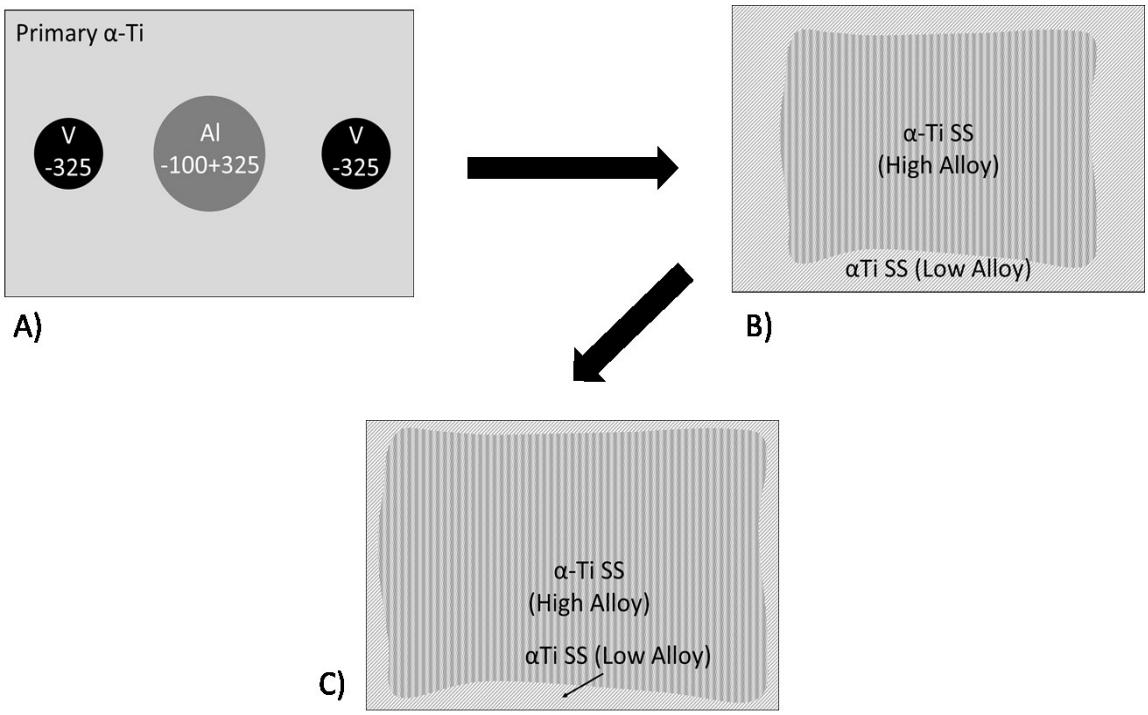

Figure 3.5.7: Diffusion model for Ti6Al4V BE at A) Green state, B) No hold state, and C) 2hr state

The observed behaviour of the ternary mixture was expected to show many of the characteristics of the two binary systems. But the interaction between both elemental additions as alloying progresses was important to understand. As Al and V alter the transformation behaviour of β-Ti to α-Ti, this interaction is particularly important. From the green state to the no hold state the observed changes to the microstructure were primarily due to the melting and dissolution of Al. A similar behaviour occurred where there was rapid melting and alloying with the surrounding Ti to form Ti aluminide intermetallics. The resulting microstructure seen in Figure 3.4.11 contained the same large voids caused by the melting of Al that was seen in the binary mixture with the majority of the microstructure consisting of plate-like α-Ti. Visible V particles were also seen in this state, with the same microstructural features that were seen in the Ti-V binary mixture. In this state it appears that both alloying additions are acting largely

independent of each other and that the interactions between the Al and V had not occurred yet. The DSC trace of the no hold state is seen in Figure 3.4.10. The measured transformation in this state qualitatively appears to be very broad with a very low peak heatflow. Further analysis of the transformation confirmed these observations. The temperature span was the largest of all the measured transformations for this investigation, while the enthalpy of transformation was the lowest. Additionally, the measured onset temperature for the β to α transformation was approximately 20°C less than the measured onset temperature for the binary Ti6Al mixture in the same state (1044.8°C vs. 1065.7°C). This lower beta transus temperature is due to the influence of the added V. The measured end temperature for the ternary mixture was markedly higher than the binary Ti4V mixture (780.2°C vs. 678.7°C), indicating that the presence of Al in the ternary BE has an alpha stabilizing influence to the mixture. These variations in transformation characteristics suggests that the earlier predictions that there was little to no interaction between the alloying elements is not correct. SEM/EDS analysis, in Figure 3.4.12 shows a V particle in the Ti matrix at the no hold state. Elemental maps of this region show that in addition to the uniform Ti concentration surrounding the V particle, the concentration of Al has reached a relatively homogeneous concentration considering the amount of thermal exposure. Some diffusion of Ti into the V particle region is observed in these SEM/EDS micrographs, however like the Ti4V system, the extent of this diffusion is limited at this state. The extent of V diffusion out into the surrounding matrix also closely resembles the Ti4V binary mixture, where relatively limited movement of V along the grain boundaries of the plate-like structure is observed. Phase composition of this state by XRD is shown in Figure 3.4.13. The key change in phase composition from the green state to the no hold state is the disappearance of V and Al spectra and the appearance of β-Ti phase. This change in phase composition supports the SEM/EDS results discussed earlier, suggesting that little pure V exists and instead a V-rich Ti,V solid solution has formed.

In the 0.5Hr state the measured DSC transformation trace shifted to lower temperatures relative to the no hold trace. The onset temperature of the β to α transformation in particular was recorded at a lower temperature (768.8°C vs 780.2°C). Additionally, the measured enthalpy for the transformation increased significantly with the increased thermal exposure (38.34 J/g vs. 25.94J/g). Optical micrographs of this state revealed that the equiaxed primary α-Ti grains were less prevalent and the lamellar α-Ti structure accounted for a much greater volume fraction of the total microstructure. Close examination of the microstructure also revealed that the V sites seen in the no hold state were no longer present. Both of these changes suggest that increased homogenization of both Al and V has occurred during this period. Analysis with SEM/EDS also found no evidence of the V-rich regions found in the no hold state. Instead much larger regions with uniformly distributed V were found likely near where the V-rich regions existed. In this state the V was fully segregated along the grain boundaries of the lamellar α-Ti. Other areas observed by SEM/EDS, however, did not detect any appreciable concentration of V. Instead, a uniform concentration of Al was measured. Visually, these two different regions were easily distinguished because of the different scattering behaviour of the V-rich and Al-rich regions, with the V- rich regions appearing much brighter.

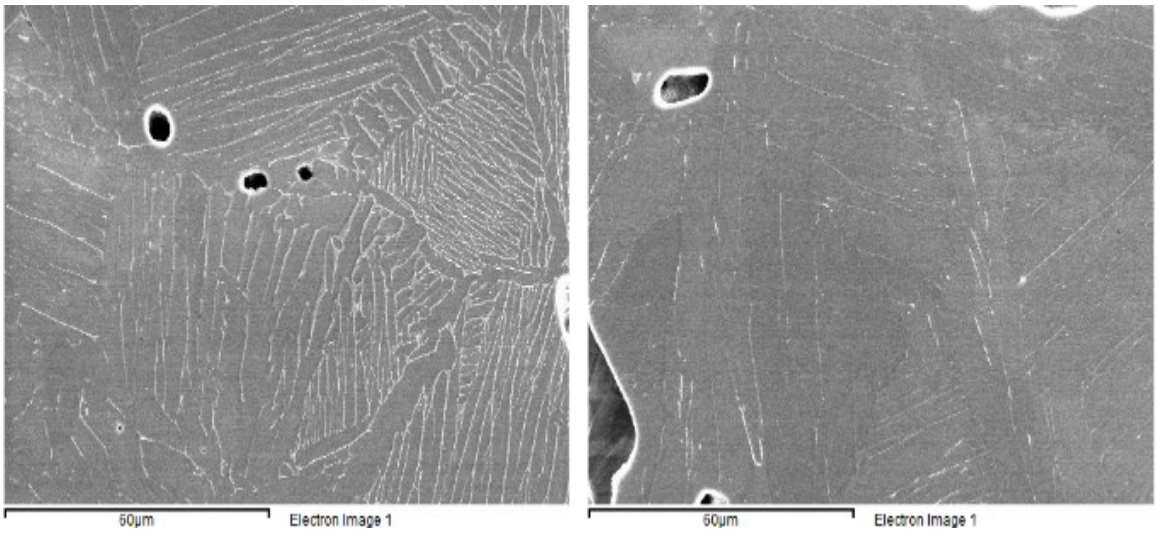

Figure 3.5.8: Sintered Ti6Al4V BE at 0.5Hr with a V-containing region (Left) and V-lean region (Right)

This difference in composition for observed microstructure with SEM is shown in Figure 3.5.8. Phase composition analysis with XRD revealed a more intense peak for the β-Ti phase which is expected due to the elimination of the V-rich regions seen at the no hold state which would have only stabilized a small concentration of the Ti, whereas now the increased homogenization allows for a larger concentration to be stabilized to room temperature.

With increased thermal exposure, the changes observed from the 0.5Hr state to the 1Hr state were less significant. The measured onset temperature for the β to α transformation with DSC was significantly lower at this state, with the transformation starting over 20°C cooler than the 0.5Hr state. The measured end temperature of the transformation and enthalpy not change appreciably. Therefore, the temperature span of the transformation decreased by over 20°C as well. Despite the narrowing of the transformation temperature span, the measured enthalpy of the transformation remained nearly unchanged (38.34J/g vs 38.13J/g). Therefore, peak heatflow increased at this state suggesting a more uniform transformation. SEM/EDS analysis revealed a similar distribution of alloying elements to

the 0.5Hr state, where a homogeneous distribution of Al was found with inhomogeneous distribution of V. Again V was confined to regions throughout the microstructure with the same segregated distribution found in the 0.5Hr. The key distinction is that in the 1Hr state these regions with distributed V occupied a larger volume fraction of the microstructure. This behaviour is similar to the binary Ti4V mixture, where slow diffusion rates of V in Ti required in excess of 1Hr to achieve an acceptable level of homogeneity. Increased intensity of the β-Ti phase was measured by XRD, which was the only observed change in phase composition. In the final sintered state at 2Hrs, the DSC trace for the phase transformation produced the largest measured enthalpy, increasing to 56.63J/g. This significant increase was due to an increased temperature span and the highest measured peak heatflow for the ternary mixture. Both of these characteristics point to a larger bulk transformation, but not necessarily a more homogeneous transformation. Observation of the optical micrographs reveal an expected progression in phase evolution, with a further reduction in equiaxed α-Ti, which was nearly absent in the 1Hr state. Indeed, in this state, it is assumed that this phase is no longer present. The plate-like α-Ti now accounts for the entirety of the phase composition with certain regions showing signs of coarsening from the 1Hr state. In addition to phase composition, comparison of the optical micrographs of the 2Hr state, Figure 3.4.11, to the no hold state reveal a reduction in the large voids that had formed due to the melting of elemental Al. Also, smaller voids are now significantly rounded. Therefore, there is a marked increase in the apparent sintered density after 2Hrs of thermal exposure. This may explain the increase in measured enthalpy of transformation by DSC. SEM/EDS analysis of the 2Hr state revealed that a marked increase in the long range diffusion of V had occurred as a result of the increased thermal exposure. The different regions of the microstructure that were analyzed all detected concentrations of V, approximately 1.5wt%. This suggests that the V inhomogeneity that persisted up to the 1Hr state is now somewhat alleviated, but further diffusion is still required. This increase in homogeneity may explain the increase in the measured temperature span of the phase transformation by DSC. Phase analysis by XRD also supports this increase in

V homogeneity with the measured changes to the β-Ti peak, whose intensity has decreased significantly from the 1Hr state.

3.5.4 PA Powder

Due to the inherent nature of the PA powder, the DSC traces for all sintered states exhibited a similar behaviour. In general, the peaks for all sintered states in Figure 3.4.14 could be characterized as broad, with low enthalpy. There was no significant variation in peak temperature or onset temperature. This indicates that the metallurgical effects that caused these variations in the BE mixtures were not occurring during the sintering of the PA powder. The high degree of homogeneity of the PA powder in the green state eliminates many of the diffusion-based problems that occurred during the sintering of the BE mixtures. End temperature was the only variable that showed any significant variation as a result of increased sintering. This suggests that despite the excellent homogeneity in the green state a considerable amount of thermal exposure is necessary to achieve necessary V diffusion. The low measured enthalpy for the phase transformation in all states is likely due to the poor observed density of the final sintered product. In both the No Hold, Figure 3.4.15 and 2Hr state, there is considerable open porosity in these micrographs compared to the BE mixtures. XRD results for each sintered state support the findings with DSC. Phase composition in all states remains very constant, no distinguishable variation. SEM/EDS analysis of the sintered states revealed a very homogeneous composition, with all measured regions within an acceptable margin of the desired bulk chemistry. Therefore, the sintered PA powder can be characterized by a very high degree of chemical homogeneity. However, the final product in all states was significantly less dense than either MA mixture.

3.6 Summary and Conclusions

A methodology for the use of DSC to analyze the phase transformation from β to α-Ti of PM titanium alloys has been developed. Additionally, the effect of elemental alloying additions of Al and V, both in binary and ternary mixtures, has been investigated using the DSC with varying sintering times at 1200°C. The homogenization of these alloying additions was analyzed with DSC, with particular attention paid to the cooling trace after sintering with no hold, 30min, 1Hr and 2Hrs. A comparison of these BE mixtures with a PA Ti6Al4V powder was also made to understand the characteristics of each type of system. In addition to DSC, optical microscopy, XRD and SEM/EDS were also utilized in this investigation.

DSC measurements of the phase transformation of the different powder mixtures provided invaluable insight in the behaviour of the specimens as a function of sintering time. Further characterization with other analysis techniques corroborated the observed alloying behaviour seen with DSC. Once a baseline was developed using IM CpTi, the different systems were investigated.

As expected, the addition of Al and V resulted in a phase transformation that occurred at higher and lower temperatures respectively. The behaviour of the Ti6Al system can be characterized as rapid homogenization resulting in the formation of large voids with an initial two phase structure. The two phase region becomes a single plate-like structure as Al becomes fully homogenized after 1Hr of sintering time. DSC analysis of the β to α transformation on cooling transformed from the early sintering stages where a very broad peak with higher onset and low end temperatures were recorded, to a more pronounced peak with an onset temperature of 1054.6°C and an enthalpy of 68.79J/g after 2Hrs.

The Ti4V system can be characterized by much slower diffusion kinetics compared to the Ti6Al system. In the no hold state SEM/EDS analysis found evidence of V-rich regions

which stabilized a small volume fraction of β-Ti. With increased sintering time longer range V diffusion did occur with the transformation of acicular α-Ti into a plate-like α-Ti solid solution. The volume fraction of this phase structure increased with increasing sinter time. After 2Hrs complete diffusion of V had occurred however achieving the desired bulk composition would require additional sintering time. DSC analysis of the β to α transformation on cooling showed continuing changes as the degree of homogeneity of the system improved with increasing sintering time. As homogeneity improved the trace changed from a broad and short peak to a narrower and pronounced peak, with a decrease in onset temperature from 923.4°C to 893.5°C from the no hold state to the 2Hr state.

The elemental Ti6Al4V mixture exhibited many of the alloying behaviour of the two binary systems. There was rapid alloying of Al with the surrounding Ti to form intermetallics creating large open pores, and slow diffusion of V. The measured transformations in the first three sintered states had very low enthalpies, with very large temperature spans. The rate of alloying of Al and particularly V appeared to be slower for each elemental addition in the ternary mixture than in the respective binary mixtures. At the 2Hr state complete diffusion of both alloying elements had happened but the desired bulk composition had not been achieved, and therefore, additional sintering time would be required. The measured enthalpy of transformation in the 2Hr state was 56.63J/g.

The PA exhibited excellent behaviour in terms of the measured transformation by DSC. No distinguishable changes in the transformation peak occurred as a result of increasing sintering time. Complete homogeneity was verified by SEM/EDS and XRD. However, a low enthalpy of transformation in all states and this is likely due to the high quantity of porosity that existed in all states. Additionally there was not a significant observed reduction in the porosity of these sintered specimens.

In the pursuit of a fully homogenized PM Ti6Al4V by means of a BE powder mixture, a better understanding of the role of each alloying addition during the sintering of the specimen has been developed. Key aspects of a BE system based on this investigation include: the dissolution and formation of titanium aluminides during heating, particle size of both alloying additions, particularly V, and a sintering time in excess of 2 hours at 1200°C to ensure a fully homogenized specimen. The use of DSC has been shown to greatly aid in the development of PM systems, and in this case Ti6Al4V, by allowing in-situ analysis of the heatflow characteristics.

4.0. IN-SITU ALLOYING AND HOMOGENIZATION OF TI6AL4V USING AL:V MASTER ALLOY POWDER ADDITIONS

4.1. Introduction and Experimental Methods

This chapter contains a continuation of the previous study of Chapter 3 into the quantitative measurement of the extent of diffusion and homogenization during sintering of Ti6Al4V powder compacts. This investigation will focus on role of MA additions and the influence of MA particle size. Using the same methodology of the previous chapter, differential scanning calorimetry will be used to provide quantitative measurements during sintering. In particular, the β to α transformation during cooling will be analyzed in order to determine the extent of homogenization. Parallel microstructural and XRD examination will be used to validate the DSC results.

The master alloy powder blends used for this investigation were prepared using a CP Ti (ASTM Grade 3) powder and a binary 60 wt% aluminum 40 wt% vanadium MA. In addition to the MA blends an ingot metallurgy (IM) prealloyed Ti6Al4V rod was sourced for comparative experiments. All powders used for this investigation were supplied by Reading Alloys as-sieved and packed under argon. Both commercially pure CP -Ti and Ti6Al4V pre-alloyed (PA) powders were produced using the hydride-dehydride process (HDH), while the Al:V master alloys were produced by a thermite process.

The chemical composition of the IM rod was reported in the previous chapter. The chemical composition of the CP-Ti and MA alloy powders was verified by an independent third party laboratory to ensure purity, including the concentration of C, O, N, and H. Additionally, the received size fraction of all powders was verified by laser particle size analysis. The d_{50} from these laser measurements are given in Table 4.1.1.

Table 4.1.1: As-received powder composition (wt%) and characteristics

Powder	Size Fraction (mesh)	d_{50} (μm)	Ti	Al	V	C	O	N	H
CP-Ti	-100/ +325	106	balance	<50 ppm	<50 ppm	0.008	0.161	0.018	.013
60/40 Al:V	-100/ +325	73	0.014	58.6	41.0	0.028	0.111	0.0044	0.004
60/40 Al:V	-325	24	0.031	59.0	39.8	0.046	0.250	0.0044	0.010

Two size fractions of the MA (d_{50} = 24 and 70 μm) were blended with the CP Ti in a Turbula mixer for approximately 1 hour to produce two Ti6Al4V composition blends. Consolidation of all the powders was performed using manual uniaxial die compaction with a Carver press to 850MPa. Licowax lubrication was applied to the die walls to reduce wear. Sample weight and dimensions were recorded in both the green and sintered state. The samples were 4.8 mm in diameter and approximately 1mm in thickness. Thermal analysis of the sintering behaviour of the different PM alloys was performed using a Netzsch 404 F1 DSC. Samples were sintered in a yttria crucible to limit reaction between the crucible and Ti samples. Heating was performed under a high purity flowing argon atmosphere (99.999%) with a titanium "getter" ring placed below the hot zone to ensure minimal contamination of the samples by impurities in the gas stream. Each thermal profile involved heating to 1200°C at 20°C/min with either an immediate cooling or increasing isothermal hold times from 15 minutes to 3 hours. The samples were then cooled to room temperature at 40 °C/min. A selection of samples were also heated to temperatures between 850 °C and 1200 °C followed by rapid cooling.

Microstructural examination on post DSC treated samples was performed using both a Hitachi S-4700 FEG SEM with an Oxford INCA EDS analysis system for phase composition, and a Zeiss optical microscope. Samples were mounted in a conductive resin and polished to a mirror-like finish using SiC papers, diamond suspension and colloidal silica (Struers). A Bruker D8 Advance XRD with a Cu Kα source was used for phase identification of as pressed and DSC heated powder compact samples.

The previous chapter presented the development of a DSC method, based on the analysis of the β to α phase transformation during cooling, which is capable of analyzing homogenization during BE sintering. The same technique will be also be used to analyze Ti6Al4V MA sintering in this study.

4.2. Results

4.2.1. Initial Heating

It is postulated that in-situ alloying and interdiffusion between the Al:V MA and CP-Ti powders could begin during initial heating up to 1200°C. To investigate this possibility an examination of the initial DSC heating traces of the MA mixtures in comparison to the 100% CP-Ti sample was completed. The α to β transformation of unalloyed CP-Ti compared to both MA mixtures is shown in Figure 4.2.1. Measurements of the onset temperature, peak width, end temperature and enthalpy of transformation obtained from the DSC peaks are given in Table 4.2.1. It should be noted that the data of Table 4.2.1 is the average of up to 14 separate sample measurements. The standard deviation of the enthalpy, peak width and end temperature measurements was in the range of 5 to 10%, while onset and end temperature had a standard deviation of less than 1%.

All powder compacts have very similar onset temperatures in the range of 877 to 879 °C which, given the variability of the measurement, is in agreement with the value of 882 °C

for pure Ti. The 100% CP-Ti represents only 90wt% of the MA mixtures and therefore the initial enthalpy of transformation of the Ti6Al4V blends should be reduced to 60 J/g. This is the case for the Ti6Al4V coarse MA mixture but not for the fine MA blend. In addition, the DSC trace for the fine MA mixture exhibits an exothermic shift in the baseline prior to the alpha to beta phase transformation while the coarse MA mixture exhibits an exothermic peak in the temperature range of 1050 to 1200°C. These differences compared to the pure CP-Ti trace are expected to be due to metallurgical reaction between the MA particles and Ti matrix.

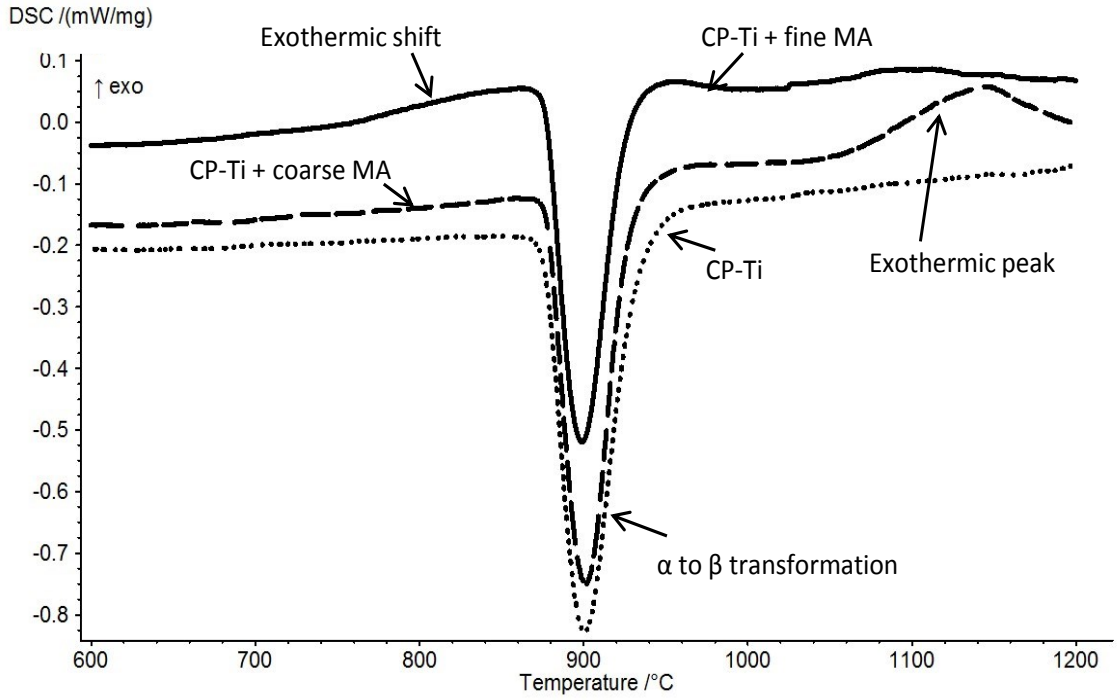

Figure 4.2.1: Change in transformation behaviour with the addition of 60/40 AlV MA to CP Ti during heating to 1200°C

Table 4.2.1: DSC Measurements for the α to β Phase Transformation during initial heating for CP-Ti and master alloy blended Ti6Al4V mixtures.

Sample	Enthalpy (J/g)	Peak Temperature (°C)	Onset Temperature (°C)	End Temperature (°C)	Peak Width (°C)
100 % CP-Ti	73	904	879	930	77
Ti64 with 72 μm MA	59	902	878	926	75
Ti64 with 24 μm MA	54	890	877	924	75

The cause of these differences in the DSC traces was investigated by heating the blends to four different temperatures of significance, followed by rapid cooling (i.e. nominally 100 °C/minute). From the transformations observed in Figure 4.2.1, these temperatures were chosen to represent the onset, peak, and end temperature for each MA trace (i.e. 850, 900, and 950 respectively). Following cooling, the samples were mounted and polished and their microstructure observed.

Optical micrographs presented in Figure 4.2.2 a), b) and c) show the extent of diffusion between the Ti matrix and the coarse MA particles as a function of the peak interrupted temperature. At 850°C (i.e. Figure 4.2.2 a) the microstructure exhibits isolated MA particles surrounded by an α-Ti matrix. At 900 and 950 °C an intermediate layer appears between the coarse MA particles and the Ti matrix

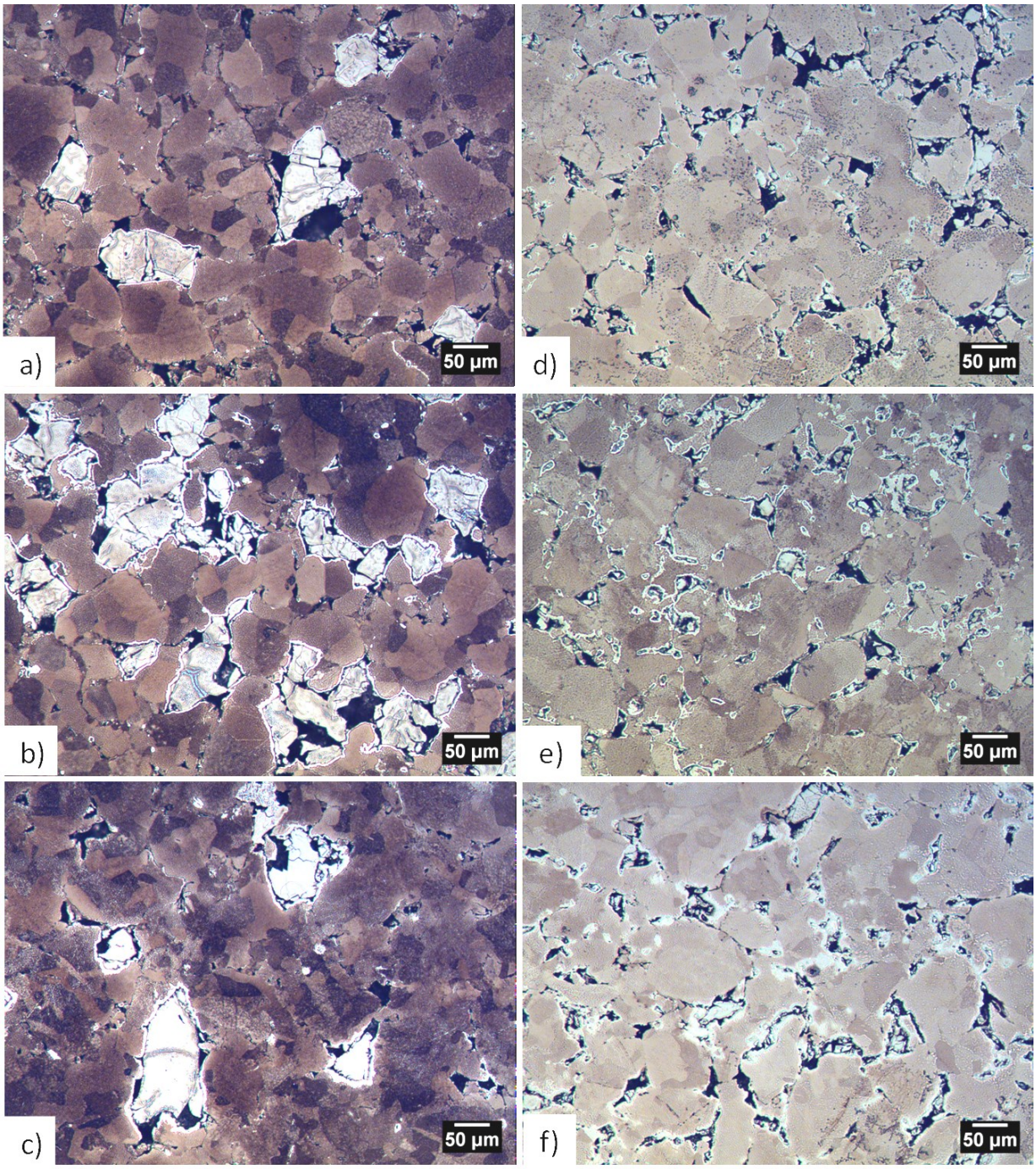

Figure 4.2.2: Optical micrographs of CP Ti + Coarse AlV MA heated to a) 850°C b) 900°C c) 950°C and CP-Ti fine MA heated to d) 850°C e) 900°C f) 950°C

The same regions depicted in Figure 4.2.2 were analyzed with SEM/EDS to determine the chemical composition of the different regions. The SEM micrographs are shown in Figure 4.2.3. The compositions measured by EDS at specific points noted on Figure 4.2.3a) b) and c) for the coarse MA mixture, are listed in Table 4.2.2. Figure 4.2.3 and Table 4.2.2 indicate that at 850°C the microstructure of the coarse MA mixture still consists of Al:V MA particles imbedded in a pure Ti matrix. However at 900 and 950 °C, the intermediate layer visible in the optical micrograph of Figure 4.2.2 has a mixed composition which includes Ti, Al and V. This indicates the development of a Ti containing intermetallic compound. The core of the coarse MA particle has a slightly higher Ti content compared to that measured in the as received powders, indicating that a minor amount of Ti has diffused into the coarse MA particle.

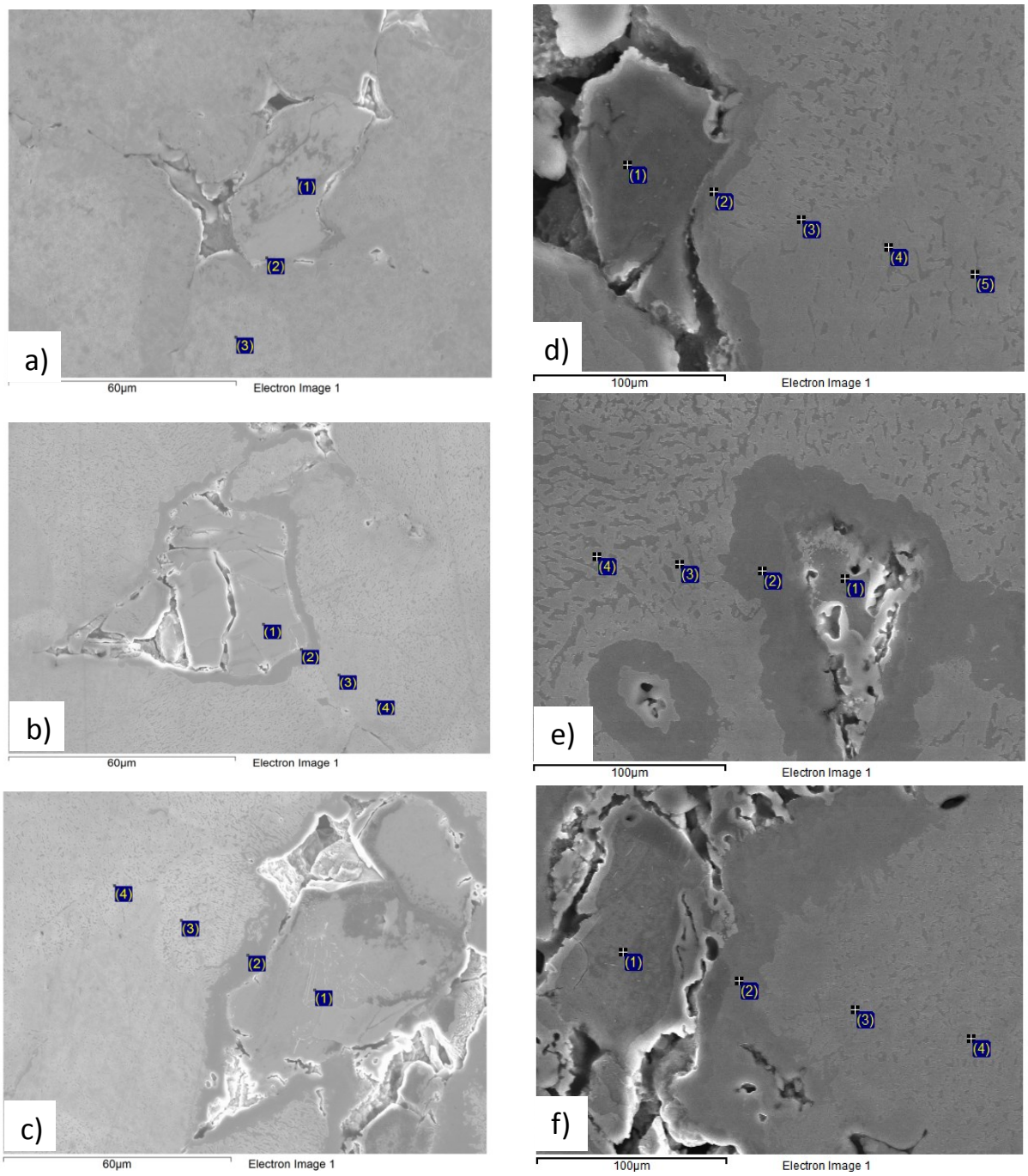

Figure 4.2.3: SEM micrographs of CP Ti + Coarse AlV MA heated to a) 850°C b) 900°C c) 950°C and CP-Ti fine MA heated to d) 850°C e) 900°C f) 950°C indicating locations of EDS analysis

Table 4.2.2: EDS chemical analysis results for interrupted coarse MA samples (wt%) from images of Figure 4.2.3 a), b) and c).

Quench Temperature	Element	Site 1	Site 2	Site 3	Site 4
850 °C (a)	Ti	0.51	0.96	100	-
	Al	60.05	58.53	0	-
	V	39.95	40.52	0.00	-
900 °C (b)	Ti	0.87	57.74	99.86	99.94
	Al	45.37	28.24	0.07	0.02
	V	53.75	14.01	0.07	0.04
950 °C (c)	Ti	0.54	94.00	99.97	99.96
	Al	58.58	5.36	0.03	0.04
	V	40.88	0.64	0.00	0.00

The optical micrographs in Figure 4.2.2 d), e) and e) show the microstructure of interrupted fine MA Ti6Al4V blended samples. These micrographs demonstrate the finer distribution of these MA particles, relative to the coarse MA. Similar to the coarse MA, there is visual evidence of a boundary region forming in the 900°C sample. The region is seen to expand significantly at 950°C.

Micrographs for the SEM/EDS chemical analysis for the fine MA interrupted samples are shown in Figure 4.2.3 d), e) and f). The composition measured by EDS at the specific points is listed in Table 4.2.3. Unlike the coarse MA blend, there is some evidence of an intermetallic layer forming at the fine MA/CP-Ti interface at 850 °C. (i.e. point 2 in Figure 4.2.3 d)). The thickness of this intermetallic layer increases at 900 and 950 °C, particularly compared to that observed for the coarse MA blend. Also compared to the coarse MA mixture, there is a higher Ti content at the core of the fine MA particles and a slightly higher Al and V content in the CP-Ti matrix surrounding the MA particles.

Table 4.2.3: EDS chemical analysis results for interrupted fine MA samples (wt%) from images of Figure 4.2.3 d), e) and f).

Quench Temperature	Element	Site 1	Site 2	Site 3	Site 4	Site 5
850 °C (d)	Ti	1.21	82.34	100	100	100
	Al	56.57	15.10	0	0	0
	V	42.22	2.56	0	0	0
900 °C (e)	Ti	1.73	80.34	98.71	99.47	-
	Al	51.84	14.95	0.33	0.18	-
	V	46.43	4.71	0.97	0.36	-
950 °C (f)	Ti	0.89	88.09	99.52	99.77	-
	Al	57.72	11.20	0.26	0.08	-
	V	41.39	0.71	0.22	0.14	-

All of the above data indicates that there is some level of metallurgical reaction between the MA and CP-Ti particles during heating in the temperature range of 850 to 950°C. The diffusion of Ti into the MA particles and the formation of Ti containing intermetallics, reduces the phase fraction of alpha-Ti available to undergo the α to β phase transformation during heating. This results in a lower enthalpy measurement determined from the DSC trace. This Ti consumption is greater in the fine MA blend, resulting in a

more significant reduction in enthalpy of transformation of 54 J/g compared to the expected 60 J/g.

Figure 4.2.4 presents a comparison of the microstructure of a coarse and fine MA blend "quenched" from 1200 °C. The coarse MA sample exhibited many undissolved MA particles dispersed throughout an unalloyed alpha CP-Ti matrix. Each MA particle is surrounded by a diffuse boundary layer consisting of Widmanstatten structure. The presence of this type of microstructure demonstrates that heating to 1200 °C has caused the development of an alloy region in the matrix around the MA particles.

Figure 4.2.5 presents SEM micrographs of the vicinity around the MA particle for both the coarse MA and fine MA mixture quenched from 1200 °C. The figure includes the locations of EDS spot analysis, the results of which are presented in Table 4.2.4. This data confirms that the Widmanstatten region contains a high Al content with some V present. Outside the Widmanstatten boundary layer, the composition reduces back to near pure Ti. The EDS analysis also shows that diffusion of Ti into the core of the coarse MA particles has increased, while diffusion of Al out into the matrix has increased. The core of the coarse MA particle remains vanadium rich.

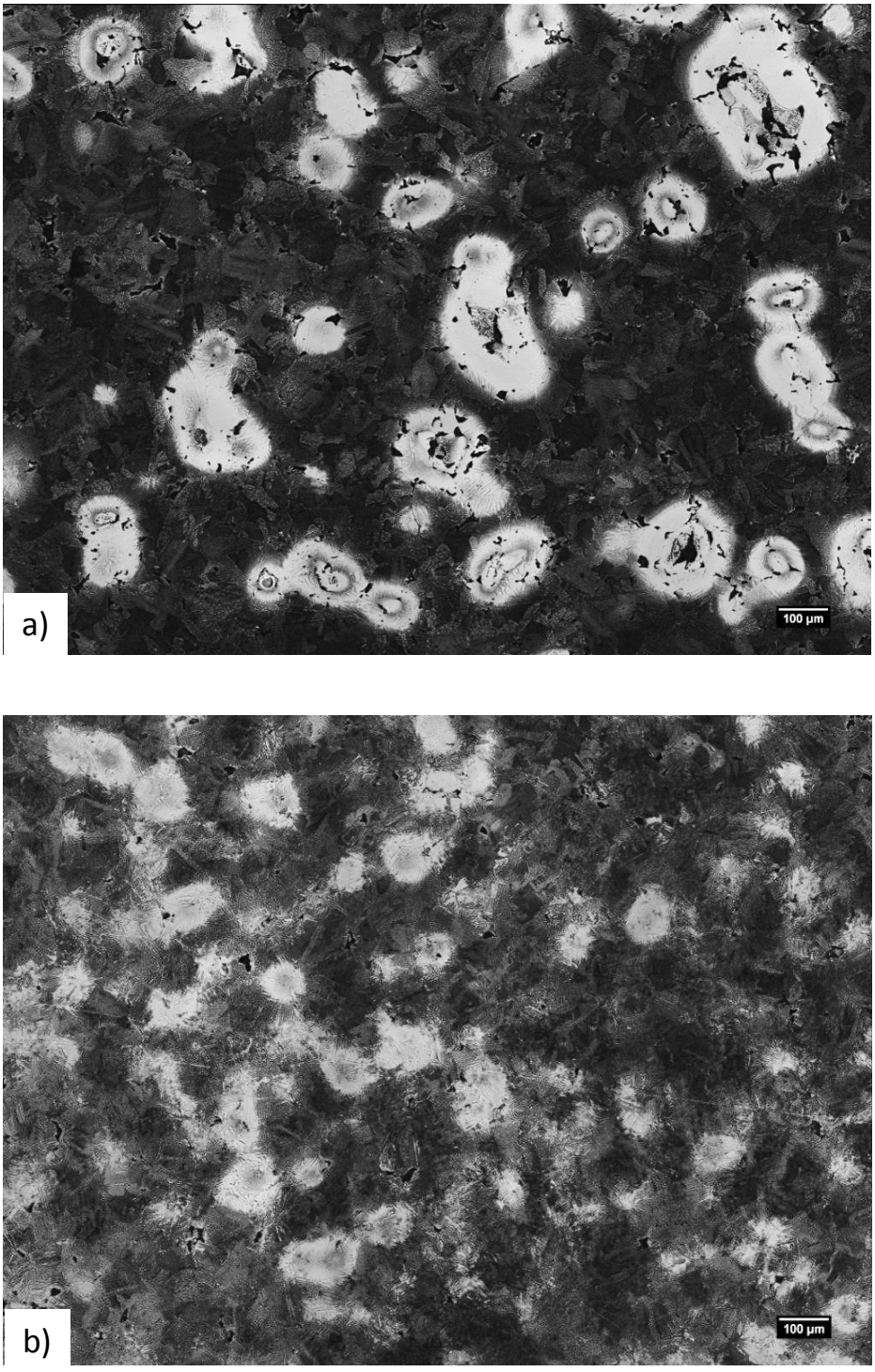

Figure 4.2.4: Optical micrographs of a) CP Ti + Coarse AlV MA and b) CP Ti + fine AlV MA heated to 1200°C and quenched.

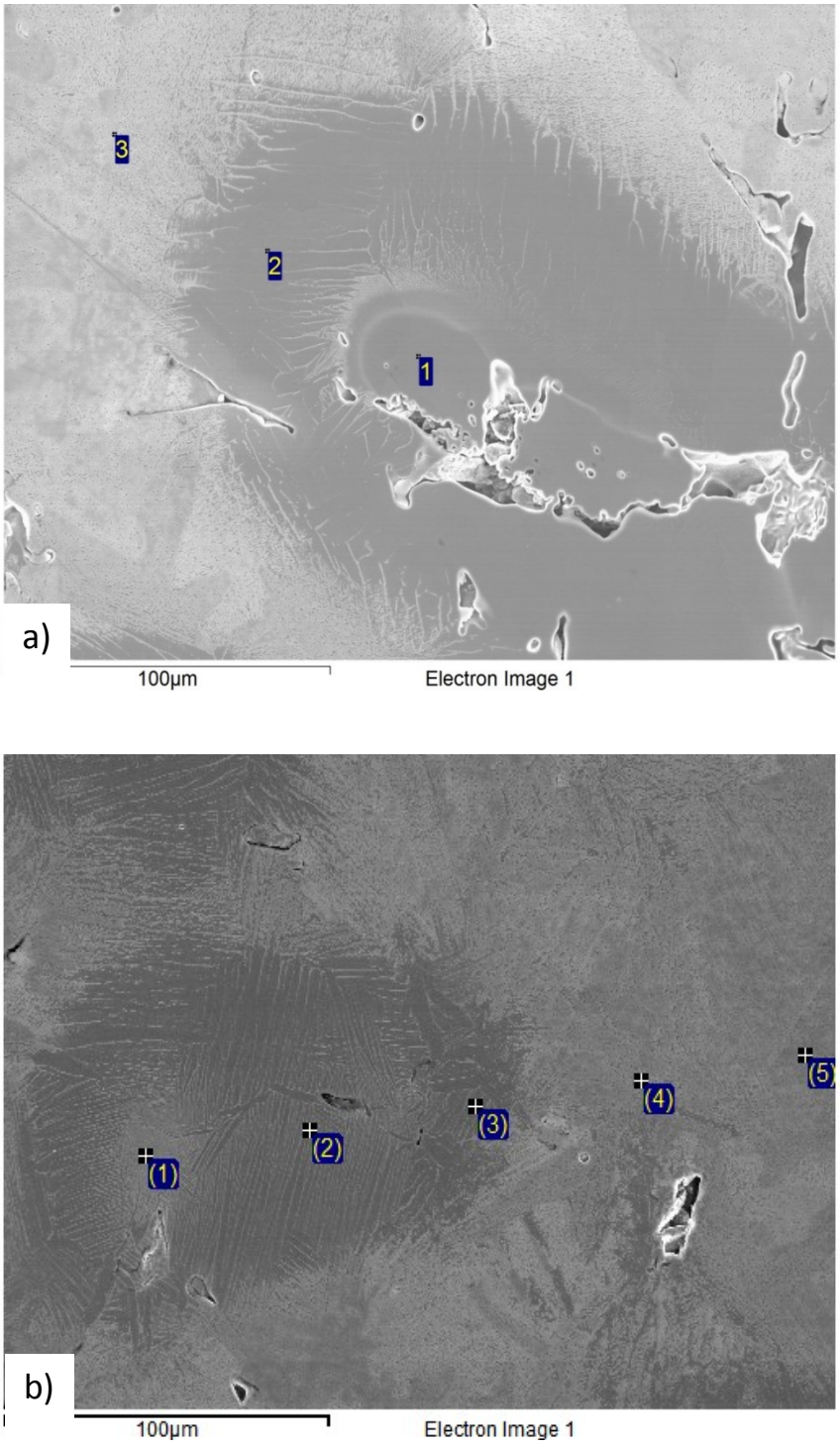

Figure 4.2.5: SEM micrographs of a) CP Ti + Coarse AlV MA and b) CP Ti + fine AlV MA heated to 1200°C and quenched.

Table 4.2.4: EDS analysis of selected sites surrounding a MA particle location for the MA mixtures heated to 1200 °C and quenched. Site locations are given in Fig. 4.2.5

Mixture	Element	Site 1	Site 2	Site 3	Site 4	Site 5
Coarse MA Ti6AL4V	Ti	32.84	89.97	99.43	-	-
	Al	13.51	8.98	1.06	-	-
	V	53.65	1.06	0.03	-	-
Fine MA Ti6AL4V	Ti	81.15	89.86	94.70	97.84	98.84
	Al	4.9	5.00	3.03	1.53	0.83
	V	13.95	5.13	2.27	0.63	0.33

The microstructure of the fine MA sample heated to 1200 °C also consists of dispersed clusters of Widmanstatten structure within an alpha Ti matrix. SEM/EDS analysis of the core of these regions indicate that they have a slightly elevated V content but also a high percentage of Ti with some Al. This composition is very different than the original MA composition and, unlike the coarse MA mixture, is Ti rich rather than V rich. This indicates that the process of MA particle dissolution is more advanced in the fine MA mixture at this stage of heating compared to the coarse MA mixture. Both the etched microstructure of Figure 4.2.4 and the SEM/EDS analysis of Figure 4.2.5 and Table 4.2.4 indicate that the diffusion of Al and V has extended further into the matrix in the fine MA mixture resulting in an increased area fraction of Widmanstatten microstructure.

4.2.2. Effect of Hold Time

The above results indicate that there is interdiffusion between the CP-Ti matrix and MA powders in the Ti6Al4V MA blends during the heating stage of the sintering process. This is particularly true between 950 and 1200 °C, where the Ti matrix is in the beta phase. However the quenched samples from 1200 °C also indicate that a significant amount of inhomogeneity still exist in both the coarse and fine MA blends at this point of sintering. The extent to which homogenization occurs as a function of the sintering time in these MA blends was investigated through an analysis of the β to α phase transformation on cooling. As described in more detail in the previous chapter, the enthalpy of this transformation and the temperature range over which it occurs, is a function of the extent to which the Al and V alloy elements have distributed throughout the material.

The results shown in Figure 4.2.6 include the DSC cooling traces after increasing hold time at 1200°C for the Ti6Al4V MA blend made using coarse Al:V intermetallic particles. A cooling trace for pure CP-Ti is included for comparison. The transformation peak for the no hold sample has a unique shape consisting of a very gradual transformation near the onset of the transformation to a sharp transformation near the end temperature. This results in a maximium peak height (a.k.a “peak temperature”) occurring at the lower end of the transformation temperature range (i.e. a peak temperature of 882°C). In comparison with the CP-Ti transformation peak, it is clear that the onset temperature in the no hold MA Ti6Al4V blend is shifted to higher temperatures, which would be expected for regions of the sample with a higher Al content. The transformation at lower temperatures near the peak maximium (i.e. 882 °C) is due to regions of the sample that have remained unalloyed, at 100% Ti.

The transformation behaviour of the samples held for longer times all exhibit a different shape from that of the no hold sample. In particular, the magnitude of the transformation, as indicated by the peak height, is evenly distributed around the peak temperature with a peak shape similar to a Gaussian distribution. However, a general trend of a narrowing peak width and an increased peak height occurs with an increase in sintering time. Cooling traces for sintering times of 2 and 3 hours are not shown, but were similar in shape to the 1 hour sample.

Figure 4.2.7 presents the DSC cooling traces for the Ti6Al4V MA blends using fine Al:V intermetallic particles. The trends with sintering time are similar to that observed in the coarse MA blend. Notable exceptions include a non-skewed zero hold time peak and "sharper" transformation peaks at the longer hold times. These sharper peaks are characterized by higher peak heights and narrower peak widths. Peak shapes for samples sintered for 2 and 3 hours were also similar to the 1 hour hold samples.

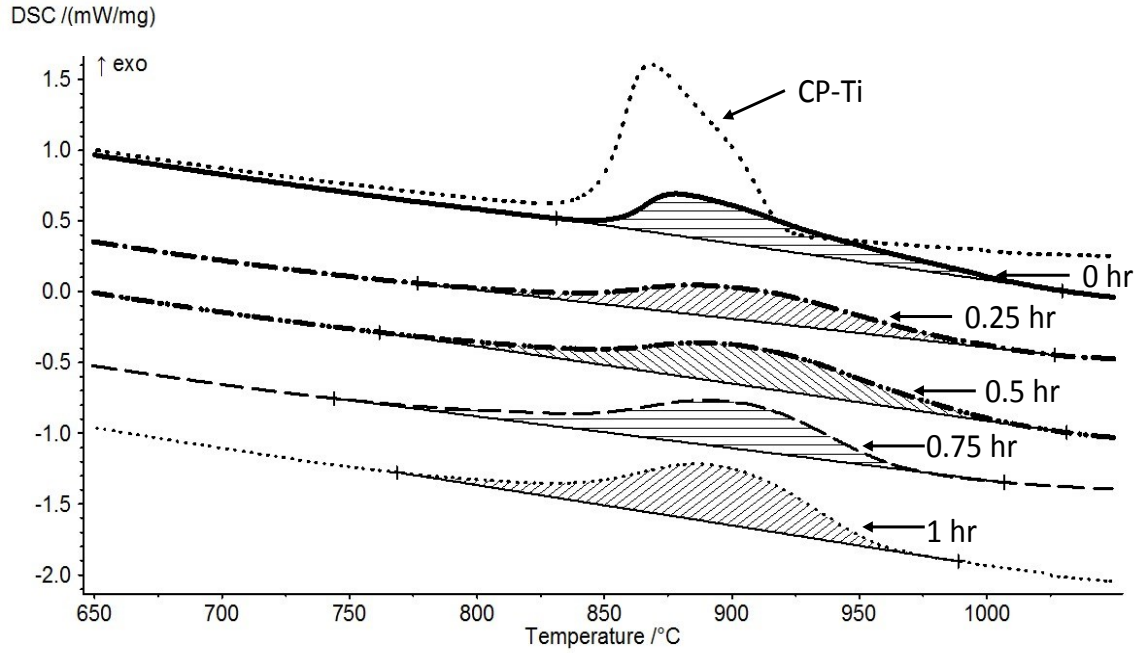

Figure 4.2.6: Comparison of the β to α transformation resulting from increasing isothermal holds in the coarse MA blend: No Hold, 0.25, 0.5, 0.75 and 1 hour compared to pure Ti.

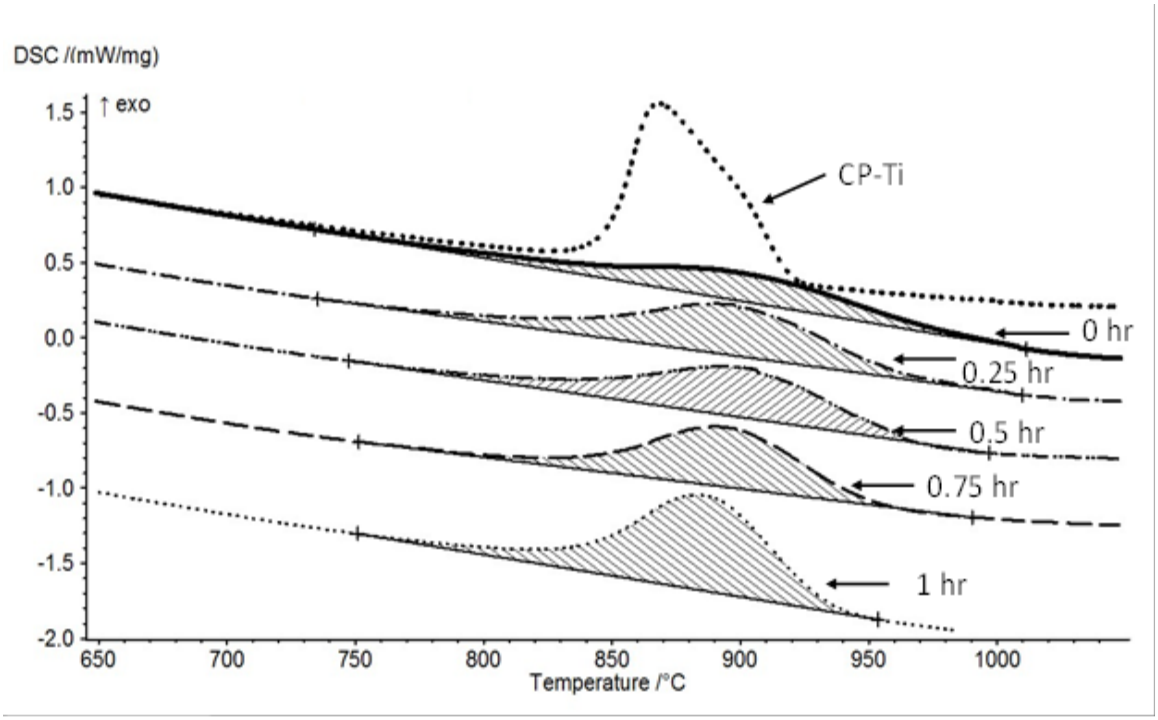

Figure 4.2.7: Comparison of the β to α transformation resulting from increasing isothermal holds in a fine MA blend: No Hold, 0.25, 0.5, 0.75 and 1 hour compared to pure Ti.

A summary of key measurements obtained from the DSC traces of Figure 4.2.6 and Figure 4.2.7 as a function of hold time at 1200 °C are presented in Figure 4.2.8. Included for comparison are the same measurements made from cooling DSC traces of an ingot metallurgy Ti6Al4V alloy, which was described in the previous chapter. For both the coarse and fine MA mixtures the onset temperature (or Beta transus temperature) is high at short sintering times indicating the presence of high Al containing regions. As the sintering time increases, the onset temperature systematically decreases and starts to approximate the measurements obtained in the homogeneous ingot metallurgy sample. Most of the change occurs in the first hour of sintering.

The end temperature behaves in a similar manner but reaches the level of the ingot sample more quickly. The coarse MA sample exhibits a lower end temperature at

intermediate sintering times. This indicates the development of more V rich regions at these sintering times.

The overall shape of the transformation peak was described by measuring the full peak width at half the maximum height (FWHM) (see Figure 4.2.8 c)) which is a common way to describe a peak with a Gaussian distribution. A high value for FWHM indicates a wide peak with a low peak height. The FWHM is high at short sintering times, but systematically decreases with sintering time. As with the onset and end temperatures, the FWHM value approaches that measured for the ingot measurements as the sintering times increases above 1 hour. Interestingly the FWHM value for the coarse MA at zero hold time is lower than at intermediate times, which is a reflection of the unusual shape of this transformation peak. The FWHM, onset and end temperatures for the fine MA mixture approach the ingot values more closely than that of the coarse MA mixture.

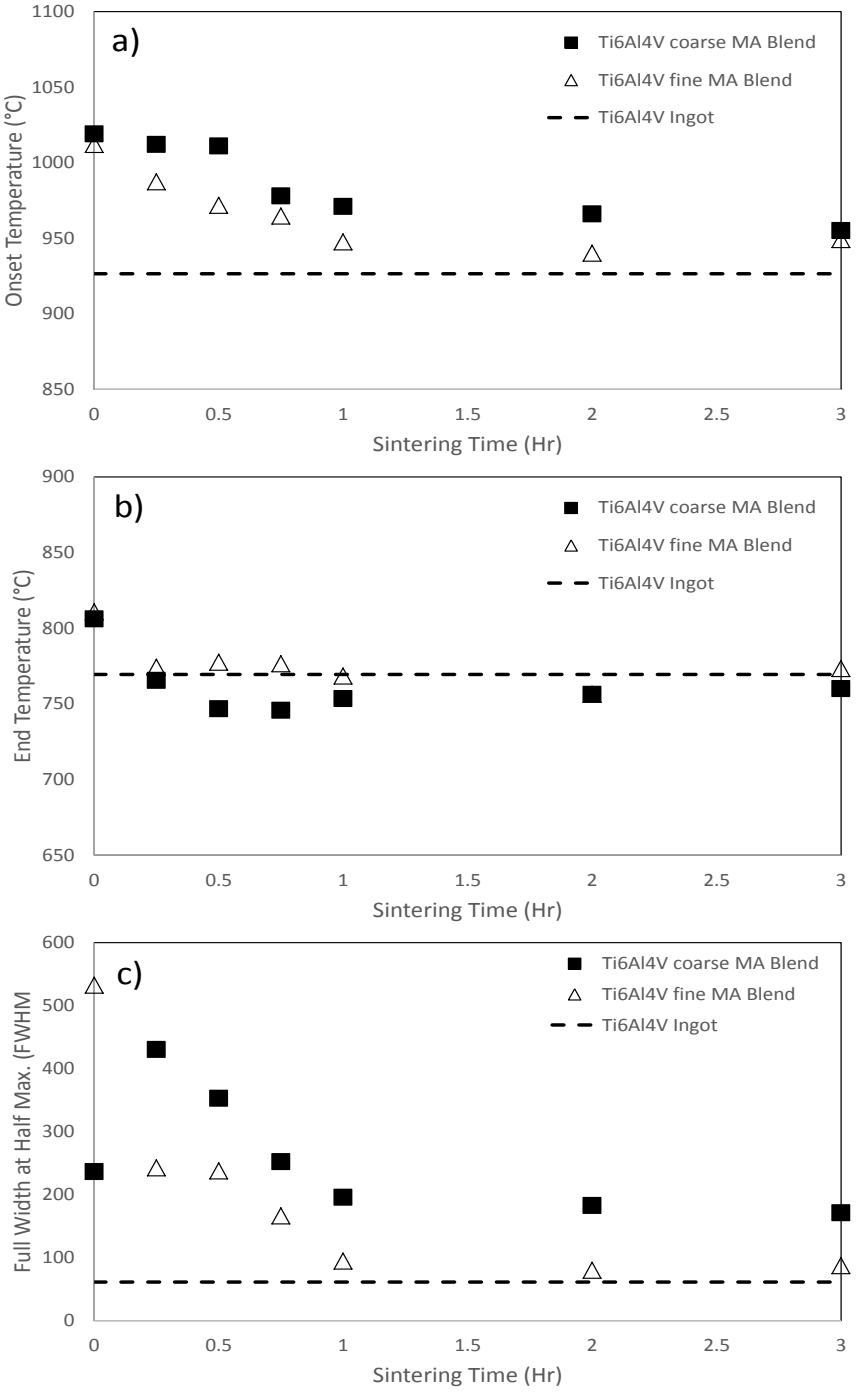

Figure 4.2.8: DSC measurements of a) onset temperature, b) end temperature, c) full peak width at half maximium (FWHM) for the β to α phase transformation of the materials of this study, as a function of sintering time at 1200 °C

In order to correlate the changes in the β to α transformation documented in the DSC traces, with microstructural changes, metallographic analysis was performed on all of the samples from Figure 4.2.6 and Figure 4.2.7. Optical micrographs of selected DSC samples for the coarse MA mixture after sintering times of zero, 0.5, 2 and 3 hours are shown in Figure 4.2.9. Samples sintered at 0.25 hours exhibited similar microstructural features to the zero hold time, while samples sintered at 1 hour had similar features to the 0.5 hour samples. For sintering times of zero and 0.25, regions of unalloyed CP-Ti were still present as well as a significant fraction of undissolved MA particles. Relatively coarse Widmanstatten microstructure (or alloyed region) surrounds the MA particles. The extent of this alloyed region has increased compared to the quenched sample of Figure 4.2.9a. After sintering for 0.5 and 1 hour, no unalloyed regions remain in the microstructure. Only a few large MA particles remain undissolved, while the Widmanstatten or alloyed region is well developed. The microstructural scale of the Widmanstatten structure is variable, which is due to different Al and V contents throughout the microstructure [57]. After 2 hours of sintering, all of the MA particles are dissolved and a fairly uniform Widmanstatten microstructure is developed. However there is still some variation in the scale of the Widmanstatten features. After 3 hours the microstructure appears very uniform, due to the establishment of a homogeneous distribution of the alloying elements.

Optical micrographs of selected DSC samples for the fine MA mixture after sintering times of zero, 0.5, 2 and 3 hours are shown in Figure 4.2.10. Samples sintered for zero hours exhibited some isolated undissolved MA particles and unalloyed regions. However, the majority of the microstructure is alloyed with Widmanstatten structure with a range of scale. Samples sintered for 0.25, 0.5 and 1 hour exhibited similar microstructural features (as exemplified by the 0.5 hour sample of Figure 4.2.10 b)). No undissolved MA particles or unalloyed regions were visible. However, the character of the Windmanstatten structure varied from lightly etched to darkly etched regions. SEM/EDS analysis indicated that the darkly etched regions had a lower alloy content compared to the lightly

etched regions. After 2 hours of sintering, only isolated regions of darkly etched, low alloy regions were present while at 3 hours, a uniform, equally etched Widmanstatten structure developed. The relatively coarse distribution of low and high alloy regions which existed at sintering times of 0.25 to 2 hours was partly due to a non-uniform distribution of the fine MA particles in the green compact. This resulted in some inhomogeneity on a scale larger than the inhomogeneity caused by the dissolution of the MA particles. Despite this non-uniform MA particle distribution, the microstructure reached a high degree of homogeneity after 3 hours of sintering.

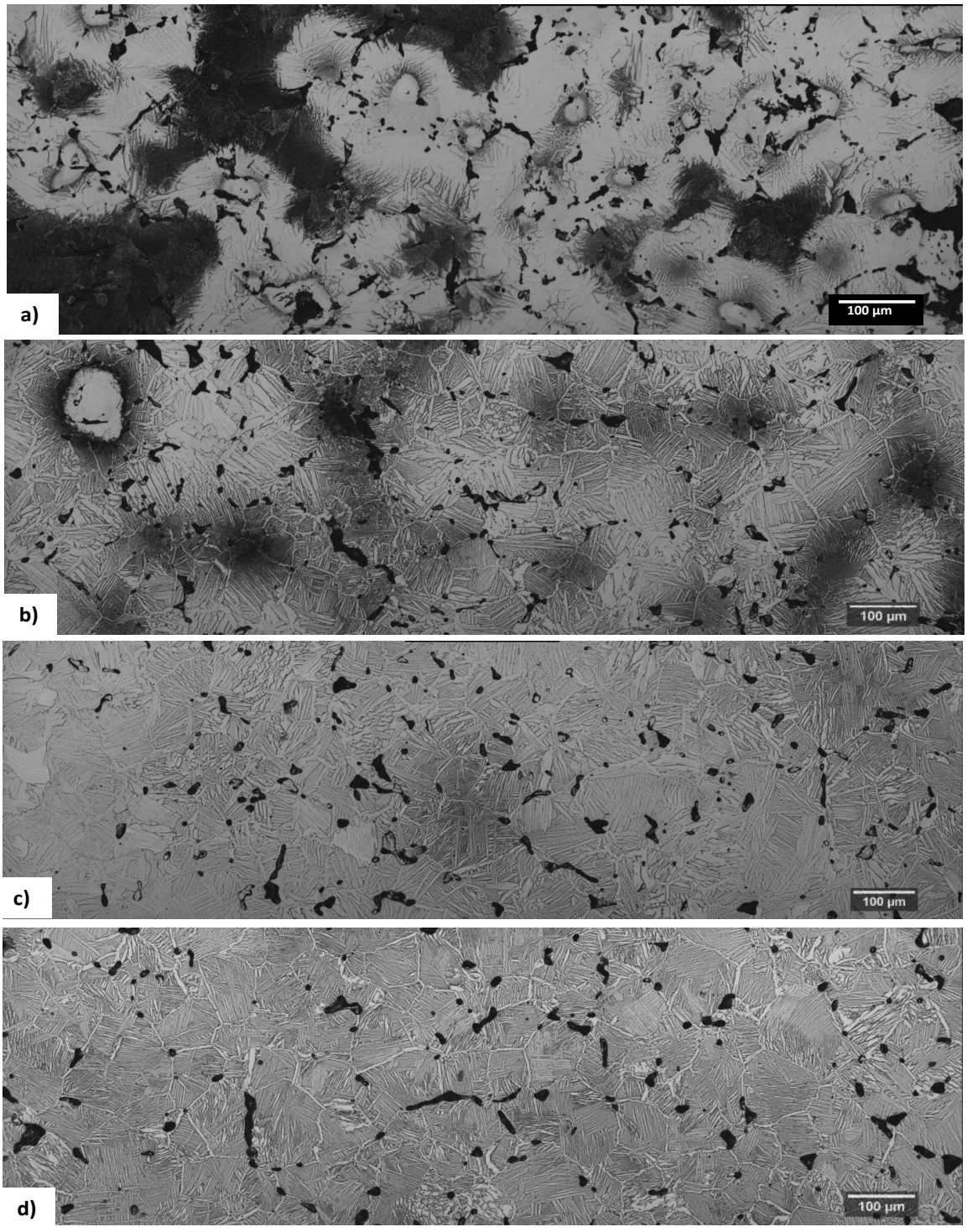

Figure 4.2.9: Optical micrographs of Ti6Al4V with Coarse MA sintered at 1200 °C for a) zero, b) 0.5 c) 2 and d) 3 hours

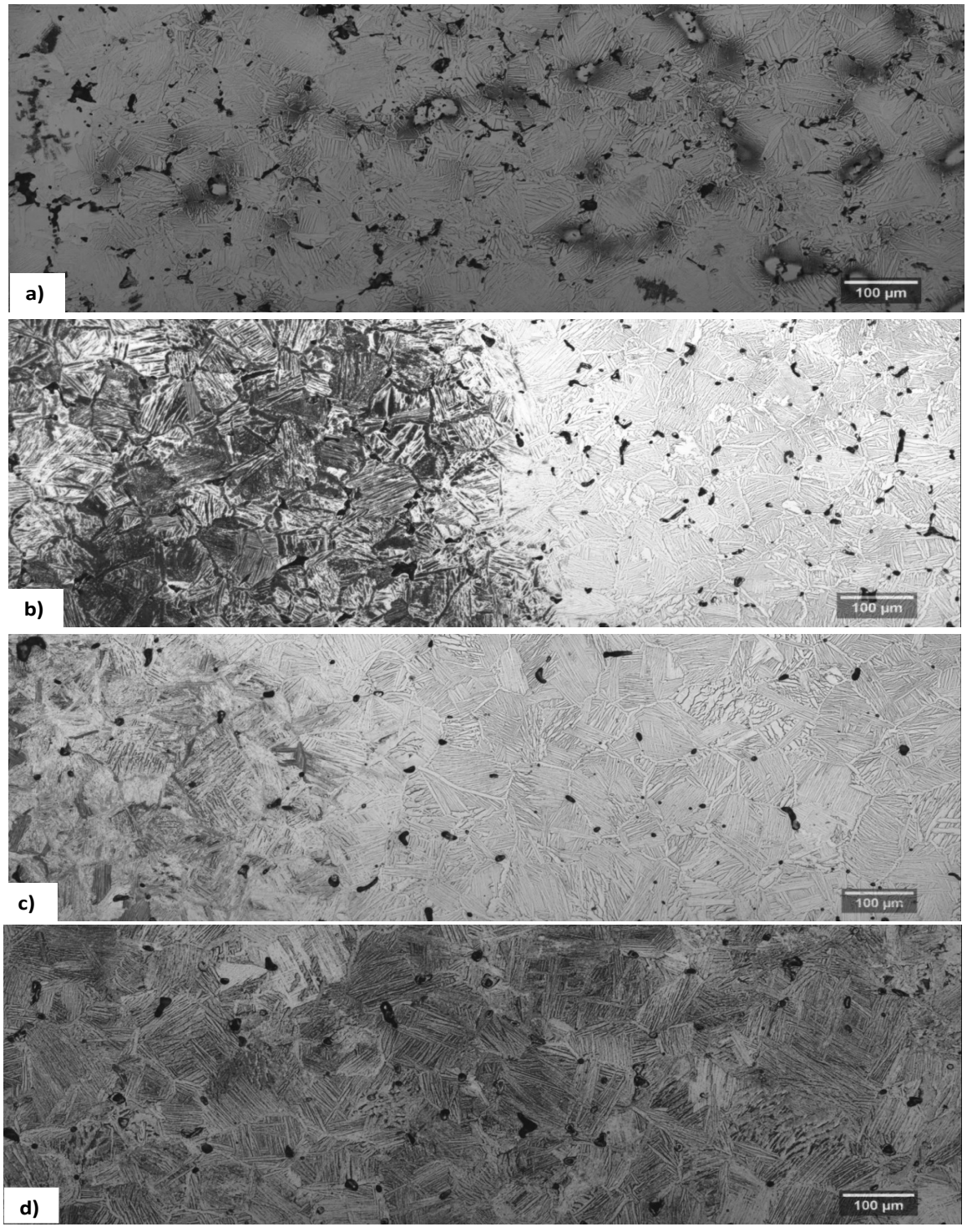

Figure 4.2.10: Optical micrographs of Ti6Al4V with Fine MA sintered at 1200 °C for a) zero, b) 0.5 c) 2 and d) 3 hours

The phase composition for the coarse MA mixture in the green state and all the sintered states is shown in Figure 4.2.11. From the measured spectra, the bulk composition of all samples appears to α-Ti, with this phase accounting for nearly all the peaks. A shift in the measured peaks was noted for all the sintered samples. The main peak for β-Ti was observed at a 2θ of 38°. It appears that this peak becomes apparent after 30 minutes of sintering. Several intermetallics were observed, with the most prominent being $AlTi_3$. The spectra for these peaks is found between the two main peaks for α-Ti, and have the highest intensity in the 30 min sample. These peaks then decrease with increased sintering and have a significantly reduced intensity after 2 hours. The aluminum-vanadium intermetallics were only observed in the green sample where the AlV MA existed.

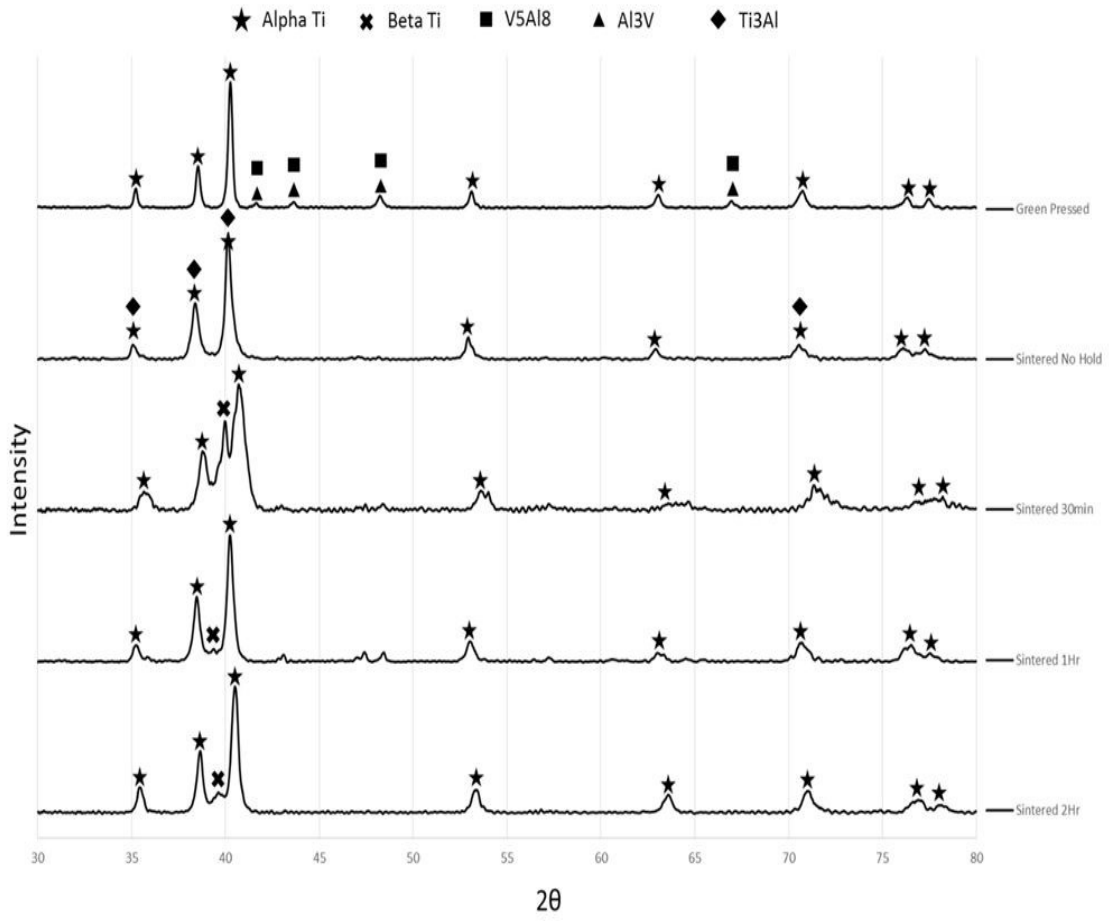

Figure 4.2.11: Measured spectra by XRD for the coarse MA mixture with corresponding phase composition

The phase composition for the fine MA mixture in the green state and all the sintered states is shown in Figure 4.2.12. Similar to the coarse MA, α-Ti accounted for the majority of the measured spectra for all samples. These peaks were also shifted from the reference angles. Similarly, the formation of β-Ti appeared in the 30 minute sample and persisted with additional sintering time. There was no evidence for the existence of Al_3Ti in all the measured spectra, despite being found in the coarse MA samples. In the green state both powders contained V_5Al_8 and Al_3V, which constituted the bulk phase composition of this state.

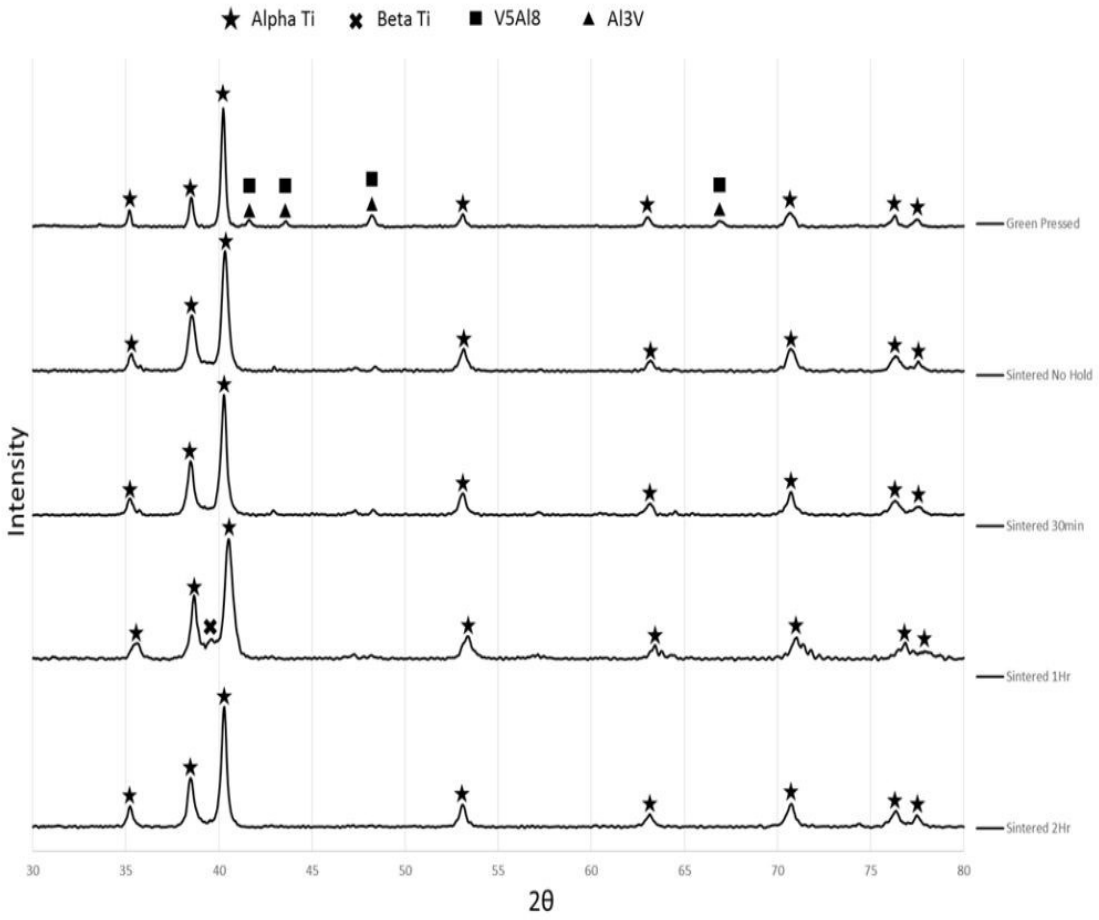

Figure 4.2.12: Measured spectra by XRD for the fine MA mixture with corresponding phase composition

4.3. Discussion

4.3.1. Microstructural evolution from initial heating

The results from DSC and microstructural analysis have been interpreted using the conceptual diffusion model in Figure 4.3.1. The microstructure of the green material can be represented by a master alloy particle (60:40 AlV) sounded by a matrix of unalloyed α-Ti, depicted as "Primary α-Ti" in this model. In this state the coarse and fine mixtures

differ only by the size of the master alloy particle relative to the matrix and the distribution of these particles.

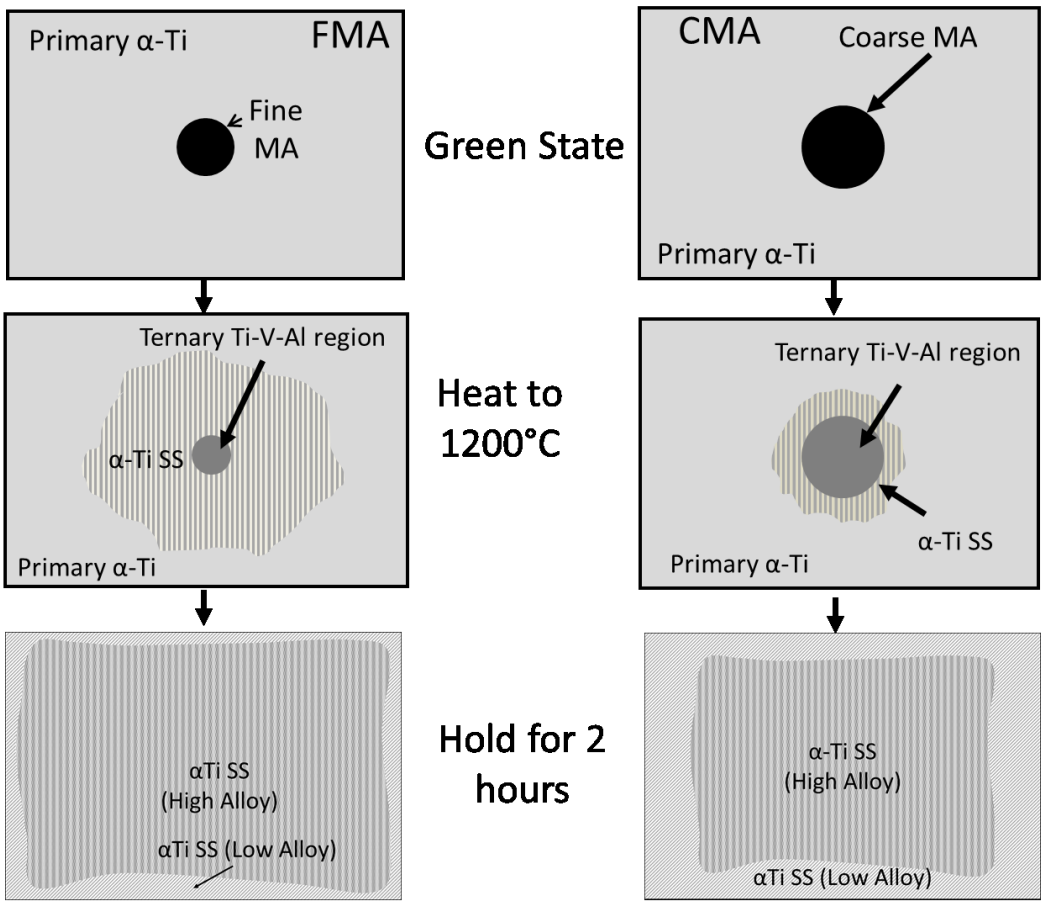

Figure 4.3.1: Conceptual diffusion model of phase evolution for fine master alloy (FMA) and coarse master alloy (CMA) at various stages of sintering

Analysis of the MA and Ti particles during heating of both MA size fractions show that there is a varying degree of alloying occurring during heating. An observed intermediate region forms for both size fractions of MA during heating, with a composition producing Ti-Al intermetallics. The size of this region grows steadily with increasing heating up to 1200°C. In both cases there is significant mobility of both Ti and Al as they diffuse in opposite directions. This contrasts the relatively slow diffusion of V from the MA core

out in to the surrounding matrix. In Table 4.2.2, the concentration of Ti is over 30wt% within the site of a MA particle by 1200°C site 1. The surrounding intermediate region has formed a lamellar structure, had has grown considerably from the boundary of the matrix and MA. The fine MA has similar features, but the kinetics have been accelerated, most likely due to the finer particle size. As a result, the MA cores that were visible at 950°C are nearly eliminated. Ti diffusion into these regions reached over 80wt%, and the intermediate region has a similar concentration of Al compared to original MA site. Similar to the coarse MA, this intermediate region has formed a refined lamellar structure that resembles the Widmanstätten of fully developed Ti6Al4V.

Comparison of the microstructure for both MA mixtures in the interrupted/quenched experiments heated to 1200°C to the No Hold samples of the effect of sintering time experiments shows significant changes. This was unexpected considering both are heated to the same temperature and the only difference is the higher cooling rate for the interrupted heating samples (100°C/min instead of 40°C/min). Thus, the observed reduction in volume fraction of primary α-Ti for both MA mixtures with the no hold heating profile occurred as a result of the longer time the sample was in the beta Ti state as a result of the slower cooling. For example, choosing a nominal beta transus temperature of 1000 °C, the time in the beta phase during cooling would be 2 and 5 minutes for the 100 °C/min. and 40 °C/min samples respectively. This points out how rapid diffusion and microstructural changes are occurring in this early stage of sintering. This change in microstructure is due to the long range diffusion of Al into the Ti matrix, creating a α-Ti solid solution.

SEM/EDS analysis of both MA mixtures sintered up to 1200 °C and quenched shown in Figure 4.2.3 and Figure 4.2.5, exhibited low concentrations of Al diffused throughout the Ti matrix. Due to the smaller particle size of the fine MA, the volume fraction of remaining primary α-Ti was significantly lower than the coarse MA. The differences in extent of alloying of Al and V in this state is shown in Figure 4.3.1 at the “Heat to

1200°C" point. A greater volume fraction of α-Ti solid solution (SS) for the fine MA (FMA) compared to the coarse MA (CMA) is the primary difference at this point. As a result, Al concentration at the remaining MA site for the fine powder is decreased, with bulk Al content existing primarily in the intermediate region as α-Ti SS and Ti_3Al, and Ti matrix as α-Ti SS. The slower kinetics of the coarse MA result in higher Al concentration in the MA site, with more remaining primary α-Ti in the matrix and a smaller intermediate region.

4.3.2. Phase Evolution of CMA Mixture

DSC traces of the coarse MA mixture support this long range diffusion of Al in this state. The 0Hr trace in Figure 4.2.6 displays a unique exothermic peak for the β to α transformation. In particular there is a very high onset temperature for this transformation, 1008°C, suggesting that regions exist with very high Al content that increase the transformation temperature due to the α-Ti stabilizing effect of Al. As temperature decreases, the measured transformation maintains a relatively low slope. This slow increase in heatflow continues to a peak heatflow of 881.2°C, very close to the transformation temperature for pure Ti. The behaviour of this peak suggests that long range diffusion of Al has occurred, but a significant concentration gradient exists, and the bulk transformation is similar to that of unalloyed Ti. As cooling continues there is marked drop in heatflow. This "shoulder" further supports the observed microstructural changes of the coarse MA at this stage that the extent of vanadium diffusion is very limited. Phase evolution characterized by XRD in Figure 4.2.11 from the green state to the no hold state shows that the existence of two Al-V intermetallics that constituted the bulk phase composition of the MA particles no longer exists. At the no hold state the measured peaks at 38.5° and 40.1° have broadened due to the formation of Ti_3Al. Characteristic peaks for this phase closely match that of α-Ti, which constituted the bulk of the phase composition.

With increasing isothermal periods at 1200°C the measured β to α transformation peak shows evidence of improved homogenization of both Al and V. The 0.5Hr trace in Figure 4.2.6 has a higher onset temperature than the 0Hr trace, but more importantly a much lower end temperature for the peak. The observed shoulder of the 0Hr trace no longer exists suggesting that V diffusion has progressed, forming phases with high β-phase stability. As a result the transformation for 0.5Hr largest temperature span. Additionally, peak heatflow for this transformation shifts to 903.6°C, meaning the temperature for the bulk transformation is now being altered by the alloying additions. Additionally, the measured enthalpy of the transformation has increased as Al and V diffusion causes the dissolution of V_5Al_8 and Al_3V. This transformation is confirmed by XRD as the characteristic peaks for both phases are no longer present in this state. Instead, the appearance of peak at 40.1° begins in this state. This peak has been confirmed by several authors to be β-Ti [18,30,32]. At 1200°C there is significant solubility of both Al and V in the bcc β-Ti phase. The slower diffusion kinetics of V after this relatively short thermal exposure would likely result in high concentrations in solution in β-Ti. During cooling some intermetallic precipitation would occur but a significant solubility remains allowing for stable β-Ti at room temperature. SEM/EDS analysis at this state shown in Figure 4.3.2 found that this phase was occurring at the site of the MA. After this amount of thermal exposure Al concentration at these sites had decreased significantly, with a relatively homogeneous concentration in the surrounding regions.

Spectrum	Al	Ti	V
(1)	13.94	55.07	30.99
(2)	14.84	58.97	26.18
(3)	15.73	64.78	19.49
(4)	16.68	71.85	11.47
(5)	16.15	71.53	12.32
(6)	16.77	75.49	7.75
Mean	15.69	66.28	18.03

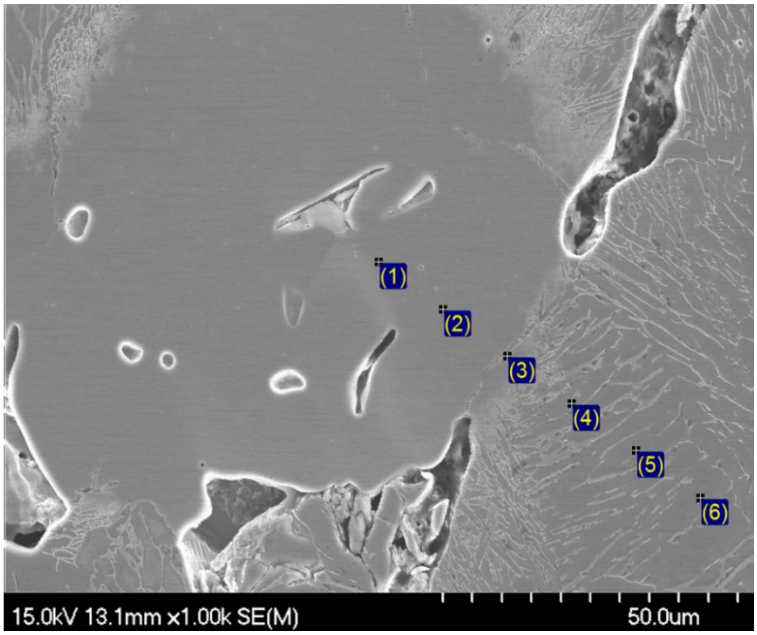

Figure 4.3.2: SEM/EDS analysis of coarse MA Ti6Al4V sintered for 0.5Hrs

However, Ti and V have inverse concentration gradients with point (1) having sufficient V concentration to result in a stable β-Ti.

Phase progression for the coarse MA transitioned to the stage shown in the model in Figure 4.3.1 during the 1 hour and 2 hour isothermal sintering profiles. From this point the transformation peak maintained a uniform profile, showing that a combined effect of both alloying elements on the transformation behaviour instead of localized effects of each. The onset temperature shows very little variation after 1 hour, which would mean the α-Ti stabilizing effects of Al are no longer varying. This does not necessarily mean complete homogenization of Al at room temperature, instead, it results in a consistent transition at the onset temperature. The most significant change in phase composition is the diminishing intensity of the β-Ti peak. As sintering progresses, the high concentration sites of V are eliminated, resulting in a more homogeneous β-Ti solid solution. Without localized regions of high V content, retained β-Ti concentration at room temperature decreases. This correlates with the XRD spectra for both the 1 hour

and 2 hour profiles. Optical microscopy of the 2 hour state reveals a uniform Widmanstätten lamellar structure. Certain regions appeared much darker in contrast to surrounding regions due to a different response to the etchant. These different etched regions were analyzed further using SEM/EDS. It was found that the dark etched regions had a slightly lower alloy concentration compared to the bulk Ti6Al4V content. Therefore further sintering for 3 hours was necessary to remove these dark etched regions and achieve complete homogenization.

4.3.3. Phase Evolution of FMA Mixture

Evolution of the fine MA mixture, in general, had many similarities to the coarse mixture. However, due the smaller particle, and thus larger surface area of the MA with the Ti matrix, exhibited faster kinetics. The DSC trace for the 0Hr profile in Figure 4.2.7 contrasts the coarse MA trace significantly. The measured onset temperature for the transformation is slightly lower but similar to the coarse MA. However, the peak shape is more symmetric and broad, as evidence by a much higher FWHM value (i.e. 530 versus 236 for the coarse MA blend). This difference is due to the more extensive dissolution of the MA particles but also a broader range of Al diffusion into the matrix. As indicated in the FMA 0hr hold micrograph of Figure 4.2.10a), this has resulted a larger removal of any unalloyed CP-Ti. Referring to the diffusion model in Figure 4.3.1, this can be conceptualized by a shrunken MA core with high diffusion of Al out of this region, and similarly high counter-diffusion of Ti into the core. The intermediate region then becomes the area with the highest concentration of Al in the form of both α-Ti solid solution and Ti_3Al. Beyond this intermediate region, the Ti matrix has been transformed from primary α-Ti into an α-Ti solid solution. Some regions of primary α-Ti remained, but the volume fraction was significantly lower than that of the coarse MA in the same state. This phase progression correlates well with DSC measurements for the 0hr state. Both peak and end temperature for the transformation were very similar to the measured temperatures for the coarse MA in the same state, however the shape of the peak was

much different. The peak behaviour was characteristic of a more homogeneous transformation, suggesting that the phase stabilizing effects of both alloying elements were contributing. Optical microscopy revealed that the vast majority of the MA sites were no longer present and that a majority of the phase composition consisted of an α-Ti SS with the characteristic lamellar structure. As with the coarse MA blend, more darkly etched regions were evident in Figure 4.1.10 b and c. SEM/EDS analysis of these fine MA mixtures at 2 hours of sintering also indicated lower alloy content in darker etched regions.

Less significant changes to the microstructure were observed in the transition from the 0Hr state to the 0.5Hr state. Phase analysis with XRD revealed that both sintered states consist of primarily α-Ti, in addition to Ti_3Al. The absence of β-Ti for the 0.5Hr is an important distinction between the coarse and fine MA after this amount thermal exposure. As mentioned previously, the existence of a strong beta phase peak for the coarse mixture was due to the slow diffusion of V out from the MA site, coupled with high diffusion of Ti into this region. Due to the smaller particle size, this phase was not detected at this state with the fine MA, and is due to two reasons. Firstly, the nature of a smaller particle size increases the surface contact area between the MA particle and the surrounding matrix, increasing diffusion flux. Secondly, the smaller particle size reduces the diffusion path length that both Ti and V must pass.

The microstructures of Figure 4.2.9c) and Figure 4.2.10c) indicate incomplete alloying in the 2Hr state of both MA mixtures, additional specimens were sintered for 3Hrs. Quantitative measurements of the DSC data for these specimens are included in Figure 4.2.8. In all metrics there is a definite trend towards stable values that also converged toward the values measured for the IM material. Optical micrographs of both specimens' revealed visual improvements in phase composition, with both having a fully developed and uniform Widmanstätten structure.

4.4. Summary and Conclusions

A methodology for the use of DSC to analyze the phase transformation from β to α-Ti of PM titanium alloys has been developed. Additionally, the effect of MA additions in two different size fractions has been investigated using DSC with varying sintering times at 1200°C. The homogenization of these additions was analyzed using DSC, with particular attention paid to the cooling trace after sintering with various sintering times. Additionally, an analysis of the α to β transformation during heating of both types of MA additions was performed. Other analysis techniques such as XRD, SEM/EDS and optical microscopy were also utilized for this investigation

Initial work to determine the suitability of DSC for the characterization of allotropic phase transformation with IM Ti6Al4V showed excellent repeatability and sensitivity. Following this, the variation in resolution of the cooling peak based on different cooling rates indicated an optimal cooling rate of 40°C/min. Finally, repeatability of a powder compact was also proven with the use of commercially pure Ti powder.

A comparison of the heating traces of the two different MA additions was performed to understand the extent of metallurgical interactions that occurred during heating. As expected, the fine MA showed a greater extent of alloying during heating, on account of its smaller particle size and larger surface area for interaction. In both cases, an intermediate region was observed after cooling from key temperatures based on the α to β transformation. This proved that a considerable degree of metallurgical interaction occurred in both systems during the heating phase of sintering.

The analysis of the CMA addition during cooling revealed in the early stages of sintering that there was a distinct difference in diffusion rates of Al and V from the MA core. EDS mapping revealed much more rapid diffusion of Al into the Ti matrix, whereas V lagged significantly. This lead to existence of V-rich regions which formed measurable

quantities of retained β-Ti. In the 1 and 2Hr states, the measured intensity of β-Ti decreased due to the improved homogenization of V. However, SEM/EDS analysis in the 2Hr state revealed that the desired uniform composition of both Al and V had not been achieved and thus further sintering would be required to produce a fully homogeneous specimen.

As stated previously, the FMA addition exhibited a similar behaviour to the CMA but with markedly faster kinetics due to its smaller particle size. Optical microscopy of the 0Hr state revealed that the MA core was no longer distinguishable from the intermediate region that formed during heating. The cooling trace of the FMA in the 0Hr state appeared qualitatively more uniform than the CMA trace in the same state, with a more uniform peak suggesting the effects of both alloying elements were altering the phase change. The existence of retained β-Ti was only observed in the 1Hr state, and then was not present in the 2Hr state, which supports the DSC measurements that more rapid alloying was occurring with the FMA. SEM/EDS analysis in the 2Hr state found improved homogenization compared to the CMA, however, there was still a degree of inhomogeneity that existed and as such, further sintering would be required.

When both specimens were sintered for 3Hrs, improvements in homogenization were noted specifically by DSC and optical microscopy. Quantitative data of the transformation behaviour by DSC revealed that the trends for these different metrics had settled at consistent values by this point. The optical micrographs of both specimens revealed a fully developed Widmanstätten structure in both cases, and also improved densification.

In the pursuit of a fully homogenized PM Ti6Al4V by means of a MA powder mixture, a better understanding of the role of the alloying elements and the effect of particle size during the sintering of the specimens has been developed. Key aspects of a MA PM system based on this investigation include: the role of MA particle size, the effect of

cooling rate, and a sintering time in excess of 2 hours at 1200°C to ensure a fully homogenized specimen. The use of DSC has been shown to greatly aid in the development of PM systems, and in this case Ti6Al4V, by allowing in-situ analysis of the heatflow characteristics.

5.0. SUMMARY AND CONCLUSIONS

This research has focused on the ultiziation of BE and MA additions for the purpose of producing fully homogeneous PM Ti6Al4V, which is a processing route which may lead to wider adoption due to the cost-competitive advantages of PM. The advantages of PM are well understood for many alloy systems, however, Ti-alloys are a relatively underdeveloped field. This research has attempted to advance the understanding of the alloying behavior PM Ti6Al4V with the use of either BE or MA additions. To accomplish this, a methodology employing DSC to analyze and characterize the heatflow characterisitics of this system has been developed. DSC allows for insitu analysis of specimens in different sintering atmospheres and heating profiles, providing very sensitive and accurate analysis. Additional analysis was performed using XRD, SEM/EDS and optical microscopy. Results were compared to DSC measurements in order to substantiate them.

5.1. Thermal analysis

In order to validate the use of thermal analysis for the different PM Ti6Al4V systems, repeatability of the DSC using wrought Ti6Al4V to measure the β to α transformation was tested. Excellent repeatability and sensitivity was found with these results. Further validation was accomplished with PM CpTi measuring the same phase transformation. Again, excellent repeatability and sensitivity was found, proving that DSC was capable of measuring this transformation in both wrought and PM systems.

5.1.1. BE Analysis

The effects of each elemental addition to Ti was analyzed with the expected results. The addition of V resulted in a lower onset and end temperature for the β to α transformation, with a lower recorded enthalpy than the CpTi. Conversely, the transformation measured

with the addition Al resulted in higher onset and end temperatures for the β to α transformation. The measured enthalphy of transformation was larger than that of the Ti4V, with a broader peak. This leads to the conclusion that the kinetics of Al diffusion in Ti was more rapid than V, and that a homogeneous speciemen is produced after approximately 1Hr of sintering at 1200°C. Additionaly, a large exothermic peak was observed during the heating of the Ti6Al mixture. This observation was in agreement with other published work, where researchers observed a rapid alloying of Al immediately after heating past its melting point. The elemental Ti6Al4V exhibited many of the characterisitics that were observed in each of the binary mixtures. Bulk homogenization of the ternary mixture appears to progress at a slower rate than either binary mixture, particularly Ti4V. Additionally, the measured enthalpy of transformation was lower than either binary mixture. This suggests that additional thermal exposure is required to achieve the desired bulk composition.

As a point of comparison, the DSC analysis of the Ti6Al4V PA powder provided important insight into the behavior of a fully homogeneous transformation. The results of all the different thermal profiles were very similar, with no appreciable changes. This showed that with even a short duration of sintering a fully homogeneous specimen can be produced using a PA powder.

5.1.2. MA Analysis

Analysis of the two MA additions during heating to specific points of α to β transformation revealed the extent of alloying that occurred during heating. DSC analysis revealed small differences in the α to β transformation for both MA additions when compared to CpTi. The fine MA displayed an exothermic shift leading to transformation, and the coarse MA displayed a small exothermic peak after the phase transformation. Of particular importance was the lack of any significant exothermic peak relating to the metling of Al, showing that a MA addition avoids this issue.

DSC cooling traces of coarse MA revealed a shoulder in the transformation peak at the earliest sintering time. This was believed to be due to the differences in diffusion rates of Al and V into the Ti matrix. As expected, the transformation peak transitioned into a more uniform peak with increased thermal exposure. In the later stages the measured peaks for thecoarse MA were noticeably more uniform than the BE Ti6Al4V mixture, with a higher enthalpy of transformation.

The DSC traces for the fine MA addition did not show any evidence of slow diffusion that was seen with the coarse MA. The earliest sintering traces show a more uniform transformation. This suggested that due to the smaller particle size, alloying of both Al and V progressed much more rapidly. At 2Hrs the DSC trace showed a very uniform peak with a higher enthalpy of transformation than the equivalent coarse MA trace.

5.2. Microstructural and phase analysis

5.2.1. BE Analysis

Microstrural anaylsis confirmed many of the obersvations made with the DSC. For the Ti6Al specimens, the existence of large voids confirmed the result of the rapid alloying of Al during heating. These voids persisted throughout all the thermal profiles, and would no likely heal with additional sintering time. SEM/EDS analysis showed that long range diffusion of Al in the earlier sintered states, and that a homogeneous speciemen was achieved between the 1Hr and 2Hr states.

The slower diffusion of V was confirmed with XRD and SEM/EDS for the Ti4V system. The existence of elemental V sites in early sintered states with SEM/EDS showed that there was significantly slower kinetics, likely due to V self diffusion. By the 2Hr state, the homogeneity had improved significantly. There was no observed β-Ti peak in the XRD spectra at this state. However, SEM/EDS maps revealed that certain regions were

still below the desired bulk composition and that additional sintering time would be needed.

Analysis of the BE Ti6Al4V revealed the same large porosity seen in the Ti6Al specimens. In the case of this ternary system these large voids seem to have additional detrimental affects. XRD analysis revealed more intense peaks for the β-Ti phase than what was observed in the Ti4V specimens. This suggested that the diffusion of V was further hindered in the ternary system, likely due in part to the greater porosity.

Similar to the observations of PA powder made with DSC, microstrucral analysis revealed a fully homogeneous microstructure. An important observation was the lower apparent sintered density of the PA specimens.

5.2.2. MA Analysis

Analysis of the both MA specimens during heating revealed the extent of metallurgical interaction that occurred up to the temperatures of interest. In both cases there was a formation of an intermetallic phase between the MA and the Ti matrix. The region was more developed in fine MA speciemens due to the smaller particle size.

SEM/EDS analysis of the early sintered states of the coarse MA confirmed that the diffusion of V lagged behind Al significantly. This was mostly alleviated with increasing sintering time. XRD analysis showed a decreasing peak intensity of the β-Ti phase with increasing sintering time. However, EDS mapping of the 2Hr state revealed that the desired bulk composition had not yet been achieved.

The more rapid alloying kinetics of the fine MA were confirmed with the microstructural analysis techniques used for this investigation. In all sintered states there was evidence of a more developed microstructure compared to the coarse MA. However, in the 2Hr

state, the fine MA mixture was also found not be fully homogeneous, and would require additional sintering.

5.3. Future Work

Due to necessary constraints, the scope of this research leaves several areas for future investigation into the alloying behavior of PM Ti6Al4V. The recommendation for areas of future work include:

- Analysis of at least one sintered state between 1Hr and 2Hrs of sintering time for all powder mixtures.
- A more comprehensive phase analysis of the two-phase Widmanstätten structure with XRD.
- Experimentation with different alloying additions such as mix of elemental and MA additions
- Determining the sintering time required to achieve a homogeneous microstructure for each powder mixture.
- Experimentation with hydrogenated Ti powders.
- Comprehensive analysis of sintered density, and the use of sintering aides to improve sintered density.

REFERENCES

[1] German RM. Sintering Theory and Practice. Wiley; 1996.

[2] World SS. Stainl Steel World 2001:17.

[3] Board NRC (U. S). NMA. Titanium: Past, Present and Future : Report of the Panel on Assessment of Titanium Availability. National Academy Press; 1983.

[4] Smith WF. Structure and Properties of Engineering Alloys. McGraw-Hill; 1993.

[5] Froes FHS, Gungor M, Ashraf Imam M. JOM 2007;59:28.

[6] Donachie MJ. Titanium: A Technical Guide. ASM International; 2000.

[7] Lütjering G, Williams JJC. Titanium : Springer London, Limited; 2007.

[8] Brown E. Introduction to Thermal Analysis: Techniques and Applications. Springer; 2001.

[9] Kosta D. Maglić, A. Cezairliyan VEP. Compendium of Thermophysical Property Measurement Methods: Recommended Measurement Techniques and Practices. Plenum Press; 1992.

[10] Michael D, Turriff R. 2007:319.

[11] Whitney M, Corbin SF, Gorbet RB. Intermetallics 2009;17:894.

[12] Froes FH, Mashl SJ, Hebeisen JC, Moxson VS, Duz VA. JOM 2004;56:46.

[13] Hongtao W, Zak Fang Z, Pei S. Int J powder Metall 2010;46:45.

[14] Chen W, Yamamoto Y, Peter WH. Powder Technol 2011;214:194.

[15] Lee YT, Peters M, Wirth G. Mater Sci Eng A 1988;102:105.

[16] Klar E. ASM Handbook, Volume 07- Powder Metallurgy. American Society for Metals; 1984.

[17] Robertson, I. M. and Schaffer GB. Powder Metall 2009;52:225.

[18] Siqueira RP, Sandim HZ, Hayama AF, Henriques VR. J Alloys Compd 2009;476:130.

[19] Wei, W. Liu, Y. Zhou, K. Huang B. Powder Metall 2003;46:246.

[20] Wenbin F, Lianxi H, Wenxiong H, Erde W, Xiaoqing L. Mater Sci Eng A 2005;403:186.

[21] Low RJ, Robertson IM, Schaffer GB. Scr Mater 2007;56:895.

[22] Fujita T, Ogawa A, Ouchi C, Tajima H. Mater Sci Eng A 1996;213:148.

[23] Ivasishin OM, Savvakin DG, Froes F, Mokson VC, Bondareva KA. Powder Metall 2002;41:382.

[24] Gupta RK, Pant B, Agarwala V, Agarwala RC, Sinha PP. J Mater Sci Technol 2010;26:693.

[25] B.Panigrahi, N.Reddy MG. J Mater Sci Technol 2007;23:363.

[26] Anokhin V, Ivasishin O, Petrunko A. Mater Sci Eng A 1998;243:269.

[27] Baker H, Okamoto H. ASM Handbook, Volume 03 - Alloy Phase Diagrams. ASM International; 1992.

[28] Goso X, Kale A. Production of Titanium Metal Powder by the HDH Process, in: Light Met. Conf. Advanced Metals Initiative; 2010.

[29] McCracken C, Motchenbacher C, Barbis D. Int J Powder Metall 2010;46:19.

[30] Fujita T, Ogawa A, Ouchi C, Tajima H. Mater Sci Eng A 1996;213:148.

[31] Ivasishin OM, Anokhin VM, Demidik a. N, Savvakin DG. Key Eng Mater 2000;188:55.

[32] Henriques V, Sandim H, Coelho G, Dasilva C. Mater Sci Eng A 2003;347:315.

[33] Raynova S., Zhang D. GB. Key Eng Mater 2012;520:289.

[34] Bolzoni L, Esteban PG, Ruiz-Navas EM, Gordo E. Powder Metall 2011;54:543.

[35] Luo SD, Guan CL, Yang YF, Schaffer GB, Qian M. Metall Mater Trans A 2012;44:1842.

[36] Sachdev AK, Kulkarni K, Fang ZZ, Yang R, Girshov V. Jom 2012;64:553.

[37] Zhigang Zak Fang, Pei Sun HW. Adv Eng Mater 2012;14:383.

[38] ASTM International. B348-13. 2014;02.04:8.

[39] Liu B, Liu Y, Zhang W, Huang JS. Intermetallics 2011;19:154.

[40] Druz V, Moxson V, Chernenkoff R, Jandeskajnr W, Lynn J. Met Powder Rep 2006;61:16.

[41] Su Y, Zhang D, Kong F, Chen Y. Mater Sci Eng A 2013;563:46.

[42] Kim I, Jeong WS, Kim J, Park K-T, Shin DH. Scr Mater 2001;45:575.

[43] Ng HP, Haase C, Lapovok R, Estrin Y. Mater Sci Eng A 2013;565:396.

[44] Haase C, Lapovok R, Ng HP, Estrin Y. Mater Sci Eng A 2012;550:263.

[45] Bolzoni L, Weissgaerber T, Kieback B, Ruiz-Navas EM, Gordo E. J Mech Behav Biomed Mater 2013;20:149.

[46] Robertson IM, Schaffer GB. Metall Mater Trans A 2009;40:1968.

[47] Esteban PG, Ruiz-Navas EM, Gordo E. Mater Sci Eng A 2010;527:5664.

[48] Ivasishin OM, Eylon D, Bondarchuk VI. Defect Diffus Forum 2008;277:177.

[49] Dąbrowski R. Arch Metall Mater 2011;56:6.

[50] Malinov S, Guo Z, Sha W, Wilson A. Metall Mater Trans A 2001;32:879.

[51] Bolzoni L, Esteban PG, Ruiz-Navas EM, Gordo E. J Mech Behav Biomed Mater 2012;15:33.

[52] Savvakin DH, Humenyak MM, Matviichuk M V., Molyar OH. Mater Sci 2012;47:651.

[53] Froes F, Friedrich H, Kiese J, Bergoint D. Jom 2004:40.

[54] Norgate TE, Wellwood G. JOM 2006;58:58.

[55] Smugeresky JE, Dawson DB. Powder Technol 1981;30:87.

[56] Bolzoni L, Esteban PG, Ruiz-Navas EM, Gordo E. J Mech Behav Biomed Mater 2012;14:29.

[57] Carman A, Zhang LC, Ivasishin OM, Savvakin DG, Matviychuk MV, Pereloma EV. Mater Sci Eng A 2011;528:1686.

[58] Kim SK, Park JK. Metall Mater Trans A 2002;33:1051.

[59] Santos D, Pereira M, Cairo C, Graca M, Henriques V. Mater Sci Eng A 2008;472:193.